Electrochemistry

Timo Jacob

Institut für Elektrochemie, Universität Ulm
Helmholtz-Institut Ulm

universität ulm

Oct 17, 2014

Helmholtz
Electrochemica

The Beginning

Bagdad-Battery (250 v. Chr.):

1936 Khujut Rabuah (Hill near Bagdad)

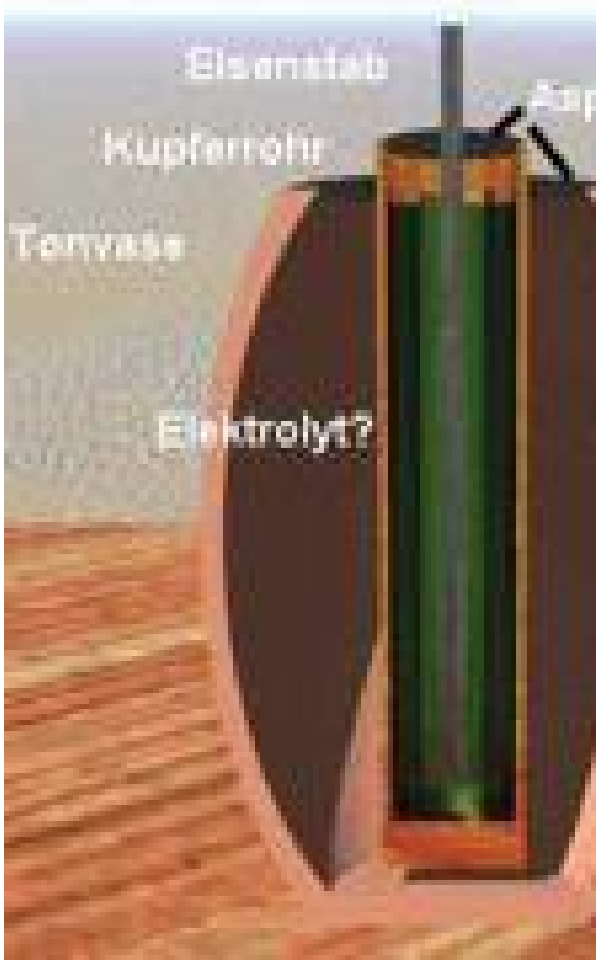

Electroch
Potentia

Halb-Reaktion					E°/V
reduzierte Form		oxidierte Form	+	z e⁻	
Li(s)	⇌	Li^+ (aq)	+	e⁻	- 3.04
K (s)	⇌	K^+ (aq)	+	e⁻	- 2.92
Ca (s)	⇌	Ca^{2+} (aq)	+	2 e⁻	-2.87
Na (s)	⇌	Na^+ (aq)	+	e⁻	- 2.71
Al (s)	⇌	Al^{3+} (aq)	+	3 e⁻	- 1.68
Mn (s)	⇌	Mn^{2+} (aq)	+	2 e⁻	- 1.18
Zn (s)	⇌	Zn^{2+} (aq)	+	2 e⁻	- 0.76
S^{2-} (aq)	⇌	S (s)	+	2 e⁻	- 0.48
Fe (s)	⇌	Fe^{2+} (aq)	+	2 e⁻	- 0.41
Cd (s)	⇌	Cd^{2+} (aq)	+	2 e⁻	- 0.40
Sn (s)	⇌	Sn^{2+} (aq)	+	2 e⁻	- 0.14
Pb (s)	⇌	Pb^{2+} (aq)	+	2 e⁻	- 0.13
H_2 + 2 H_2O	⇌	2 H_3O^+ (aq)	+	2 e⁻	0.00
Sn^{2+} (aq)	⇌	Sn^{4+} (aq)	+	2 e⁻	+ 0.15
Cu (s)	⇌	Cu^{2+} (aq)	+	2 e⁻	+ 0.34
2I⁻ (aq)	⇌	I_2 (s)	+	2 e⁻	+ 0.54
Fe^{2+} (aq)	⇌	Fe^{3+} (aq)	+	e⁻	+ 0.77
Ag (s)	⇌	Ag^+ (aq)	+	e⁻	+ 0.80
NO + 6 H_2O	⇌	NO_3^- (aq) + 4 H_3O^+ (aq)	+	3 e⁻	+ 0.96
2Br⁻ (aq)	⇌	Br_2	+	3 e⁻	+ 1.07
6 H_2O	⇌	O_2 (g) + 4 H_3O^+ (aq)	+	4 e⁻	+ 1.23
2 Cr^{3+} (aq) + 21 H_2O	⇌	$Cr_2O_7^{2-}$ + 14 H_3O^+ (aq)	+	4 e⁻	+ 1.33
2Cl⁻ (aq)	⇌	Cl_2	+	2 e⁻	+ 1.36
Pb^{2+} (aq) + 6 H_2O	⇌	PbO_2 (s) + 4 H_3O^+ (aq)	+	2 e⁻	+ 1.46
Au (s)	⇌	Au^{3+} (aq)	+	3 e⁻	+1.50
Mn^{2+} (aq) + 12 H_2O	⇌	MnO_4^- (aq) + 8 H_3O^+ (aq)	+	5 e⁻	+ 1.51
2F⁻ (aq)	⇌	F_2 (g)	+	2 e⁻	+ 2.87

reduzierende Wirkung nimmt zu

oxidierende Wirkung nimmt zu

less nob

Increasing ele
affinity

nobel

Electrochemical Potentials

Battery

$$Cu(s) \rightarrow Cu^{2+}(aq) + 2e^- \qquad E^0 = +0.34$$

$$Fe(s) \rightarrow Cu^{2+}(aq) + 2e^- \qquad E^0 = -0.41$$

$$\Delta E^0 = 0.79$$

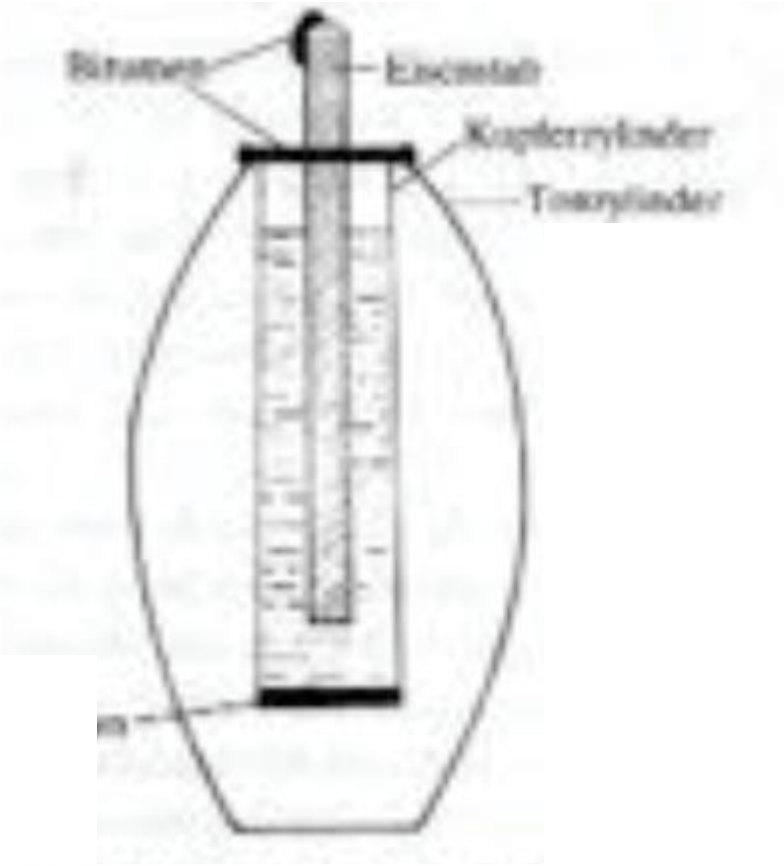

Gold Plating

...a bit later – Luigi Galvani (178

Experiment 1: Th

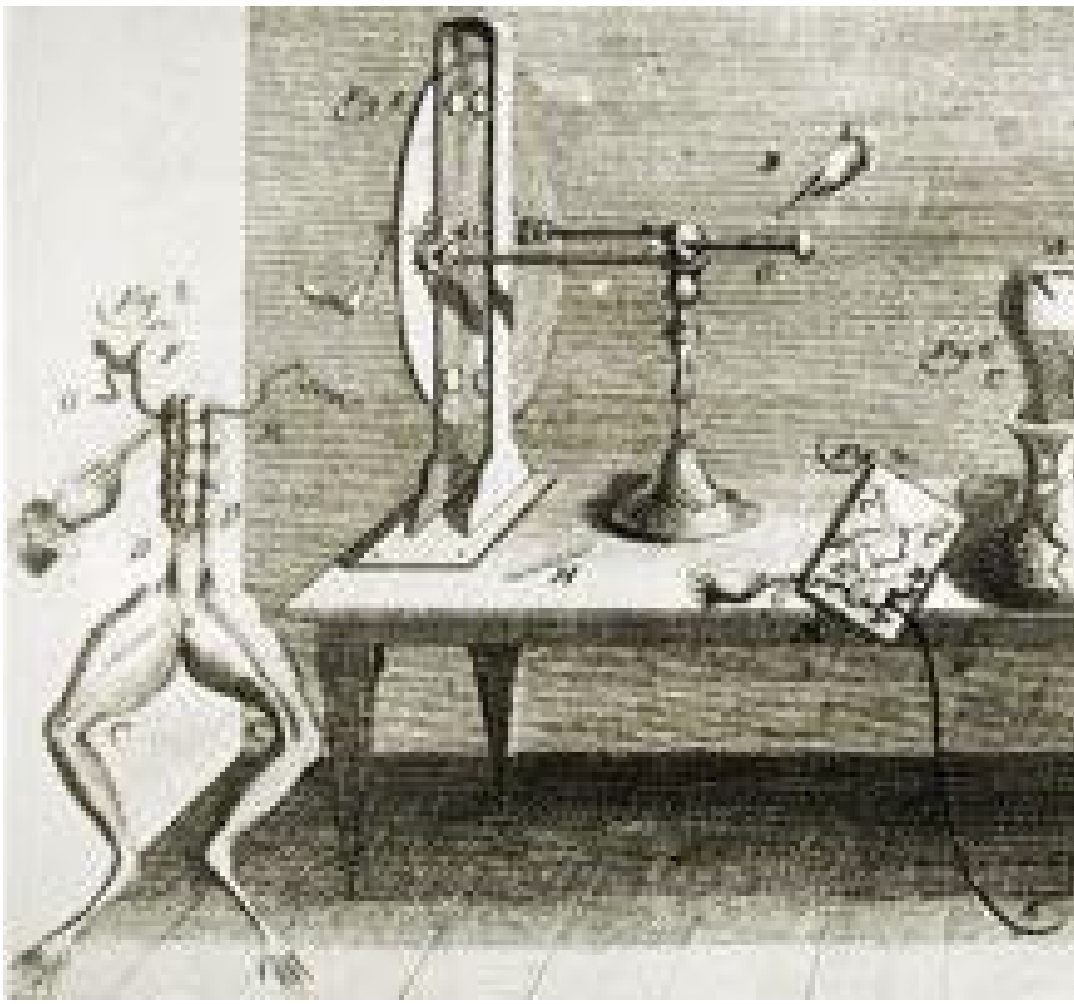

Luigi Galvani (1780)

”...suddenly all the muscles of the frog's
were seen to be violently contracted jus
though they had been seized with a viol
cramp”

De viribus electricitatis in motu musculari commens
(Description of the electrical forces of muscle mo

Luigi Galvani (1780)

Experiment 2: …I have never used that much!

Luigi Galvani (1780)

Experiment 3: at the balcony

brass (Messing) – frog-leg – iron-gate

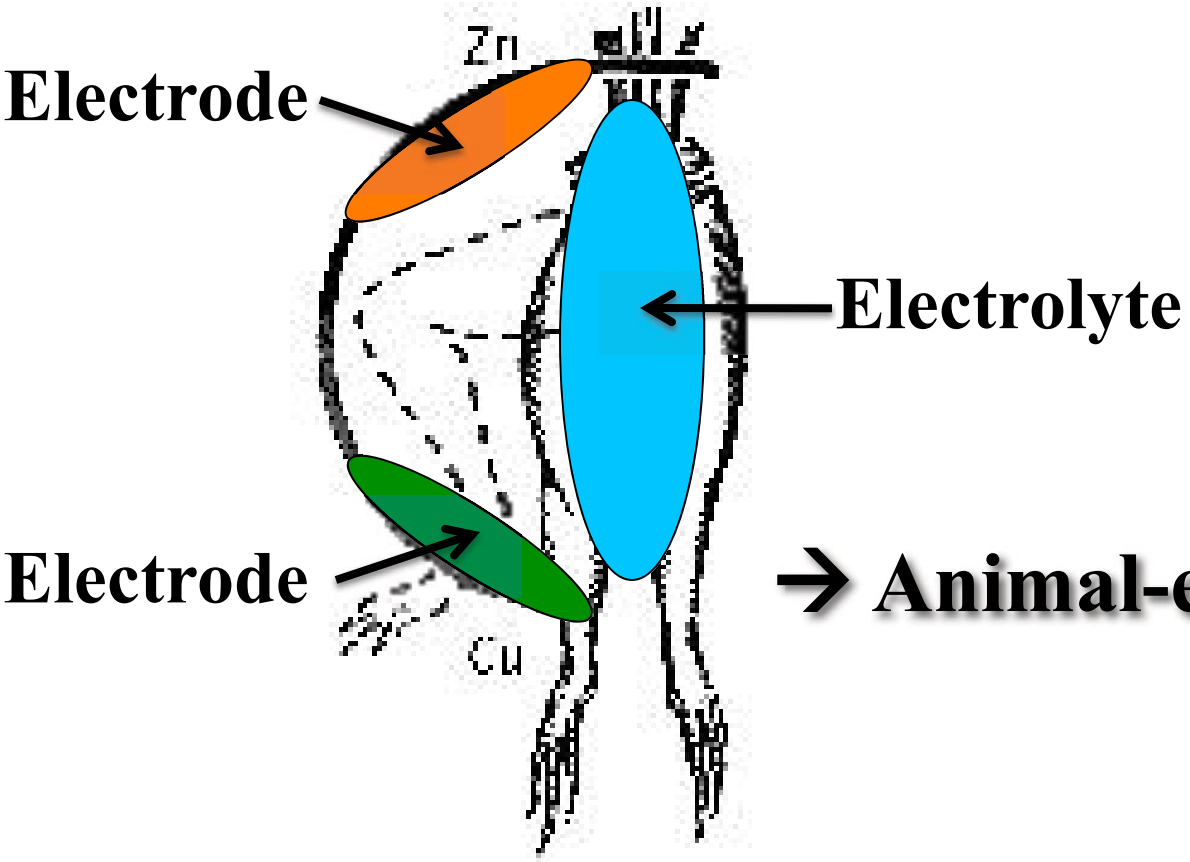

Hand battery

(http://youtu.be/

Bio-Battery

Allesandro Volta (1800) and John F. Da

Allesandro Volta (1800) und John F. Da

Anode:	Zn	$\rightarrow$	$Zn^{2+} + 2\,e^-$	$-E^0 = +0,$
Kathode:	$Cu^{2+} + 2\,e^-$	$\rightarrow$	Cu	$E^0 = +0,$
	$Zn + Cu^{2+}$	$\rightarrow$	$Cu + Zn^{2+}$	$E_{ges} = +1$

Galvanic Cell Animation

"Daniell Cell"

Zn / Zn^{2+} // Cu^{2+} / Cu

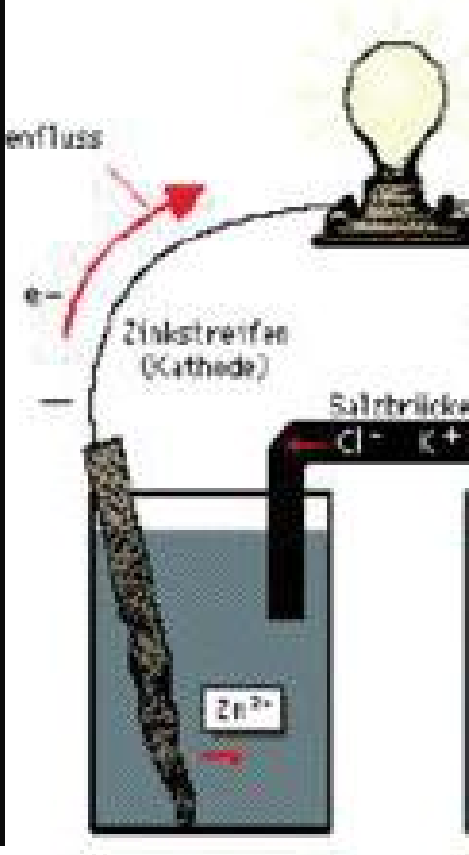

Battery-Development (http://youtu.be/WtbhIWUaRIg)

Historical View

1791	Galvani	Experiments on frog legs, muscle contrac
1800	Volta	Voltage by serial connection of metals in
1834	Farada	e a
1859	Planté	y b
1866	Leclar	nar
1891	Stoney	
1839	Grove	
1891	Nernst	Ne
1894	Ostwa	l e
1903	Arrhen	s
1905	Tafel	oub
1924-1930	Butler-Volmer	Generalization of the Tafel law

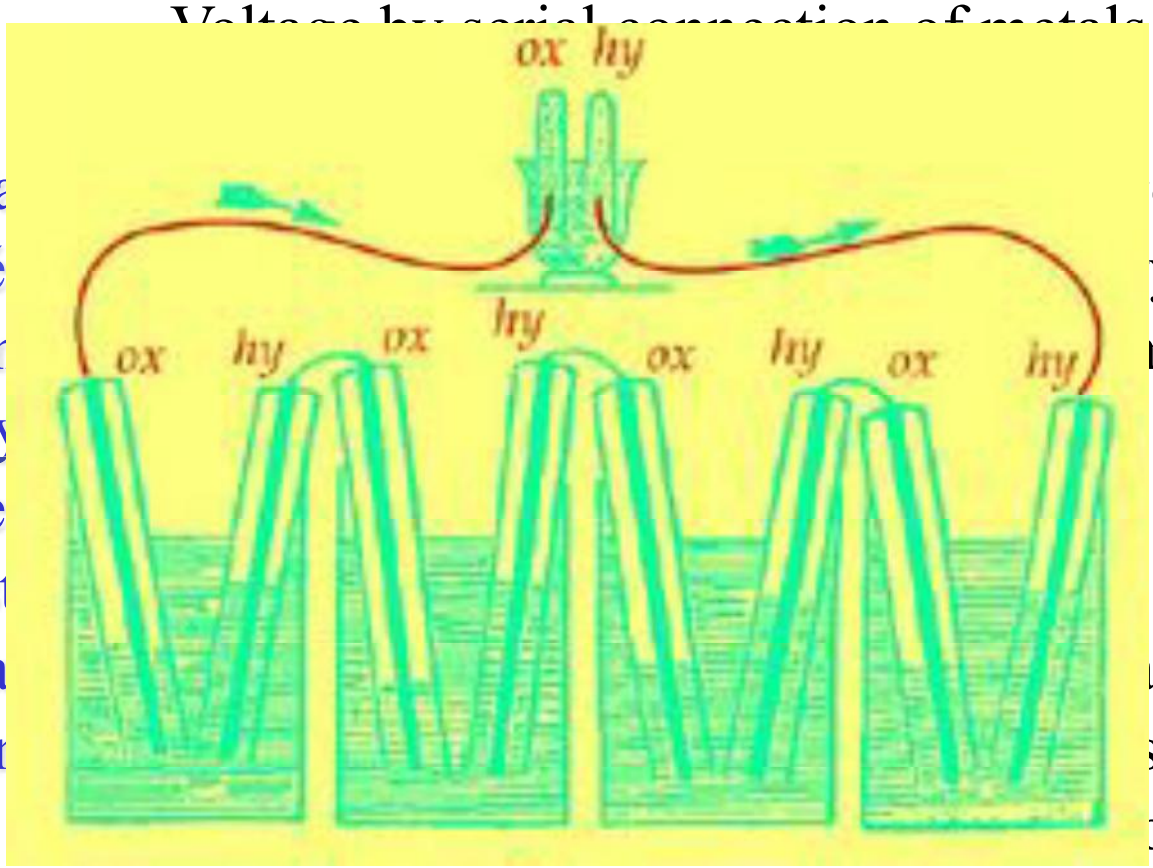

Historical View

1920	Born	Solvation of ions
1923	Debye-Hückel	Charge distribution in electrolyte solution charge
1930-1950	Frumkin	Non-equilibrium phenomena in electroch systems, over-potential, current density
>1950		Kinetic view of electrochemistry
>1960		Quantum-mechanical view of charge tran
1956-1965	Marcus	Theory of charge transfer (Nobel-price 19
1965	NASA	Hydrogen Fuel Cell in Gemini space-prog
>1994		Fuel Cell development
>1950		New batteries: Ni-Cd, HgO-Zn
>1980		Li-ion primary batteries
>1995		Li-ion secondary batteries

Johann Wilhelm Ritter (1776–1810)

Johann Wilhelm Ritter (1776–1810)

- 1798: Chemical Interpretation of galvanisation
- 1800: Water electrolysis

  $H_2O \rightarrow H_2 + ½\ O_2$
- 1800: Electrochemical passivation
- 1801: Discovery of UV-light
- 1802: Discovery of rechargeable battery
- **"Selbstversuche"**

	on the cathode	on the anode
Eyes	flash + blue light Picture decreases	flash + red light picture increases
Ears	lower tone	higher tone
Tongue	acid	basic
Nose	smell decreases	sneeze
Hand	stiffens	loosening

Overview

Fuel Cells

Applications

Photo-Electr

Li-Ion Batteries

Fundamental Electrochemistry

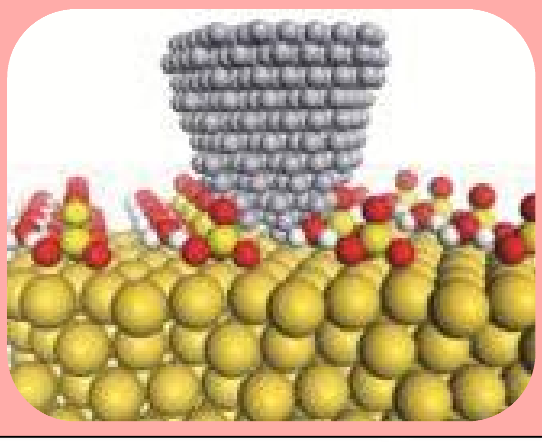

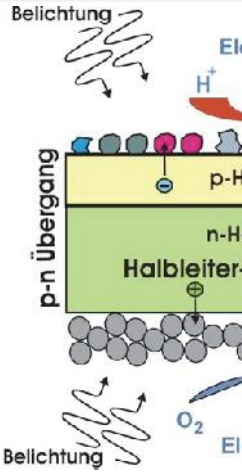

(Electro-)Catalysis

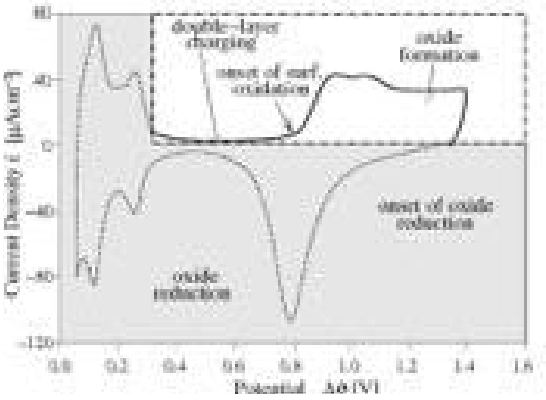

Develo

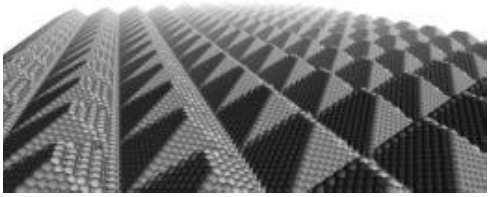

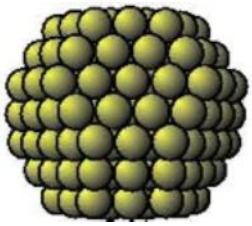

Motivation

Battery

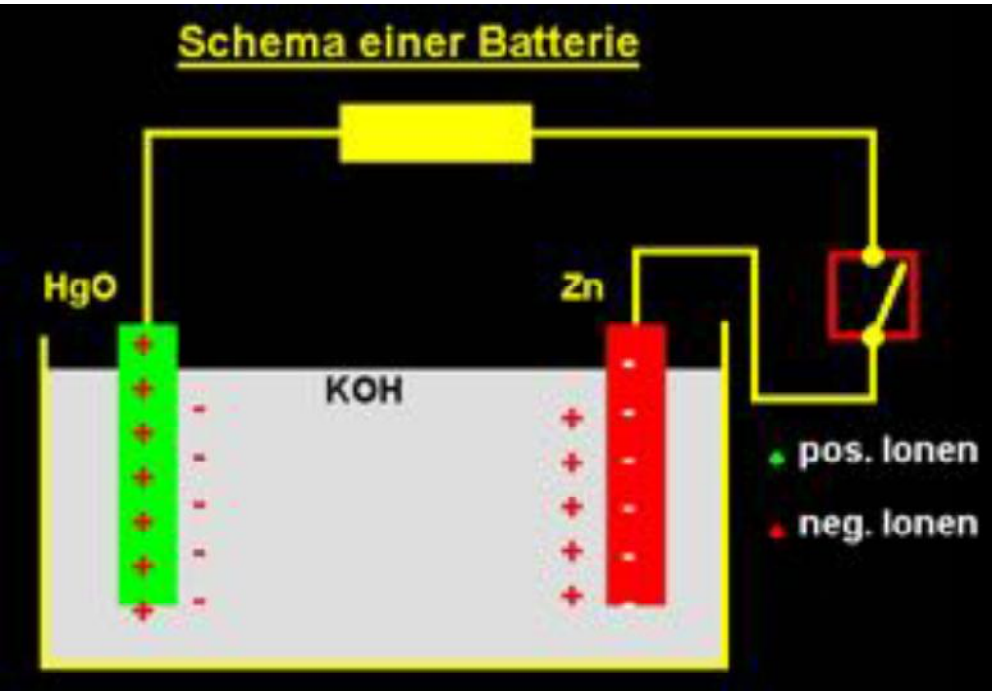

Fuel Cell

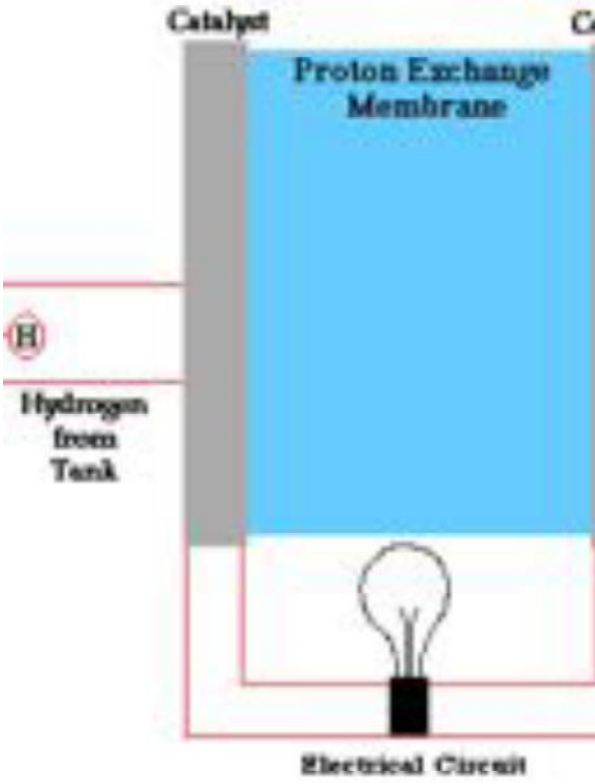

→ **Similar Principles**
(i.e. solid/liquid or solid/solid interface, respectiv

Electrochemistry

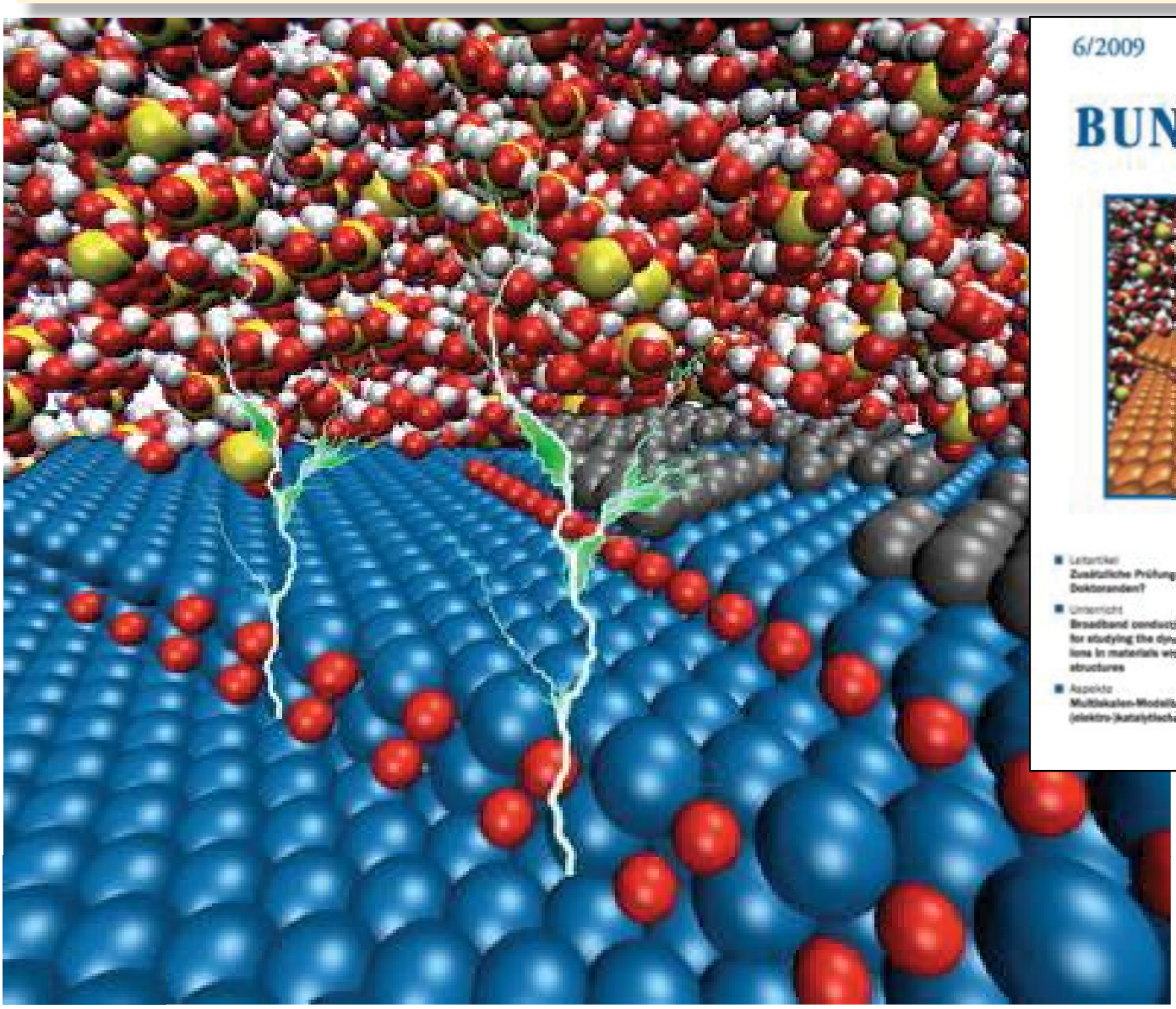

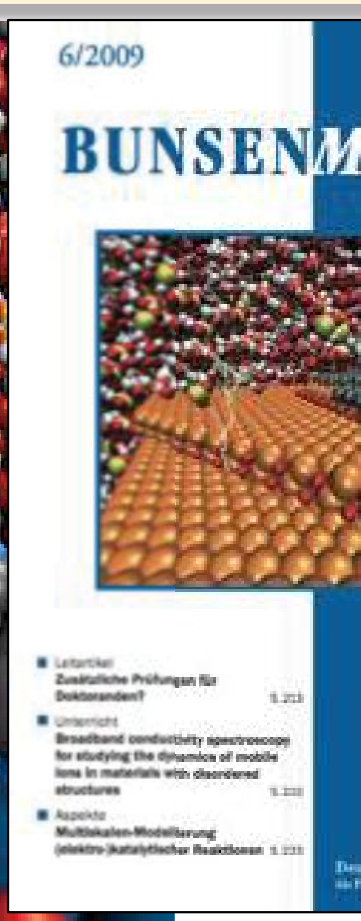

Multiphysics in Electrochemistry

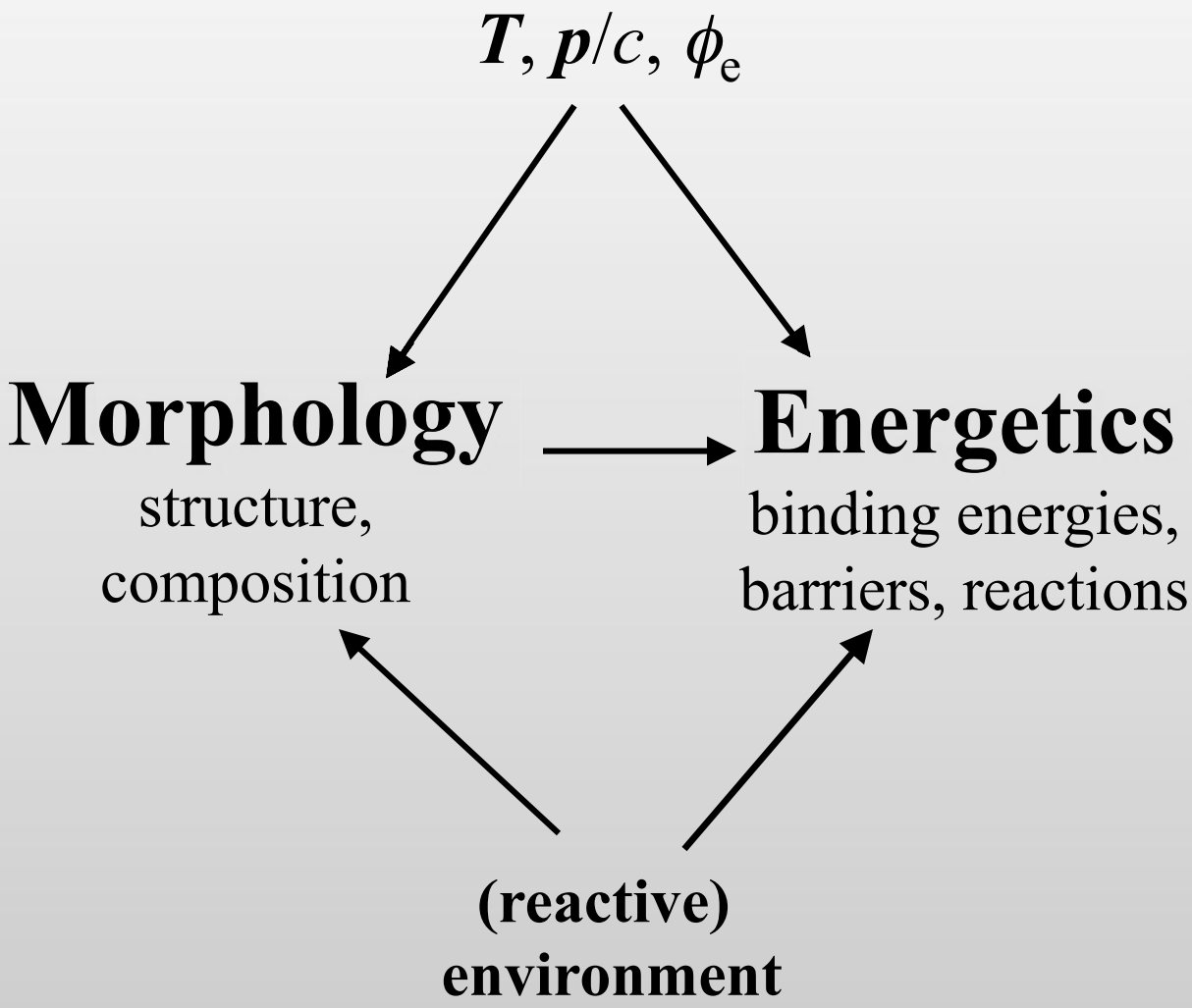

Methods

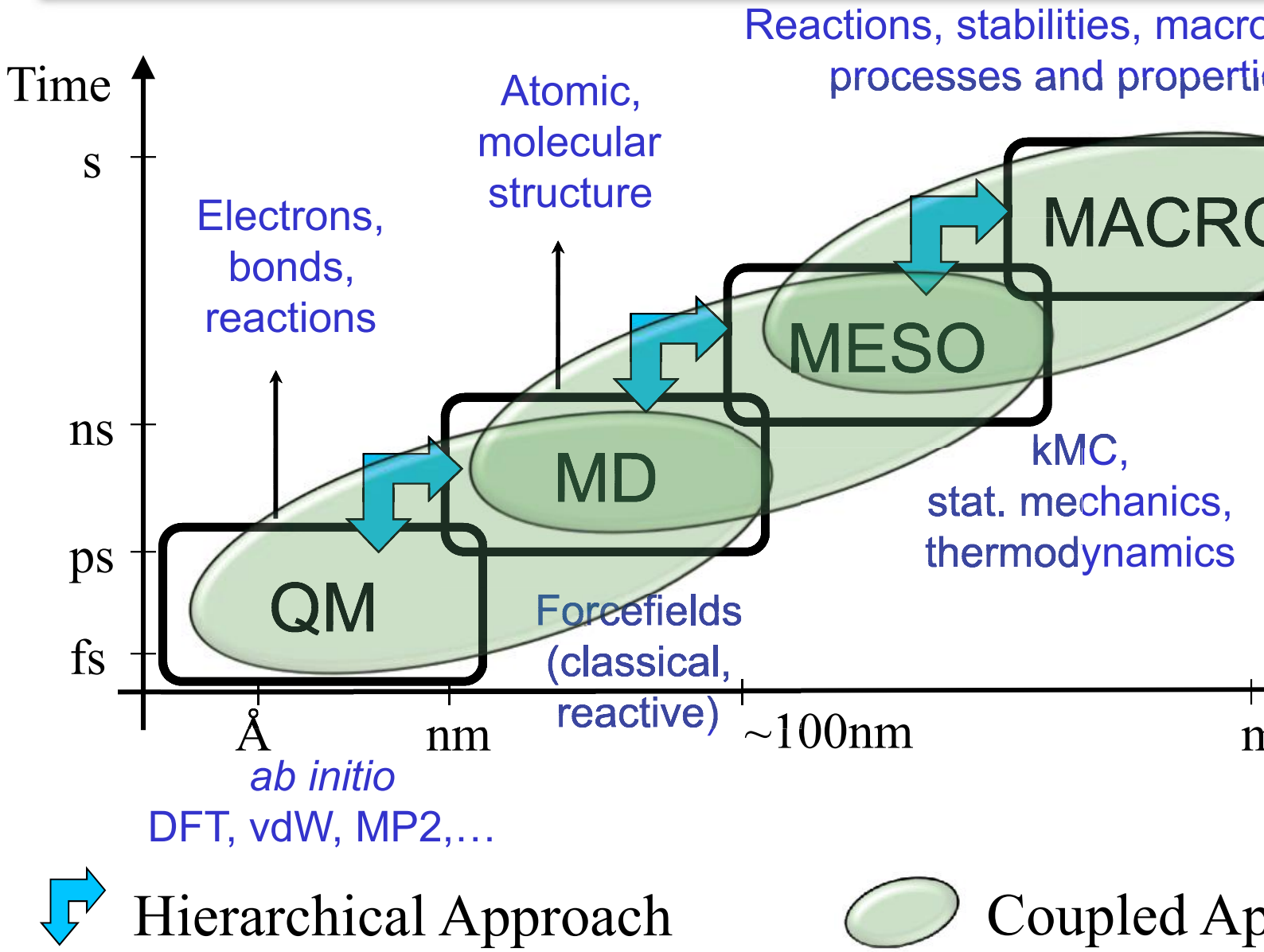
Reactions, stabilities, macro
processes and properti
Time
s
ns
ps
fs
Atomic,
molecular
structure
Electrons,
bonds,
reactions
MACRO
MESO
MD
QM
kMC,
stat. mechanics,
thermodynamics
Forcefields
(classical,
reactive)
Å
nm
~100nm
n
ab initio
DFT, vdW, MP2,…
Hierarchical Approach
Coupled Ap

Relativity in Batteries

PRL 106, 018301 (2011) PHYSICAL REVIEW LETTERS

Relativity and the Lead-Acid Battery

Rajeev Ahuja,[1,*] Andreas Blomqvist,[1] Peter Larsson,[1] Pekka Pyykkö,[2,†] and Patryk Zaleski-Ej
[1]Division of Materials Theory, Department of Physics and Astronomy, Uppsala University, Box 516, SE-751 20
[2]Department of Chemistry, University of Helsinki, Box 55 (A.I. Virtasen aukio 1), FI-00014 Helsinki,
(Received 30 August 2010; published 5 January 2011)

In conclusion, the lead-acid battery belongs to phenomena whose characteristic features are due relativistic dynamics of fast electrons when they mov a heavy nucleus. In this case the main actors are electrons of lead, in the substances involved. This may not help one to improve the lead battery, but it be useful in exploring alternatives. Finally, we no cars start due to relativity.

Electric Double-Layer

Basics

The chemical potential: $\mu_i = \left(\frac{dG}{dN_i} \right)_{p,T,N_j} \Rightarrow \mu_i(T, p_i) = \left[\overline{\mu}_i(T, p^0) +$

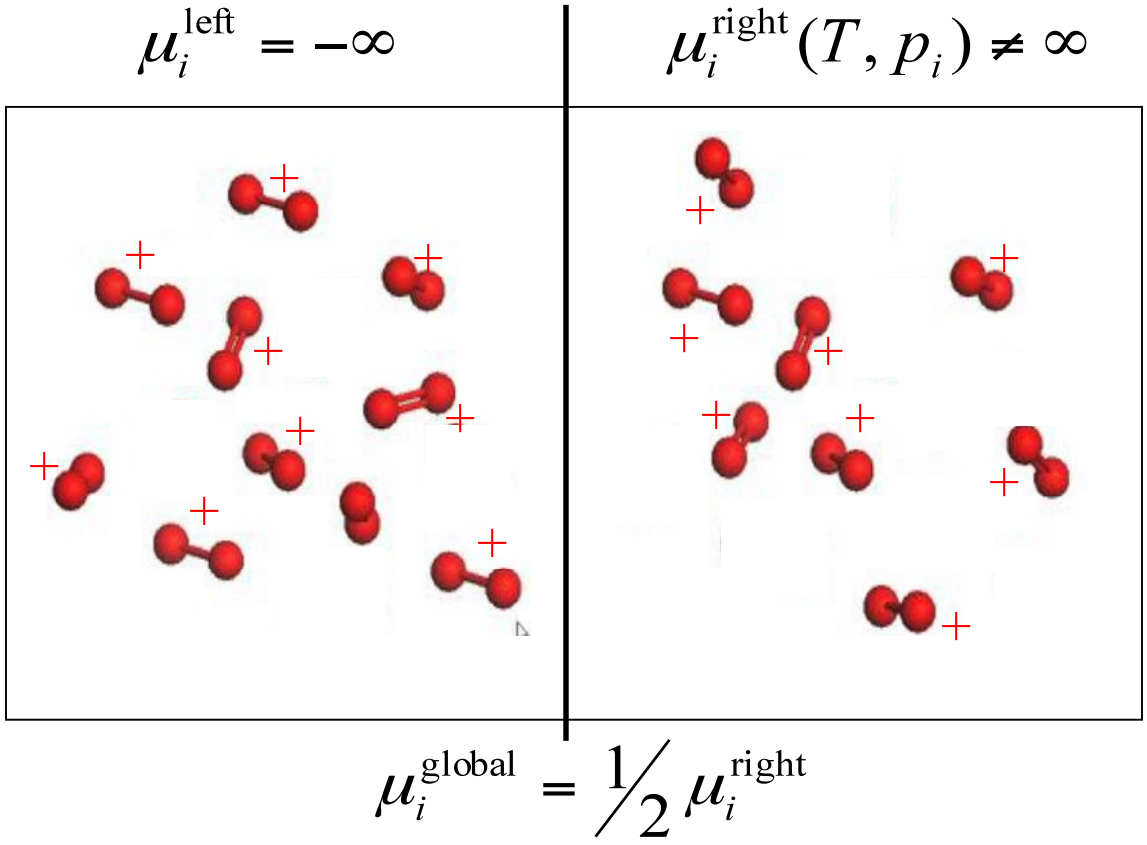

Basics

The electro-chemical potential:

$$\tilde{\mu}_i = \left(\frac{d(G + Q \cdot \phi)}{dN_i} \right)_{p,T,N_j} = \frac{dG}{dN_i} + \frac{dQ}{dN_i}\phi = \mu_i + q_i\phi$$

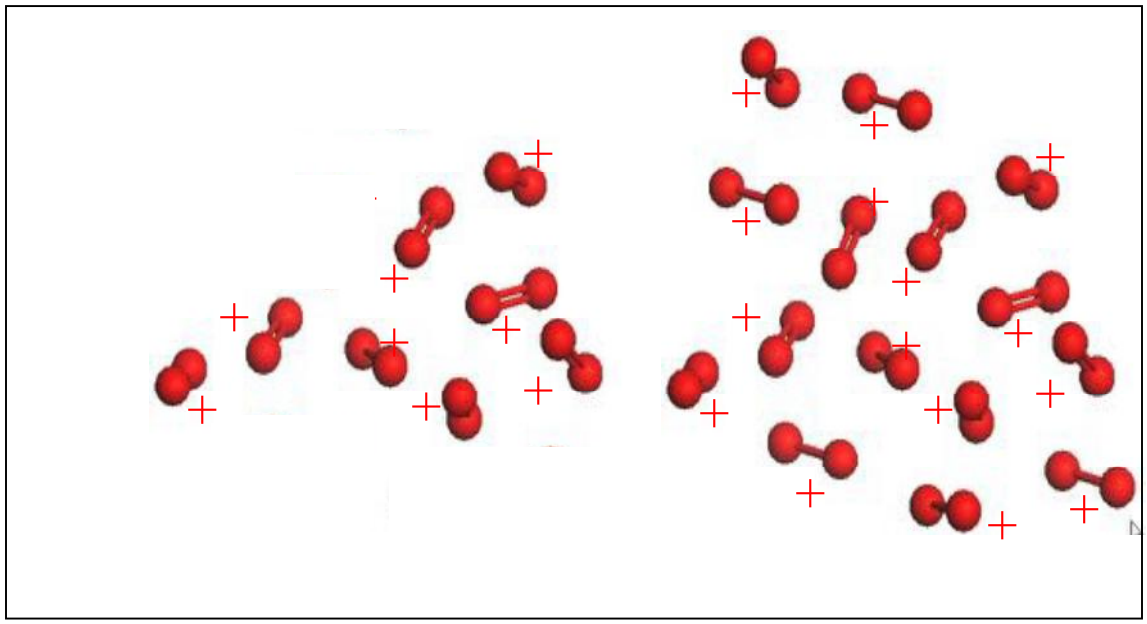

$\vec{E}$-fi

Electrochemical interface: Electro

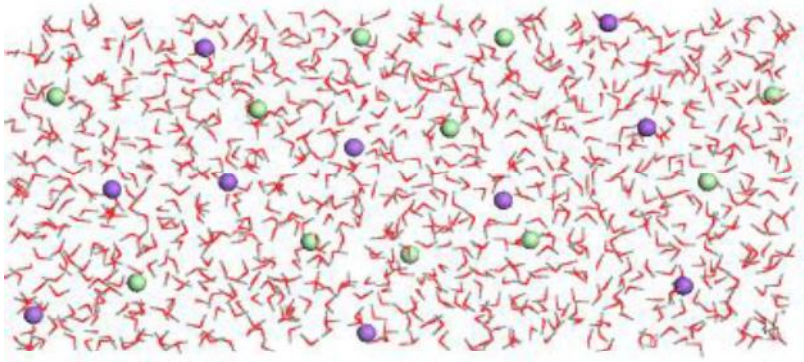

Ideal Solution
(non-interacting particles)

$$\mu_i(T,c_i) = \bar{\mu}_i(T,c^0) + k_B T \ln\left(\frac{c_i}{c^0}\right)$$

Real System

$$\mu_i(T,a_i) = \bar{\mu}_i(T,a^0) + k_B T \ln\left(\frac{a_i}{a^0}\right)$$

$$= \bar{\mu}_i(T,c^0) + k_B T \ln\left(\frac{c_i}{c^0}\right) +$$

Solvent

pure solvent

$$\mu_s(T,a_s) = \bar{\mu}_s(T,a^0) + k_B T \ln\left(\frac{a_s}{a^0}\right)$$

Solute/Ions

infinite dilution

$$\mu_\pm(T,c_\pm) = \bar{\mu}_\pm(T,c^0) + k_B T \ln\left(\frac{c_\pm}{c^0}\right) +$$

$\frac{\mu_+ + \mu_-}{2}$ $\qquad$ $\sqrt{c_+ c_-}$

The electrochemical interface (2

$\tilde{\mu}_e^A = \varepsilon_F^A + e\phi_A$

$\tilde{\mu}_e^C = \varepsilon_F^C - e$

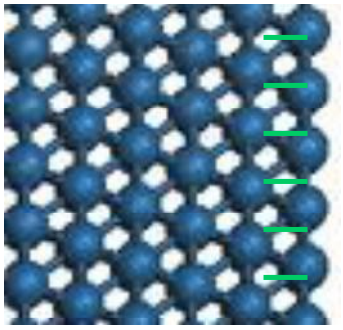

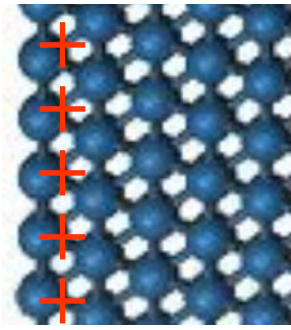

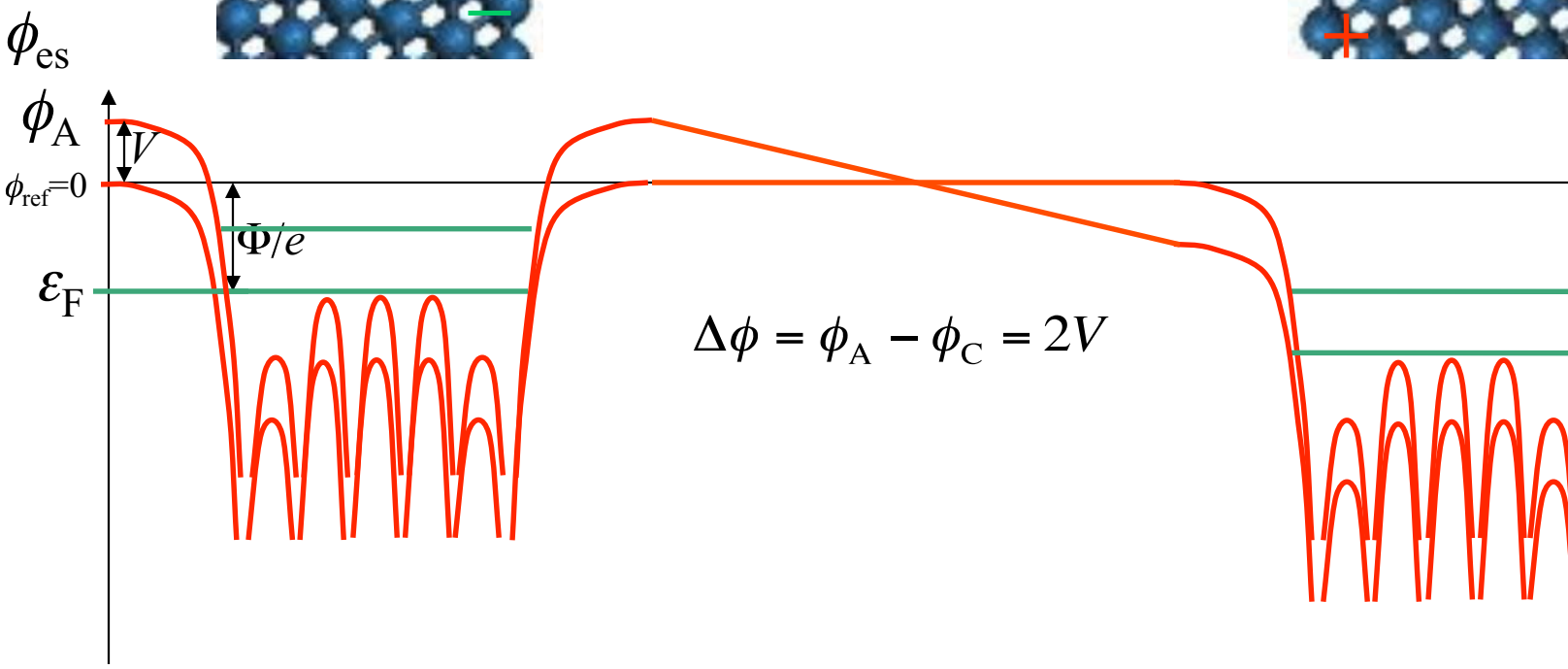

The electrochemical interface (3

$t \Rightarrow \infty$ ss (equilibrium)

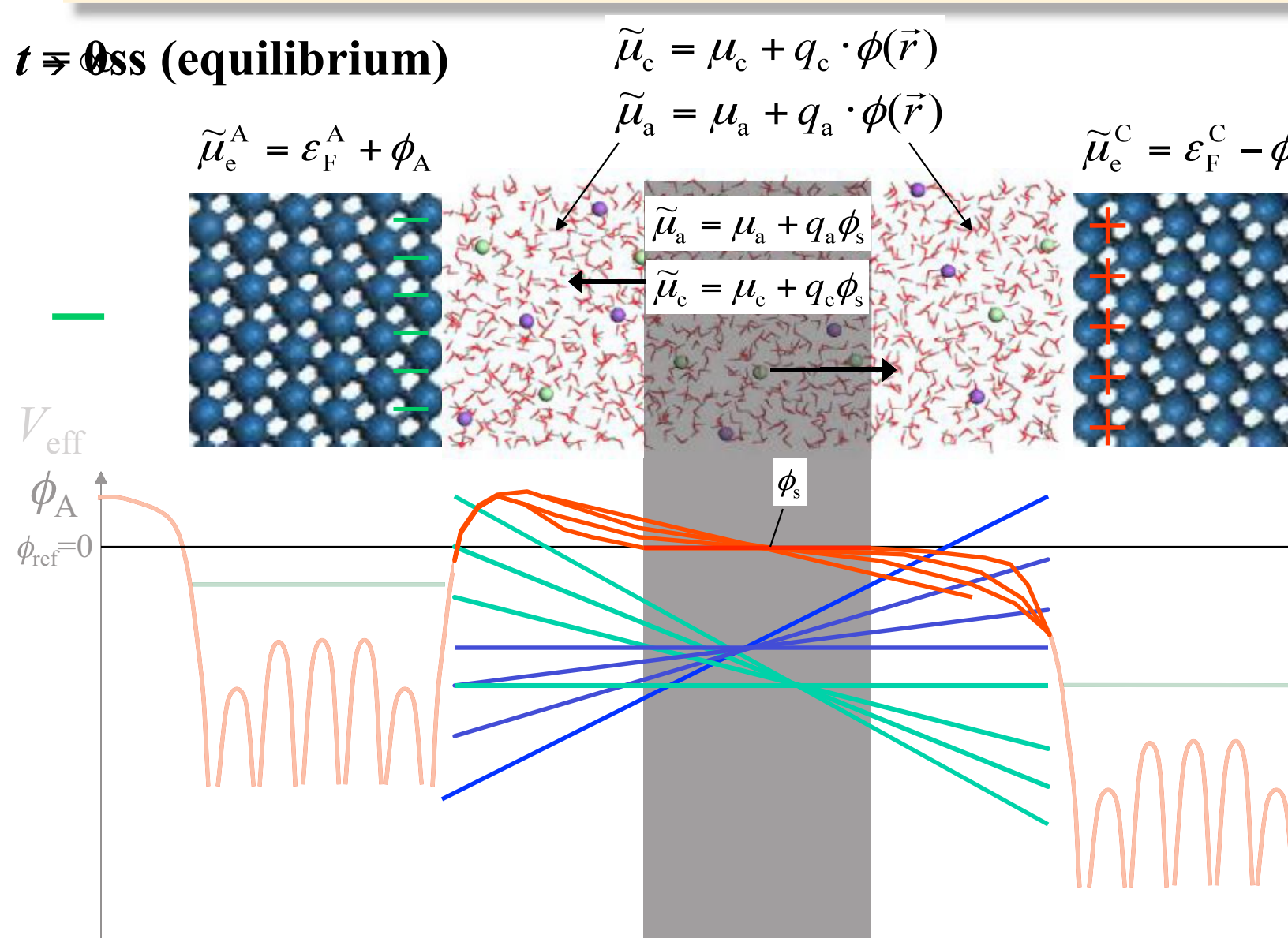

Detailed View on Double-Layer

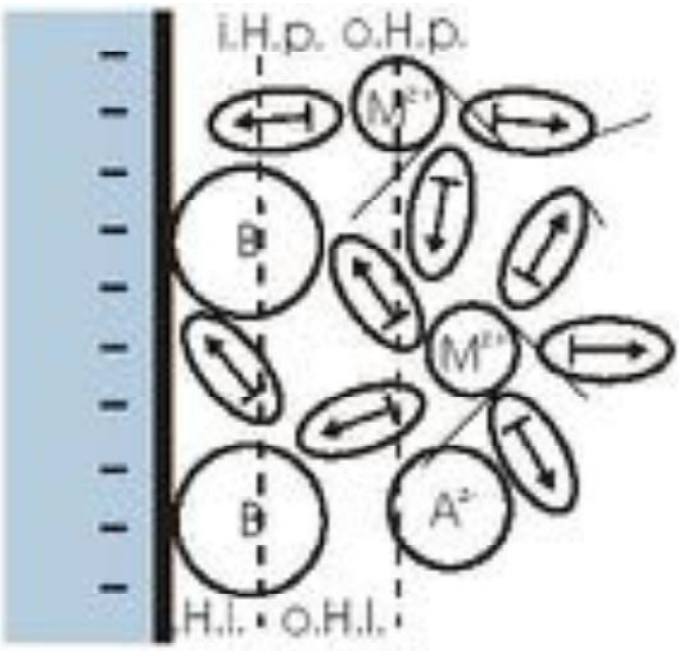

Inner Helmholtz Plane:
plane of adsorbed species (direct electrode contact)

Inner Helmholtz Layer:
Area of reactions with desolv particles

Outer Helmholtz Plane:
plane of closest possible solv particles

Outer Hemholtz Layer:
Area of redoxreaction betwe solvated particles

Condensator-model of double-layer o.H.p. model

Charge density on metal surface: $\sigma_e = q / A$

equivalent charge density in o.H.p. → electric double layer

Integral double layer capacity (relative to psz

$$C_D = \frac{q}{\varphi_e - \varphi_{pzc}}$$

Differential double layer capacity: $\tilde{C}_D = \frac{\partial q}{\partial \varphi}$

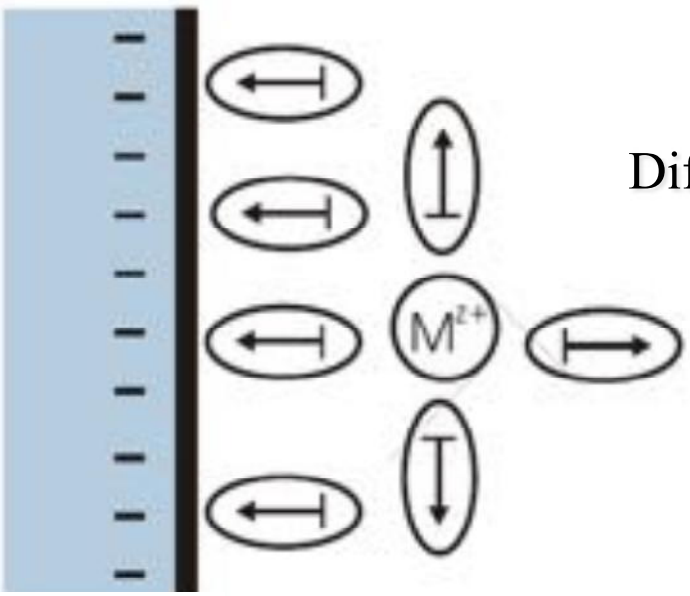

$$\frac{\partial C_D}{\partial \varphi_e} = \frac{1}{\varphi_e - \varphi_{pzc}} \cdot \frac{\partial q}{\partial \varphi_e} - \frac{q}{\left(\varphi_e - \varphi_{pzc}\right)^2}$$

$$\left(\varphi_e - \varphi_{pzc}\right)\frac{\partial C_D}{\partial \varphi_e} = \tilde{C}_D - C_D$$

$$\tilde{C}_D = C_D + \left(\varphi_e - \varphi_{pzc}\right)\frac{\partial C_D}{\partial \varphi_e}$$

Measurement of differential capacity with DC methods, electrocapillar-ex

Models for the Electric Double-Laye

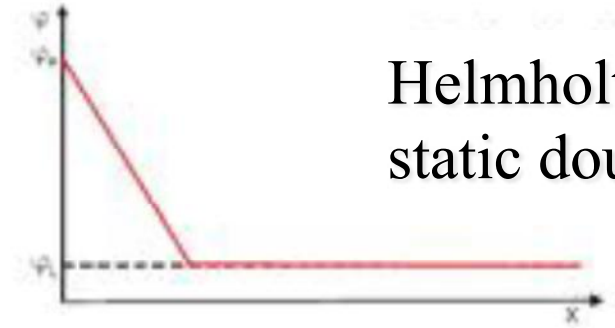

Helmholtz (1853) static double layer

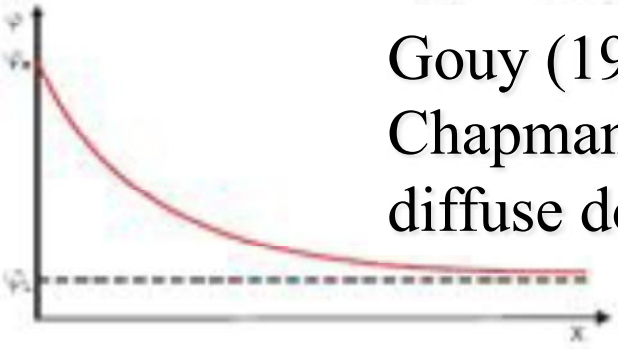

Gouy (1910) and Chapman (1913) diffuse double layer

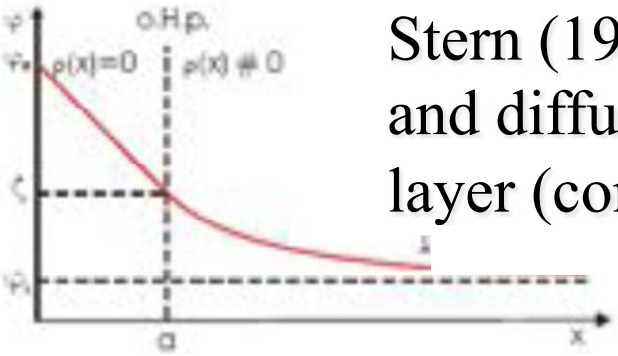

Stern (1924) static and diffuse double layer (combination)

New model also include:

- Specific adsorption at elec
- Ion-metal, molecule-meta interaction and catalytic e
- Structure of conduction ba
- Overlap between valence conduction band at phase b
- Dielectric filling of double
- Deformation of conductio

Motivation: Electrochemical Interfa

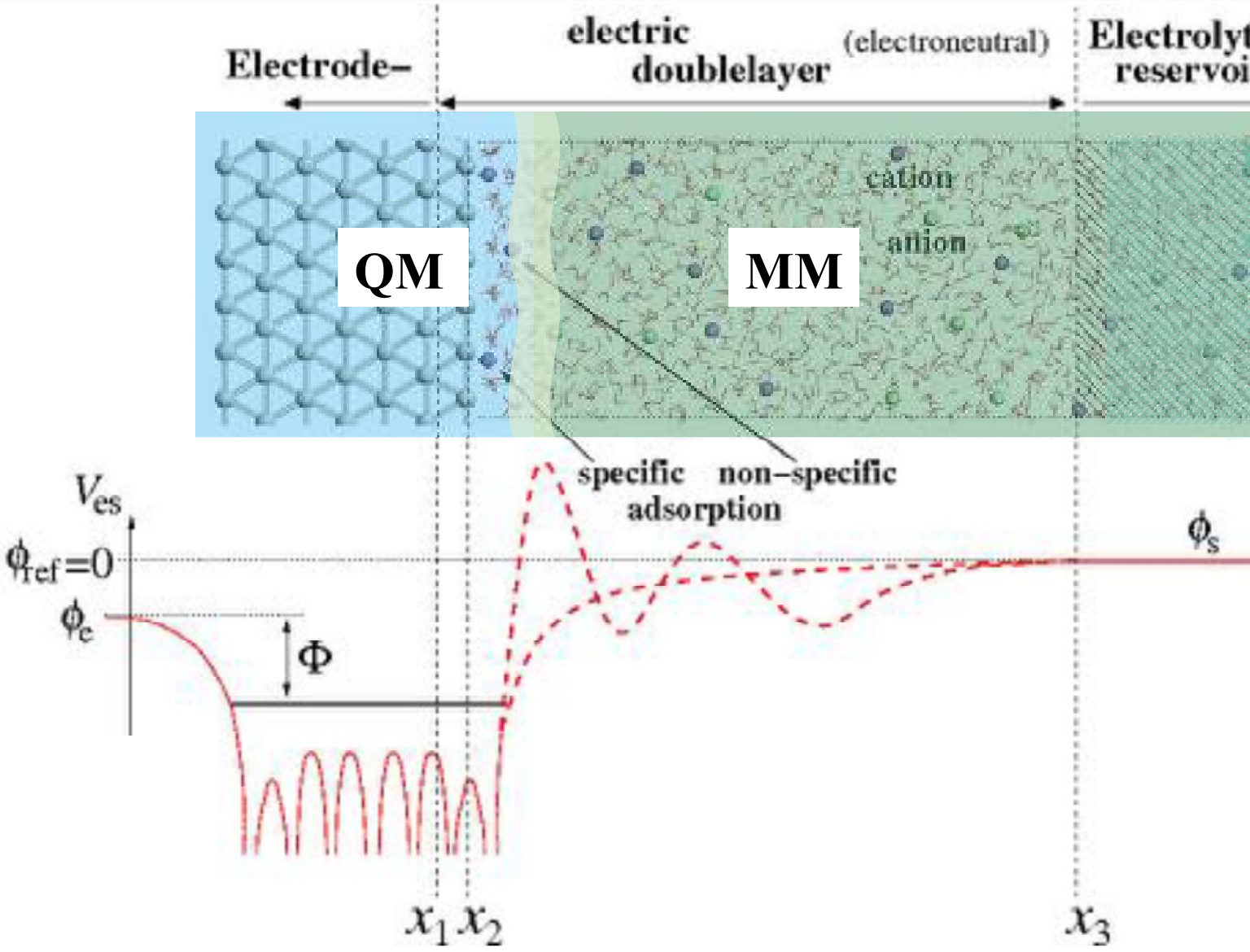

Solid/Liquid Interface

Electrode: Pt(110)

Electrolyte: 1M NaCl

T=300 K (Berendsen Thermostat)

p= 1atm.

duration: 2ns

FF: Water (F3C)
Na^+/Cl^- (OPLS)
Pt (own)

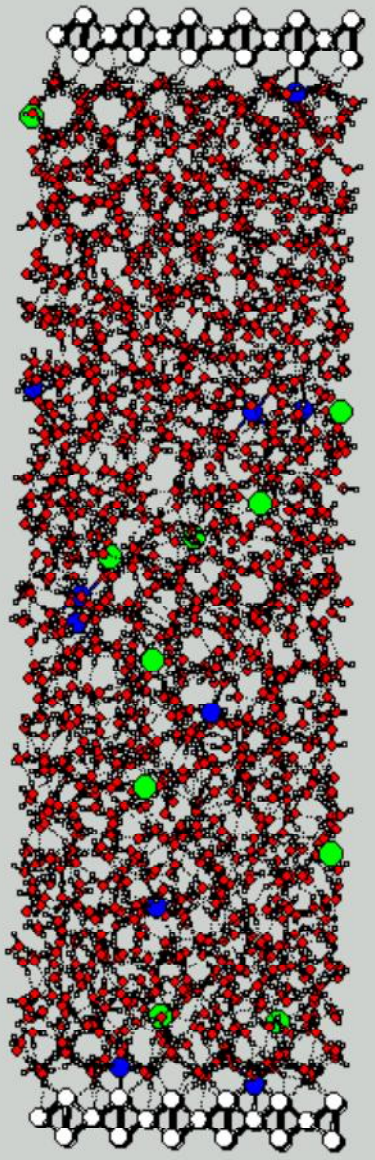

Electrode/Electrolyte Interface

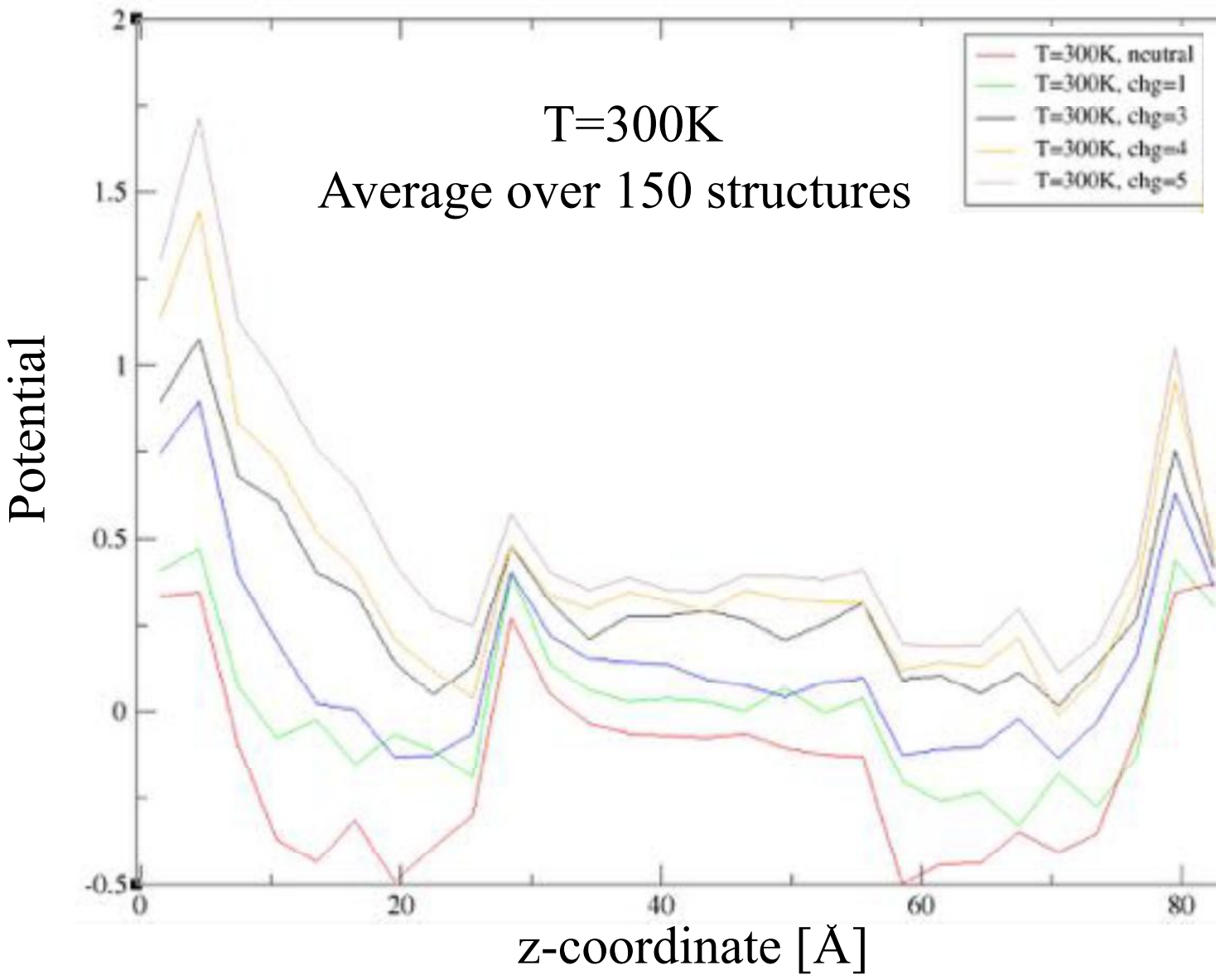

Sulfate-Adsorption on Au(111)

in situ STM/FTIRS

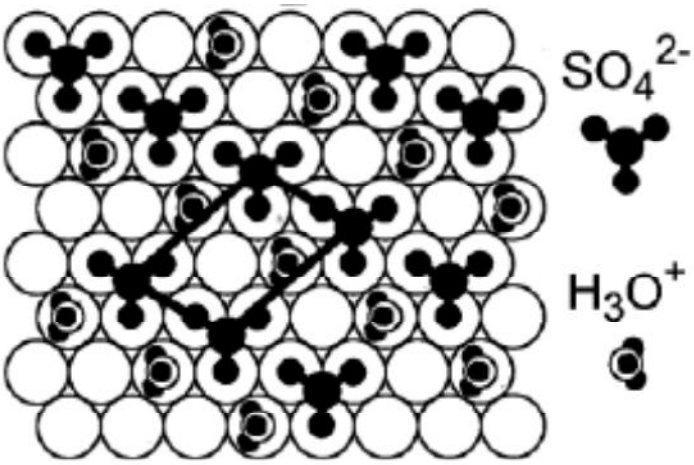

G.J. Edens, X. Gao and M.J. Weaver,
J. Electroanal. Chem., *467*, 291, 1999.

in situ STM

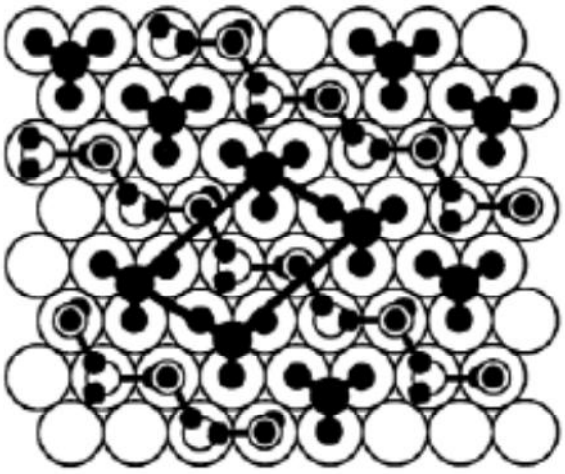

L.-J. Wan, S.-L. Yau and K. Itaya
J. Phys. Chem., *99*, 9507, 1995

in situ STM

A. Cuesta, M. Kleinert and D.M. Kolb,
Phys. Chem. Chem. Phys., *2*, 5684, 2000.

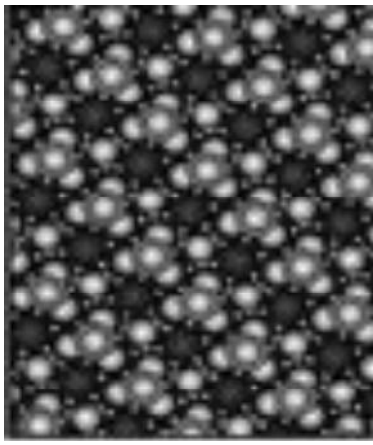

- (Bi)sulfate with H_3O^+ – Magnussen *et al.*, Shingaya and Ito
- Bisulfate with water – Uchida *et al.*

Sulfate-Adsorption on Au(111)

Sulfate

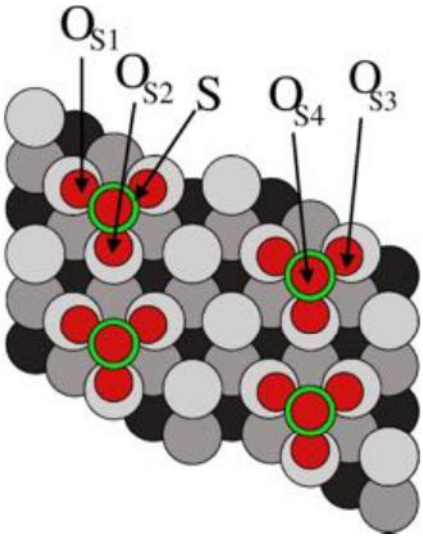

E_{bind}=2.41 eV

Sulfate+ H_2O

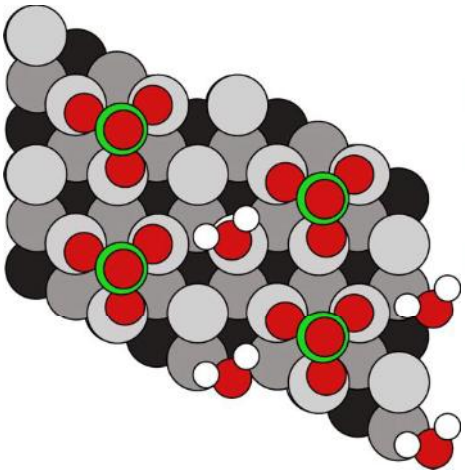

E_{bind}=3.35 eV

Sulfate+ 2 H_2O

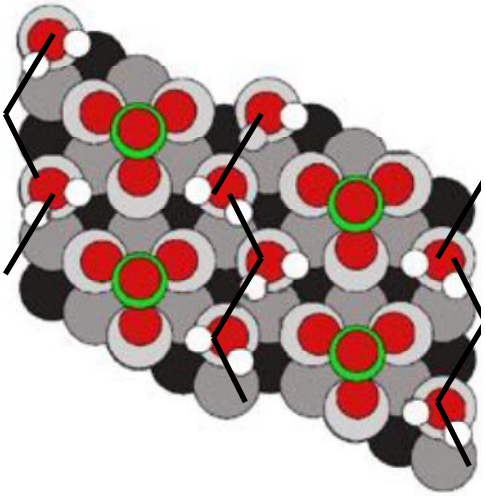

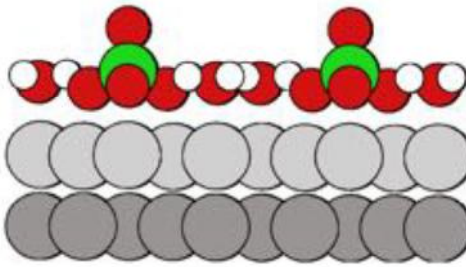

E_{bind}=4.47 eV

Sulfa

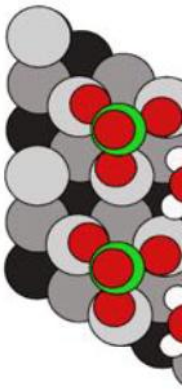

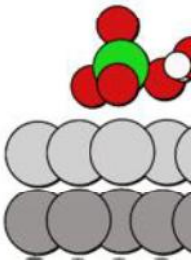

E_{bin}

Sulfate-Adsorption on Au(111

Sulfate +H_3O^++H_2O

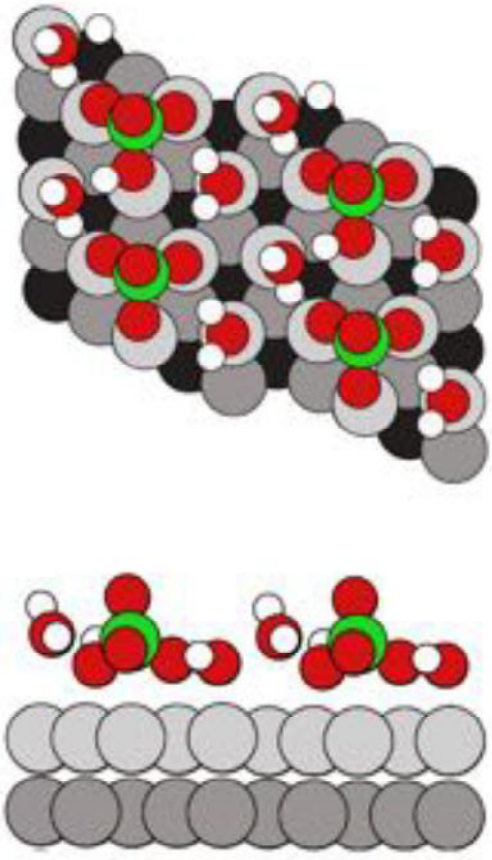

E_{bind}=8.53 eV

Bisulfate - H coordinated to O_{S4}

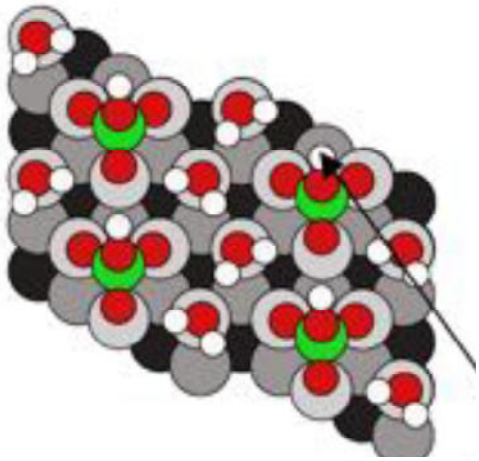

E_{bind}=8.72 eV

Summarizing

System
sulfate
+ 1 water
+ 2 water
+ hydronium
bilsulfate + 2 water (a)
bilsulfate + 2 water (b)

S. Venkatachalam, T. Jacob, *Z. Phys. Chem.* 221, 1393 (2007).

Adsorption of Sulfate + H_3O^+ on Au(1

Positive charge

Negative charge

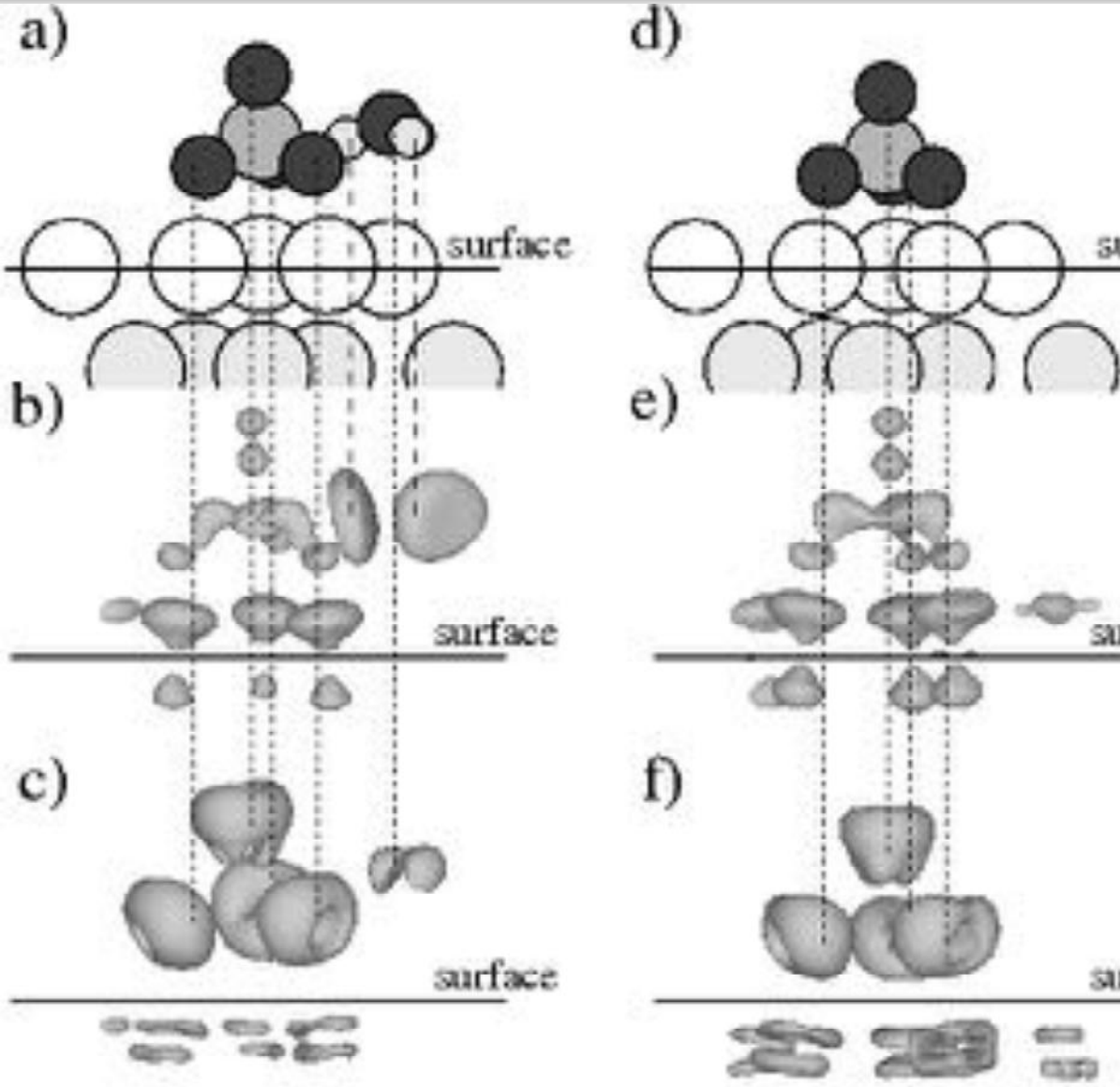

Double-Layer Structure

STM image of Au(111) in 0.1M H_2SO_4 at 850 mV (vs. SCE)

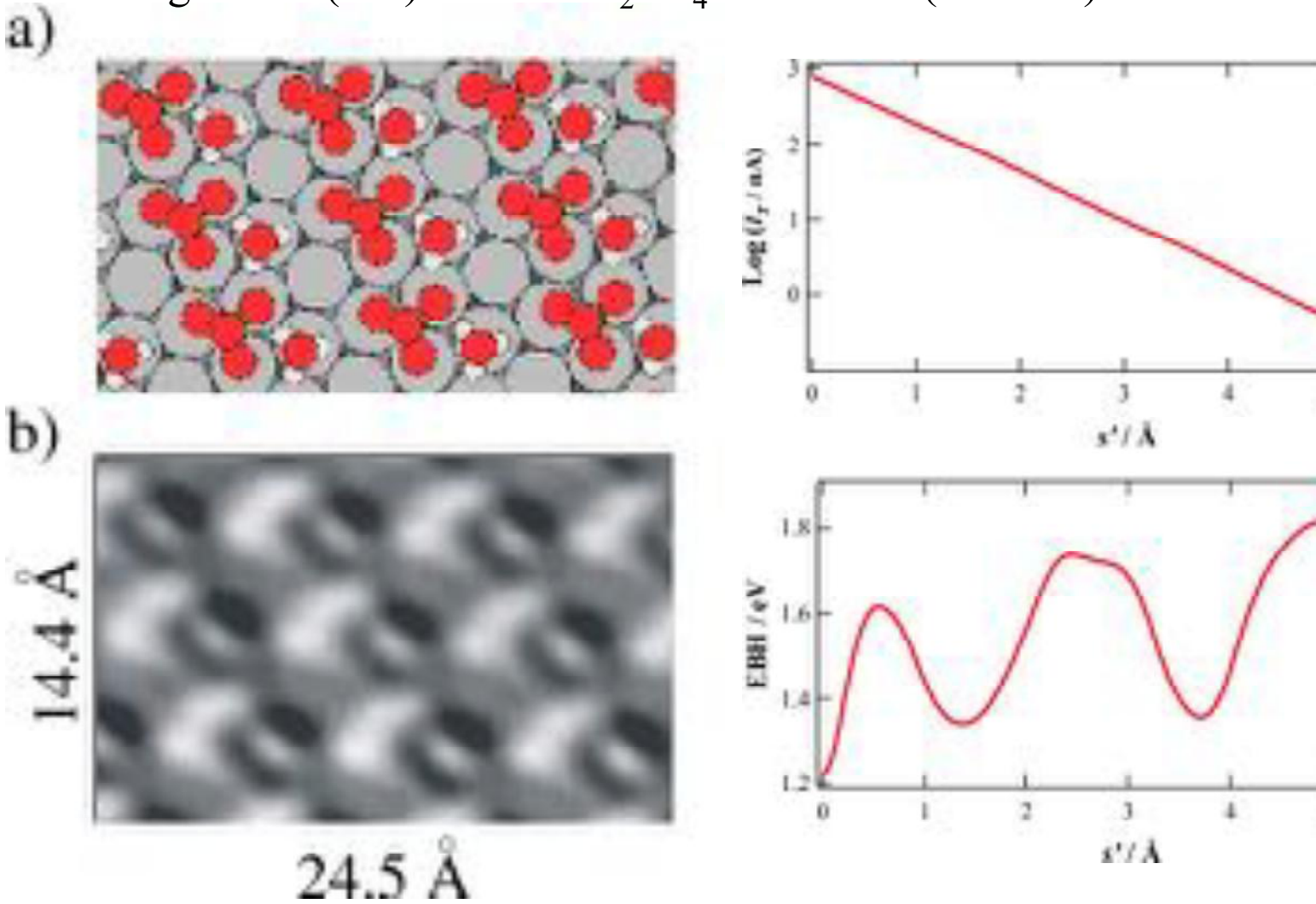

S. Venkatachalam, F. Simeone, D. M. Kolb, T. Jacob, *Angew. Chem. Int. Ed.*, 46, 8903 (2007).

Double-Layer Structure

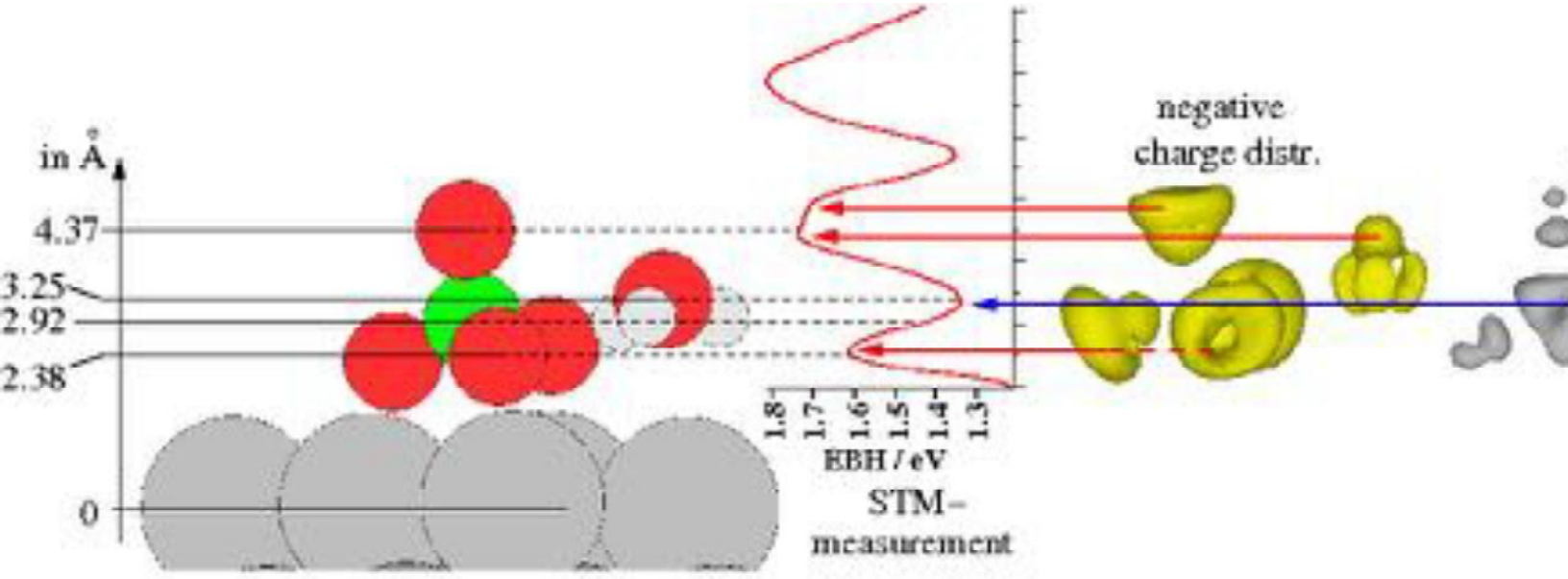

S. Venkatachalam, F. Simeone, D. M. Kolb, T. Jacob, *Angew. Chem. Int. Ed.*, 46, 8903 (2007).

STM-Measurements at different potent

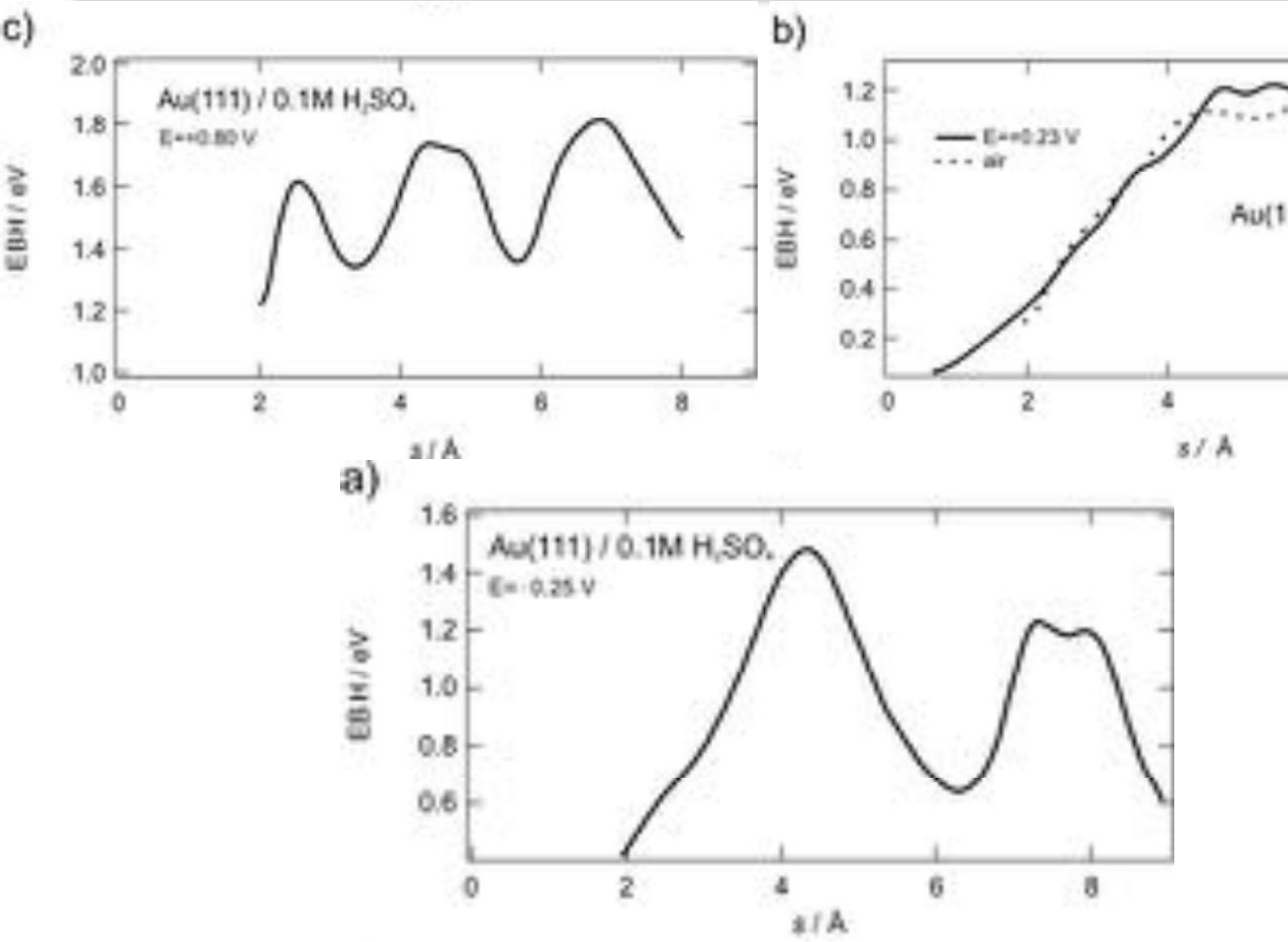

Hexagonal ice–like water bilayer at E<E

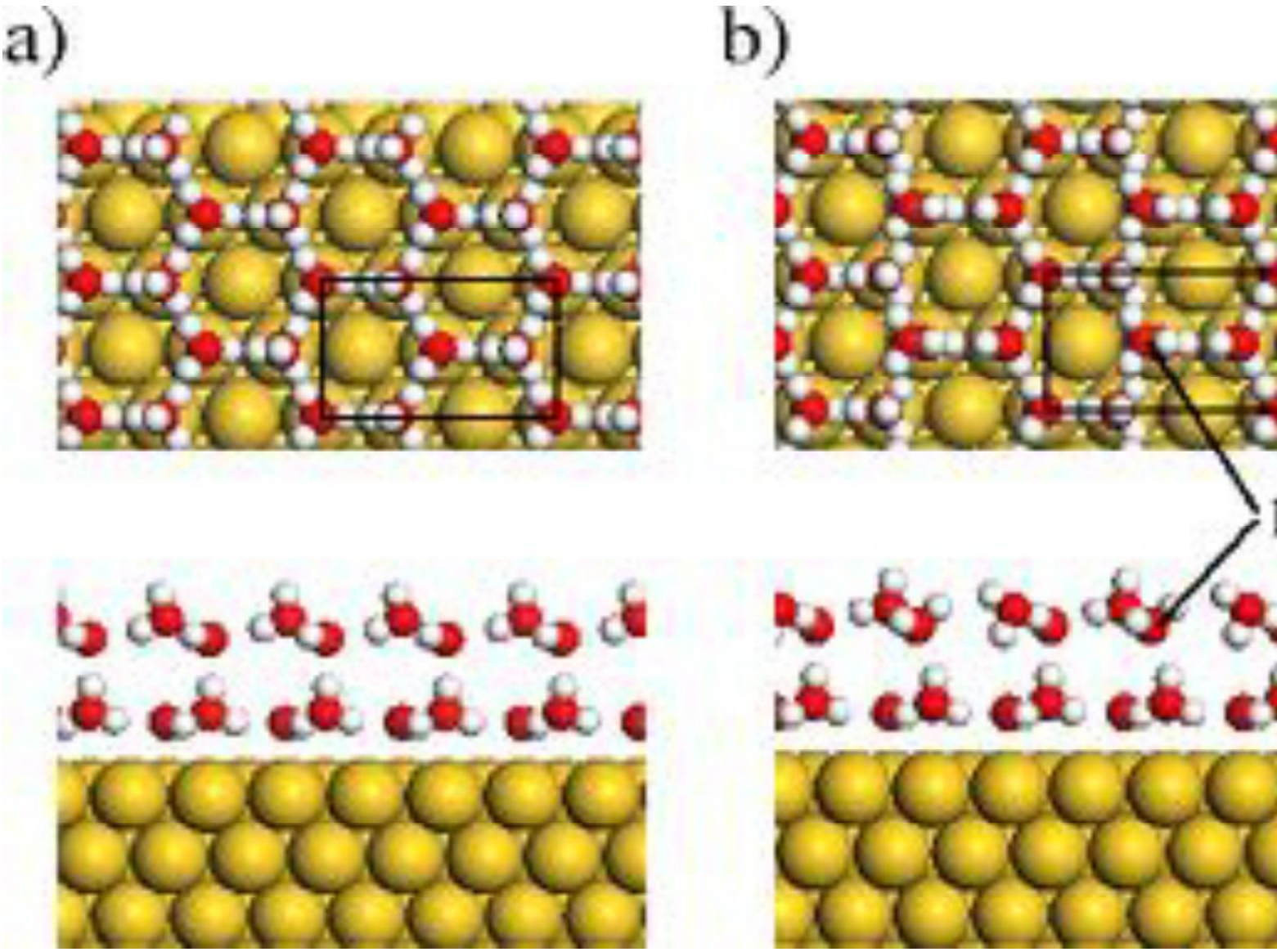

Comparison with STM-measureme

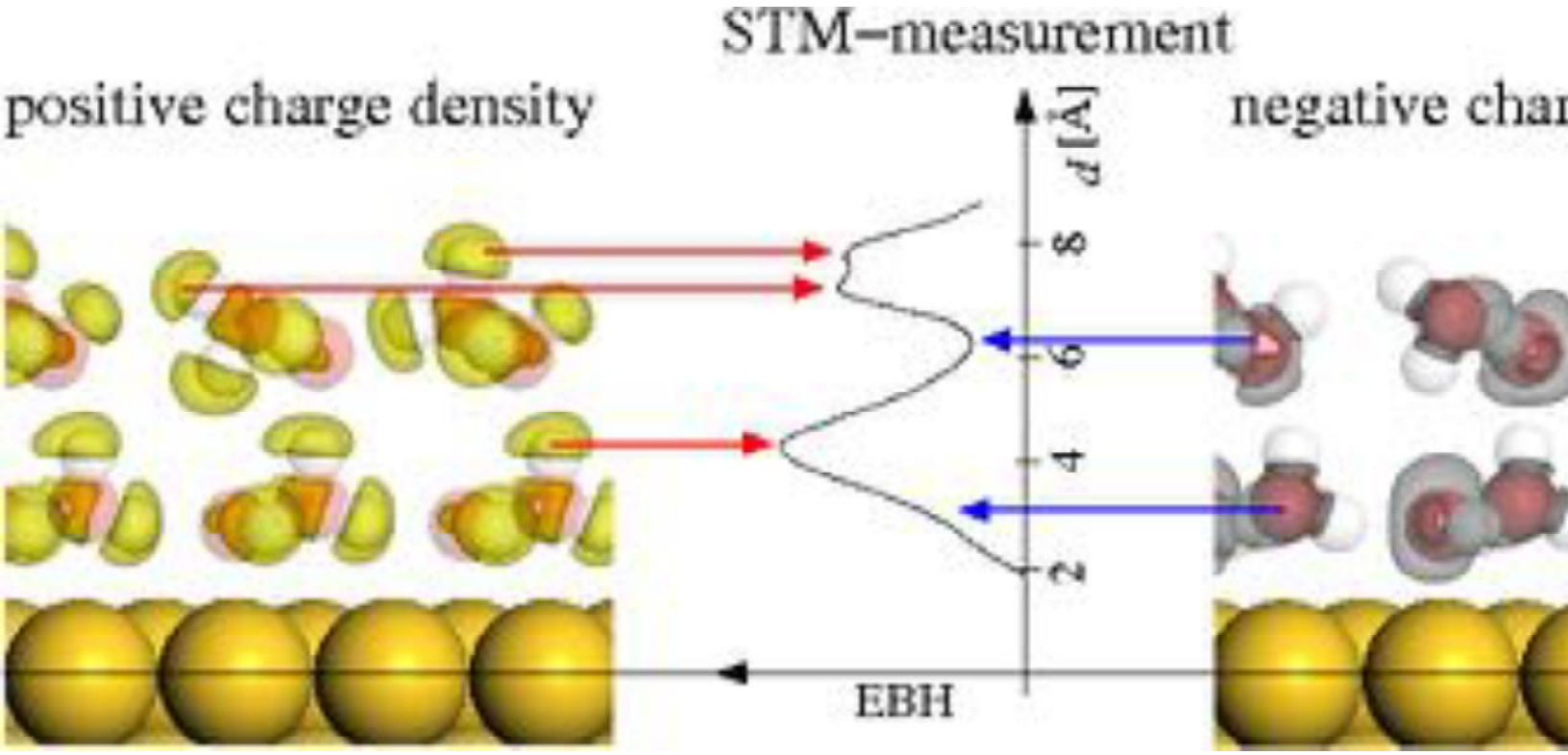

F. C. Simeone and D.M. Kolb, S. Venkatachalam and T. Jacob, *Surf. Sci.*, **7**, 1401 (2008).

Electrocatalysis:
Oxygen Reduction Reaction on Pt

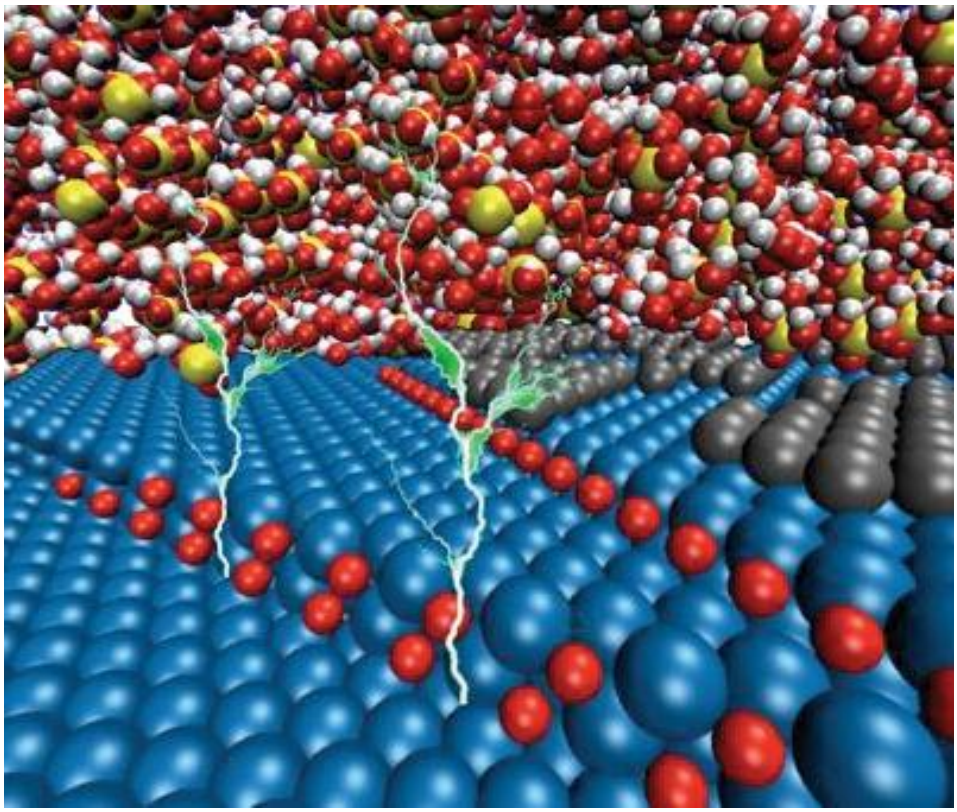

ORR on Pt

What is known about the ORR?

The first electron transfer is rate determinin

$$O_2^* + e^- \rightarrow O_2^{*-}$$

$$O_2^* + H^+ + e^- \rightarrow OOH^*$$

Damjanovic, A.; Genshaw, M. A.; Bockris, J. O. M.

J. Phys. Chem. 1964, 45

ORR on Pt

Google search:
"Damjanovic Genshaw Bockris 4057"

Damjanovic, A.; Genshaw, M. A.; Bockris, J. O. M.
J. Phys. Chem. 1964, 45, 4

A. Damjanovic, M. A. Genshaw and J. O'M. Bockris,
J. Chem. Phys. 45 (1964)

A. Damjanovic, M. A. Genshaw, and J. O'M. Bockris,
J. Chem. Phys., 45, 4057 (

Damjanovic A., Genshaw M.A., Bockris J.O'M.,
J. Phys. Chem. 1996. V. 45. P.

Damjanovic, A.; Genshaw, M. A.; Bockris, J. O. M.
J. Phys. Chem. 2001, 45,

ORR on Pt

A. Damjanovic, M. A. Genshaw, and J. O'M. Bockris,
J. Chem. Phys., 45, 4057

→ doesn't discuss the ORR explicitly

→ describes how to interpret electrochemical kin
experiments with different reaction pathways

A. Damjanovic and V. Brusic,
***Electrochim. Acta* 1967, 12, 615**

explicitly argues for: $O_2^* + H^+ + e^- \rightarrow OOH^*$

and against: $O_2^* + e^- \rightarrow O_2^{*-}$

Theoretical Studies

Surface science experiments of O_2 on Pt(111)

Table 1. Experimental O_2 binding energies to Pt(111)

Author	Experiment	Binding energy
Gland (1980)	TDS	0.3 eV
Steininger et al. (1982)	EELS	ca. 0.5 eV
Parker et al. (1989)	TPD	0.38 eV

STM experiments: Stipe et al. (1997)
O_2 binding at bridge site is preferred
O_2 dissociates to $2O^*$ via fcc site

Comparison to literature

Modern calculated binding energies of O_2 to Pt(111), ΔE values in (eV)

Author	Method / xc-functional	Basis set / PP	Model	Model geometry	Coverage (ML)	Binding site	ΔE (gas)
Eichler, Hafner (1997) Eichler, et al. (2000)	SP-PW91	US (300 eV)	4 layers	a = 3.98Å	1/4	bridge fcc hcp	0.72 0.68 0.58
Bocquet, et al (1999)	SP-PW91	US (400 eV)	4 layers	a = 3.98Å	1/4	bridge fcc hcp	0.53 0.47 0.40
			2 + 2 layers			bridge fcc hcp	0.64 0.46 0.65
Anderson, Albu (2000)	MP2	LANL2DZ 6-31G*	Pt, (5 + 0)	t-shaped bent	Low	—	[illegible]
Li, Balbuena (2001)	(U)-B3PW91	LANL2DZ 6-311G	[illegible]	linear rhombus bipyramid square-pyramid	Low	bridge	0.72 0.72 [illegible] [illegible]
Sidik, Anderson (2002)	B3LYP	LANL2DZ 6-31G*	Pt, (5 + 0)	linear	Low	bridge and-on	0.98 0.43
Šljivančanin, Hammer (2002)	PW91	US (340 eV)	2 + 2 layers	a = 4.02Å	1/9	bridge fcc	0.8 0.8
	RPBE					bridge fcc	0.1 0.1
Balbuena, et al (2003)	(U)-B3PW91	LANL2DZ 6-31G	[illegible]	linear triangle	Low	bridge	1.62 1.08
Panchenko, et al. (2004)	PW91	PAW (400 eV)	3 + 1z layers	d = 2.82Å	not explained	bridge fcc hcp	0.63 0.52 0.46
Xu et al. (2004)	SP-PW91	US (340 eV)	2 + 2 layers	a = 4.00Å	1/4	bridge fcc hcp	0.62 0.62 0.45

Comparison to literature

Okamoto (2006)	SP-PBE	US (340 eV)	2 + 4 layers	a = 3.96Å	1/4	bridge	0.72
			Pt_{13}	Icosahedral	Line	bridge	1.74
Roques Anderson (2005)	SP-PW91	US (400 eV)	2 + 2 layers	a = 3.99Å	1/4	bridge fcc hcp	0.88 0.67 0.53
Hyman Medlin (2006)	SP-PW91	PAW (400 eV)	5 layers	a = 3.99Å	1/5	fcc	0.88
Jacob (2006)	PW91 PP	LACV3P [illegible]	Pt_{13} [illegible]	d = 2.78Å (4 atoms [illegible])	Line	bridge fcc	0.69 0.71
Liu, Hsu et al. (2006)	SP-PW91	PAW (290 eV)	2 + 2 layers	a = 3.99Å	1/4	bridge fcc	0.72 0.68
Qi et al. (2006)	SP-PBE	PAW (400 eV)	2 + 2 layers	a = 3.98Å	1/4	bridge fcc hcp	0.65 0.53 0.43
Jinnouchi Anderson (2008)	SP-PBE	NC	1 + 2 layers	a = 4.00Å	1/4	bridge	0.80
	SP-RPBE			a = 4.03Å		bridge	0.38
Walch et al (2008)	B3LYP	LANL2DZ (+1f) / 6-31G*	[illegible]	d = 2.77Å	Line	bridge	1.34 1.42 1.67 1.95
Wasileski Janik (2008)	SP-PW91	PAW (400 eV)	2 + 2 + 2 layers	(calculated lattice)	1/9	bridge	0.84
[illegible] et al (2009)	SP-PW91	PAW (400 eV)	1 + 3 layers	a = 3.99Å	1/16	bridge	−0.75
Ou et al (2008)	SP-PBE	US (408 eV)	2 + 1 layers	a = 3.92Å	1/4	bridge fcc hcp [illegible]	0.65 0.62 0.34 [illegible]
[illegible] et al (2009)	SP-PW91	PAW (400 eV)	Pt_n		Line		$\Delta E_{[illegible]}$ 1.82
Sha et al (2010)	PBE	NC	2 + 4 layers	a = 3.98Å	1/4	bridge fcc hcp	0.61 0.48 0.36

Considered pathways

Determine the actual ORR mechanism dependent on *T, p, U*

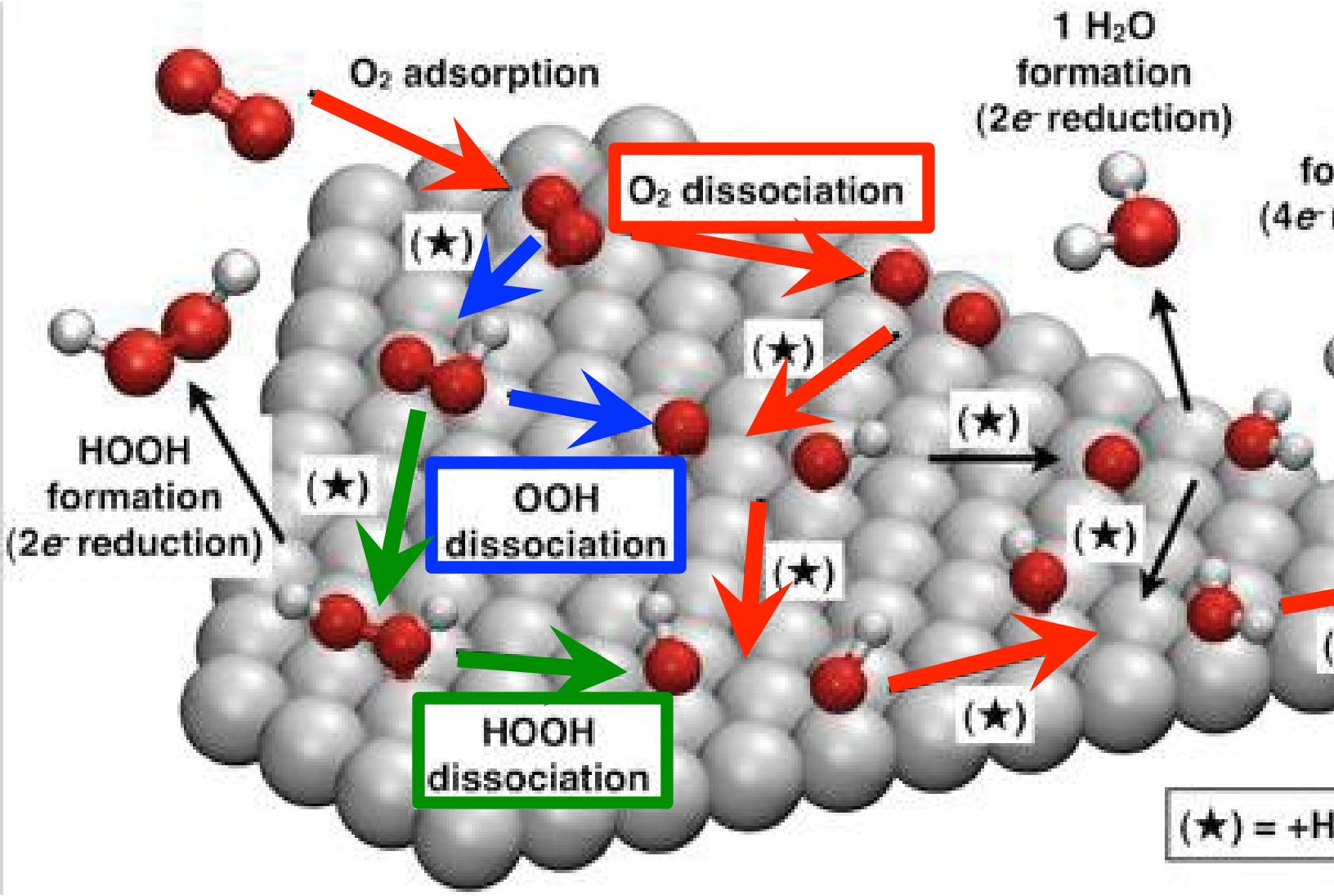

Energy Contributions

Gas-phase: $\Delta G := \Delta E^{\mathrm{DFT}}$

Water: $\Delta G := \Delta E^{\mathrm{DFT}} + \Delta E^{\mathrm{solv.}} + \Delta E^{\mathrm{ZPE}}$

Langmuir–Hinshelwood-type

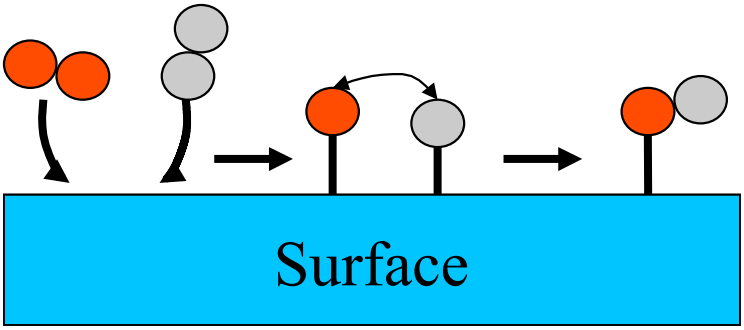

Eley–Ridea

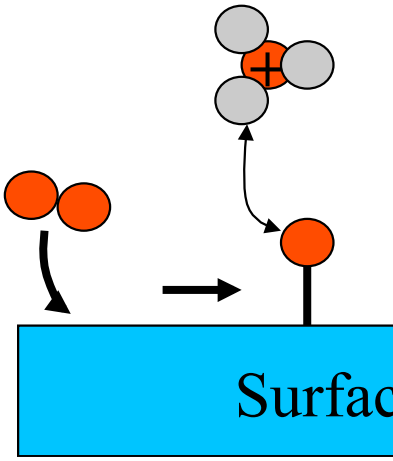

Ambient Conditions:

$$\Delta G_{298} = \Delta E^{\mathrm{DFT}} + \Delta E^{\mathrm{solv.}} + \Delta E^{\mathrm{ZPE}} + \Delta H^{\mathrm{vib.}} - T$$

O_2-Dissociation Mechanism (Eley-Rideal + Langmuir Hinshelwood)

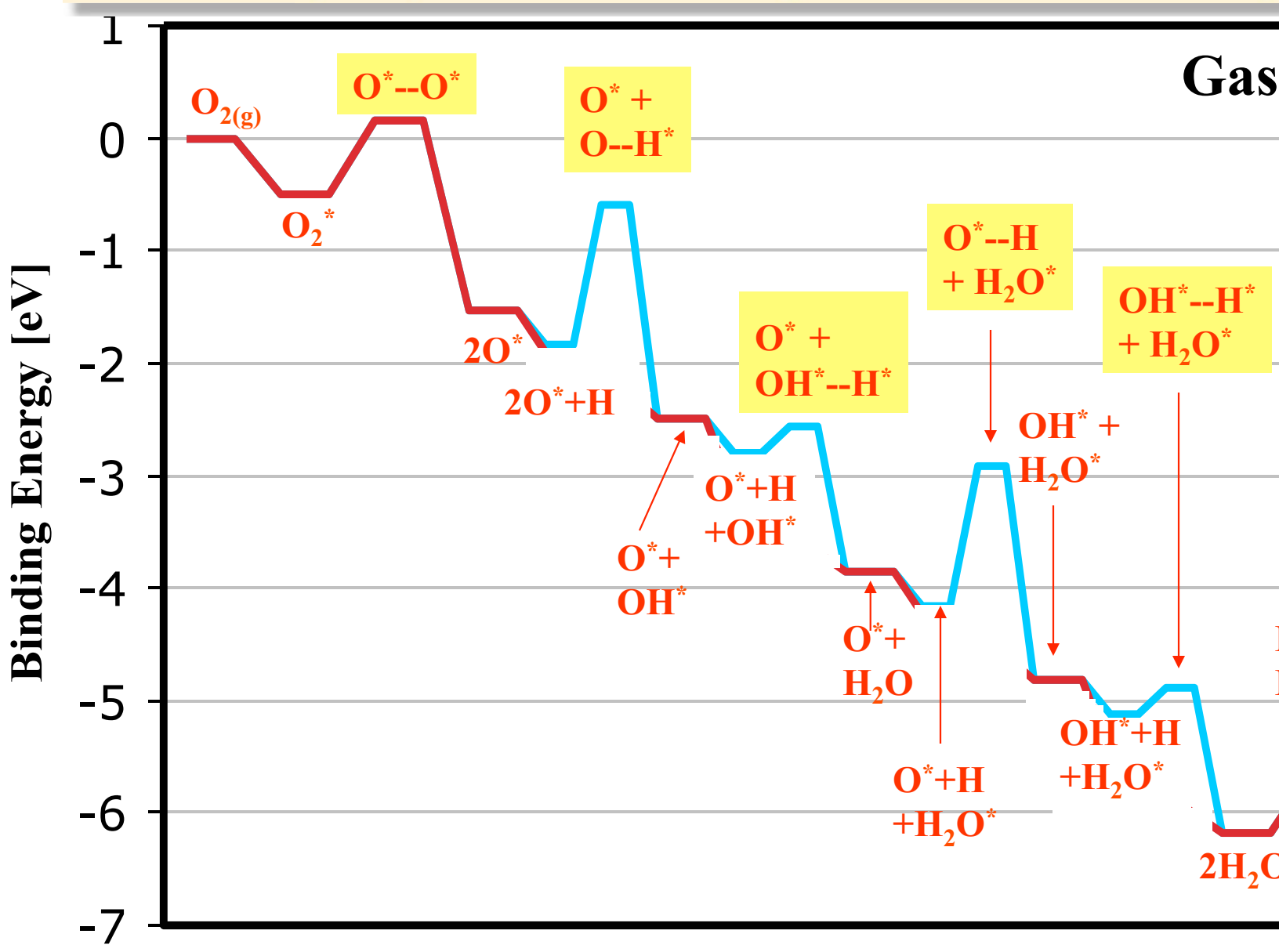

O_2-Dissociation Mechanism (Eley-Rideal + Langmuir Hinshelwood)

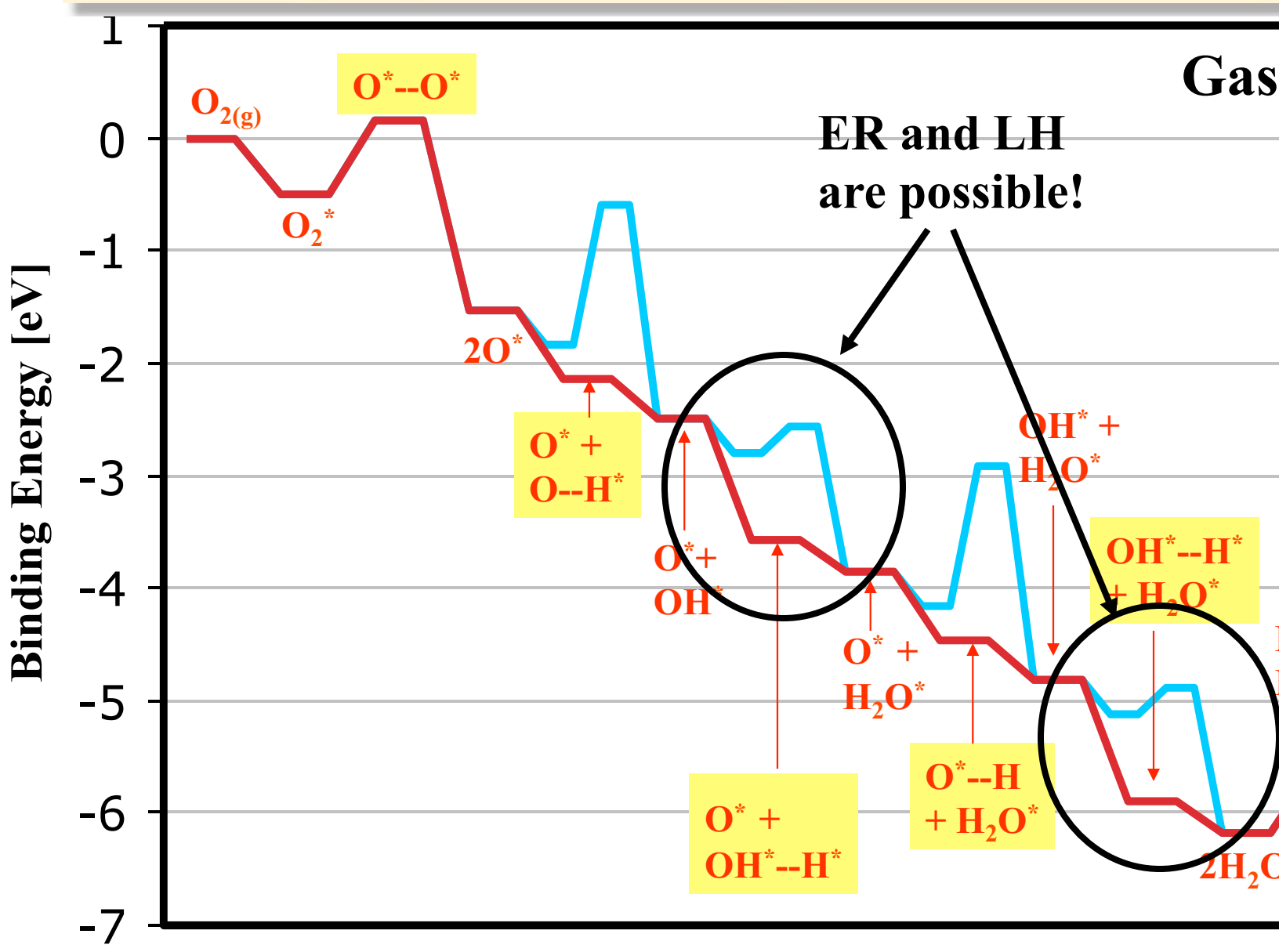

O_2-Dissociation Mechanism (Eley-Rideal + Langmuir Hinshelwood)

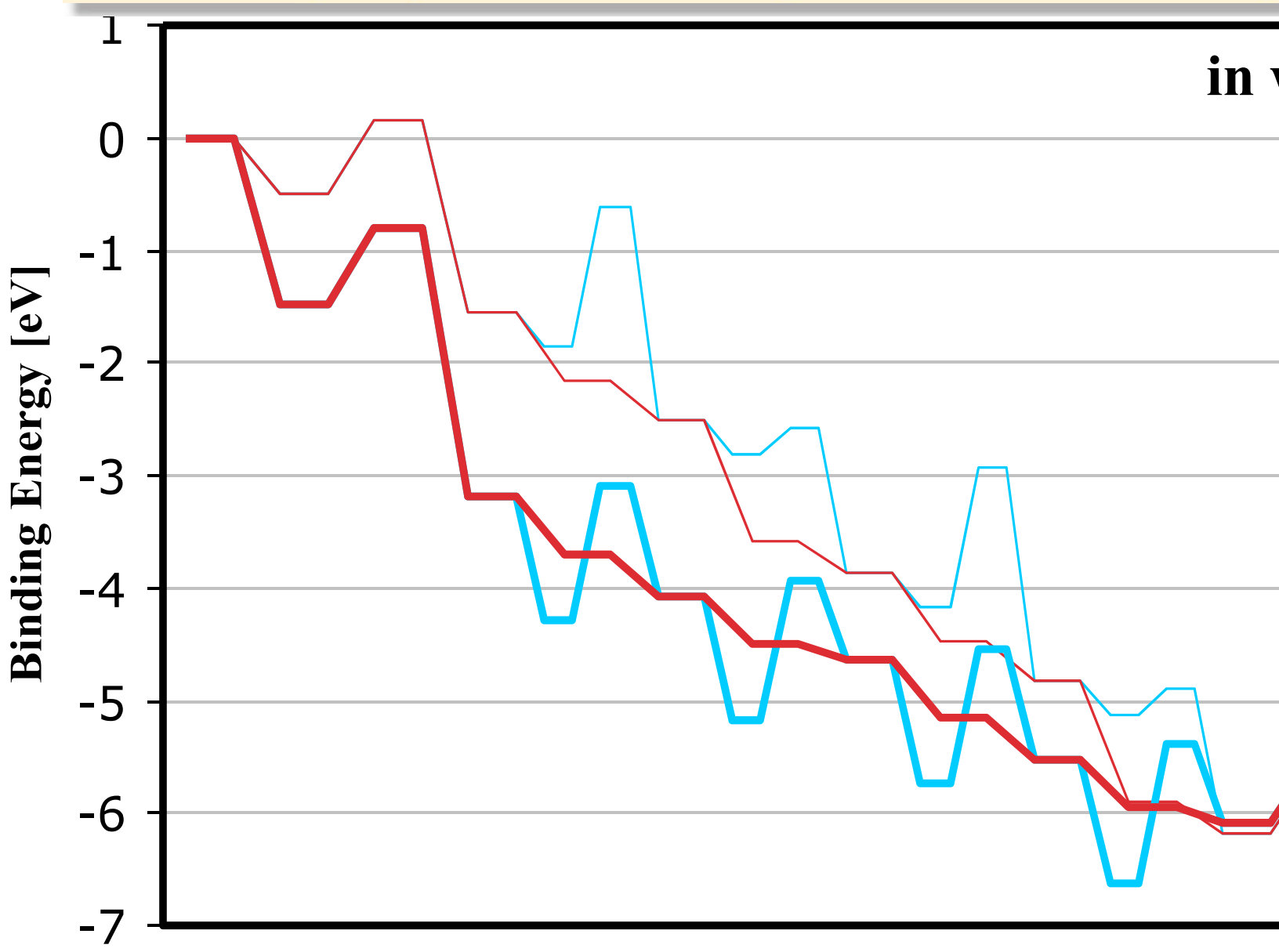

O_2-Dissociation Mechanism (Eley-Rideal + Langmuir Hinshelwood)

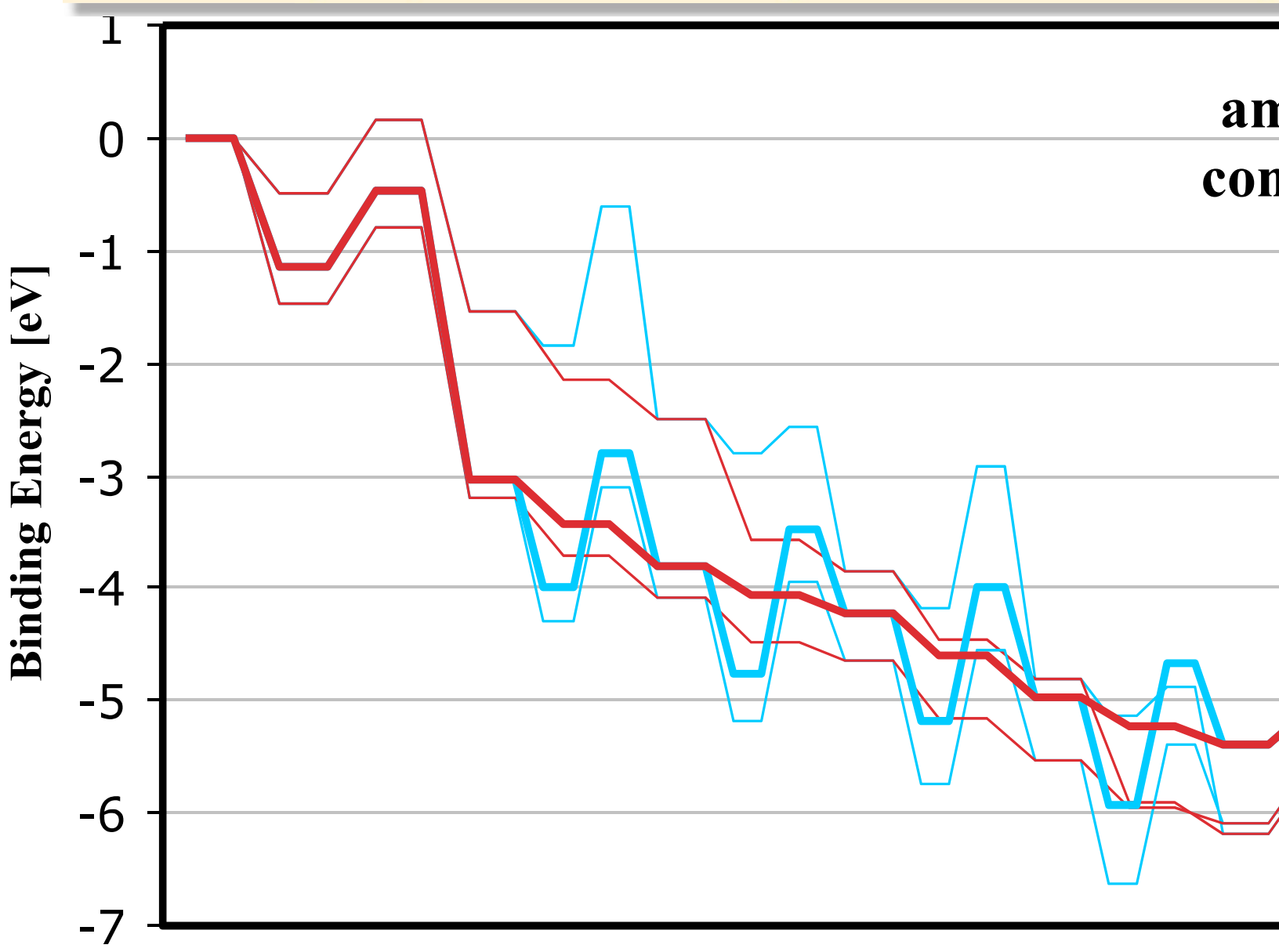

O_2-Dissociation Mechanism (Eley-Rideal + Langmuir Hinshelwood)

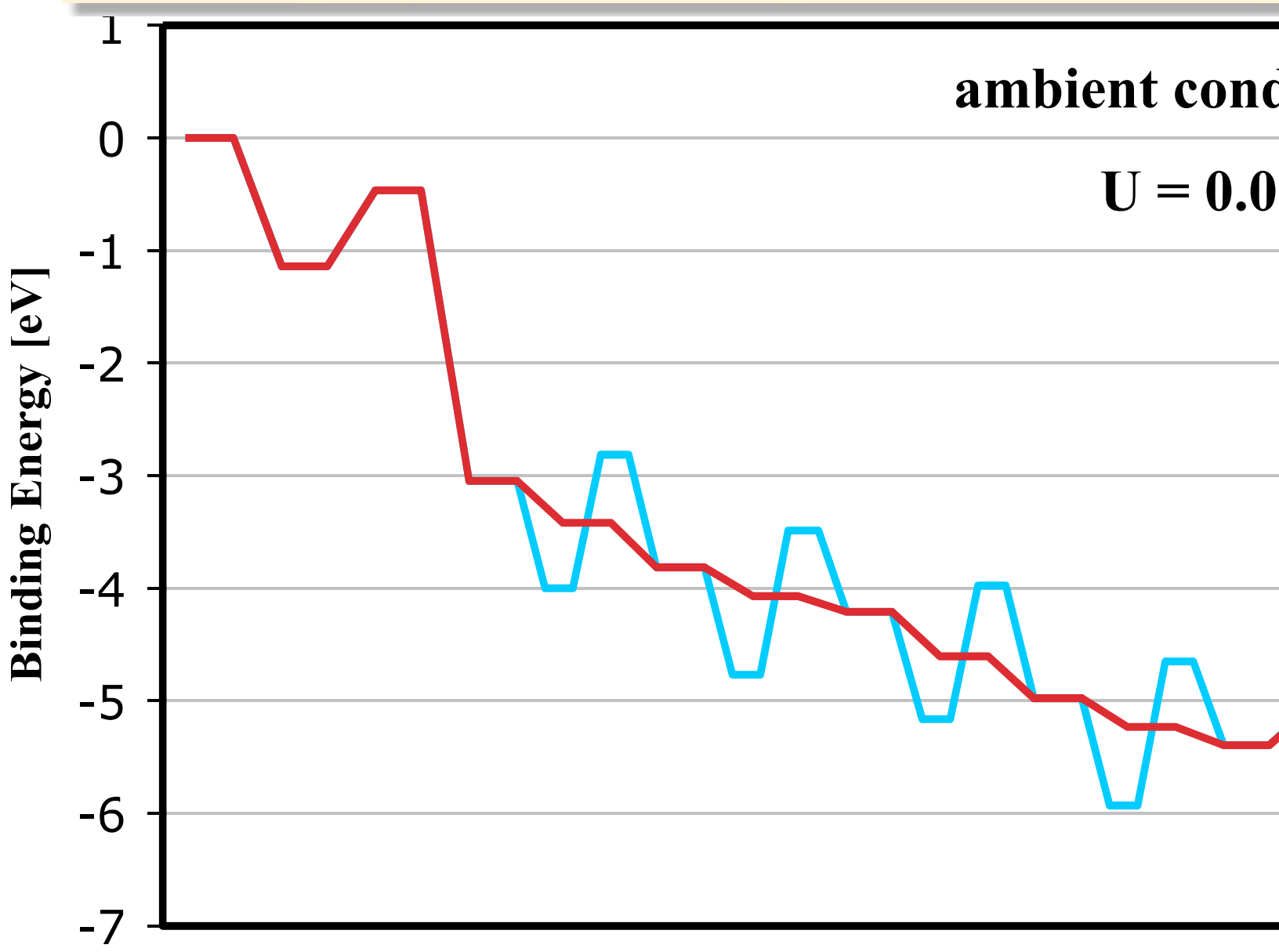

O_2-Dissociation Mechanism (Eley-Rideal + Langmuir Hinshelwood)

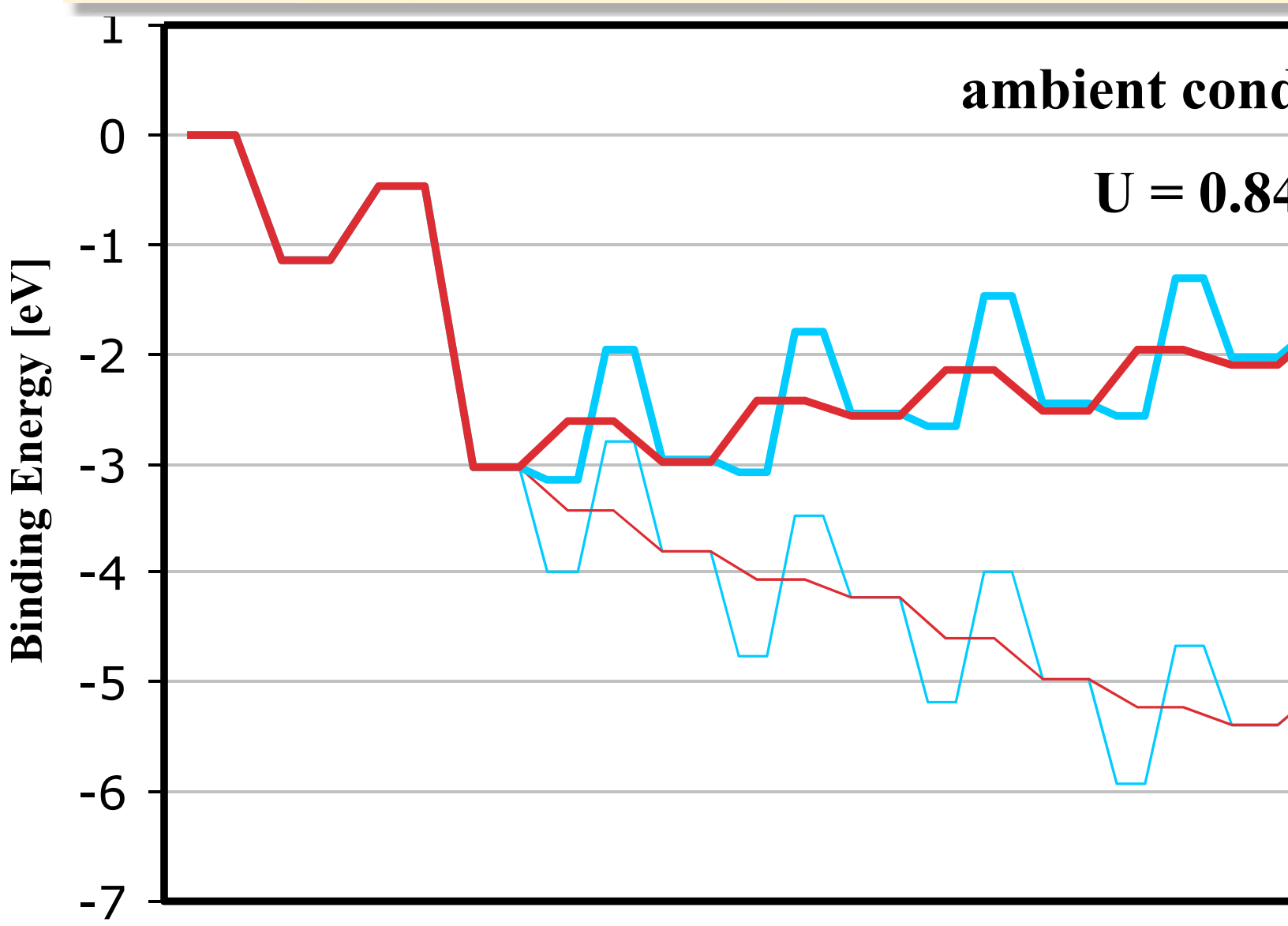

O_2-Dissociation Mechanism (Eley-Rideal + Langmuir Hinshelwood)

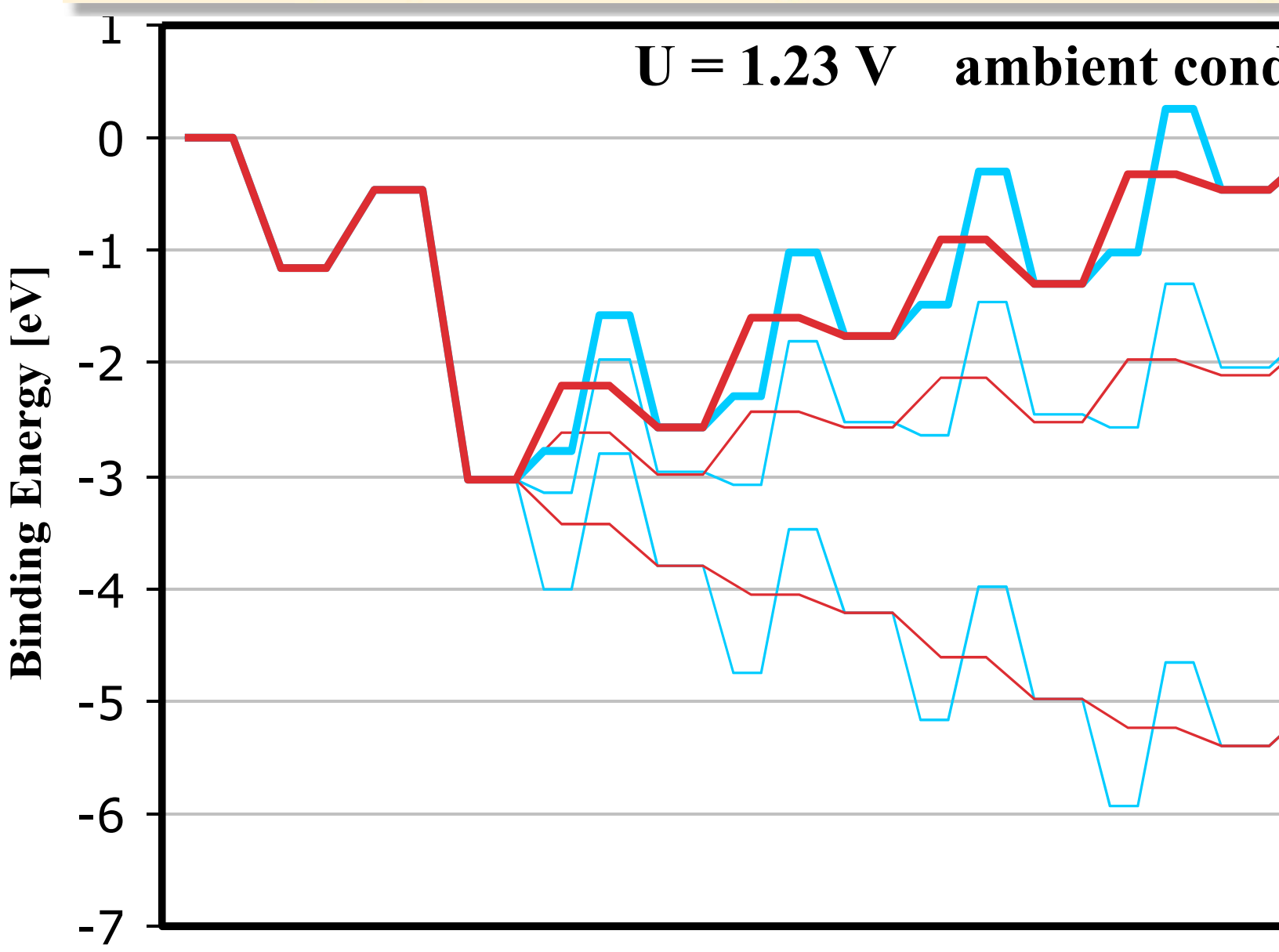

All Mechanisms
(Eley-Rideal + Langmuir-Hinshelwood)

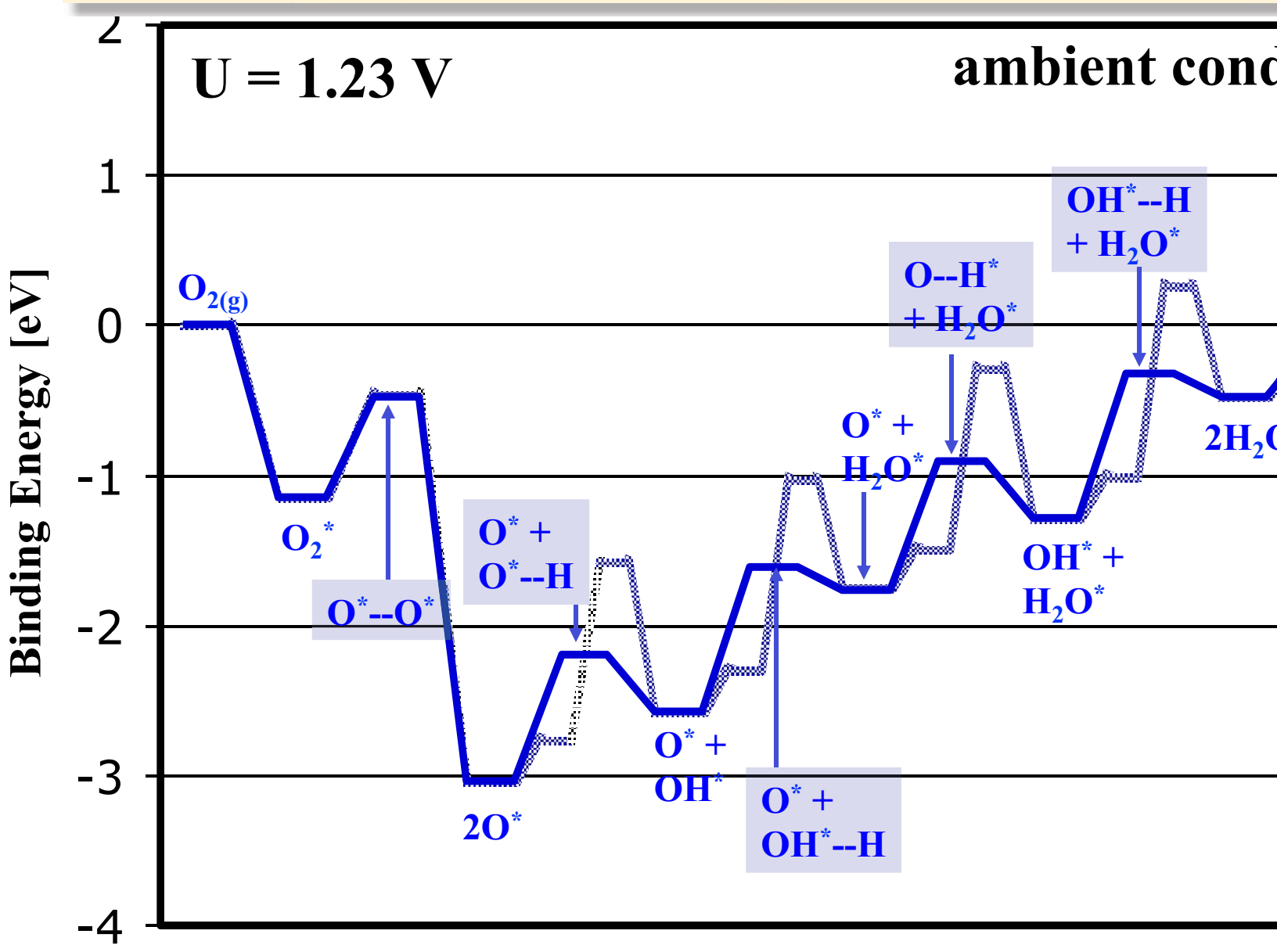

All Mechanisms
(Eley-Rideal + Langmuir-Hinshelwood)

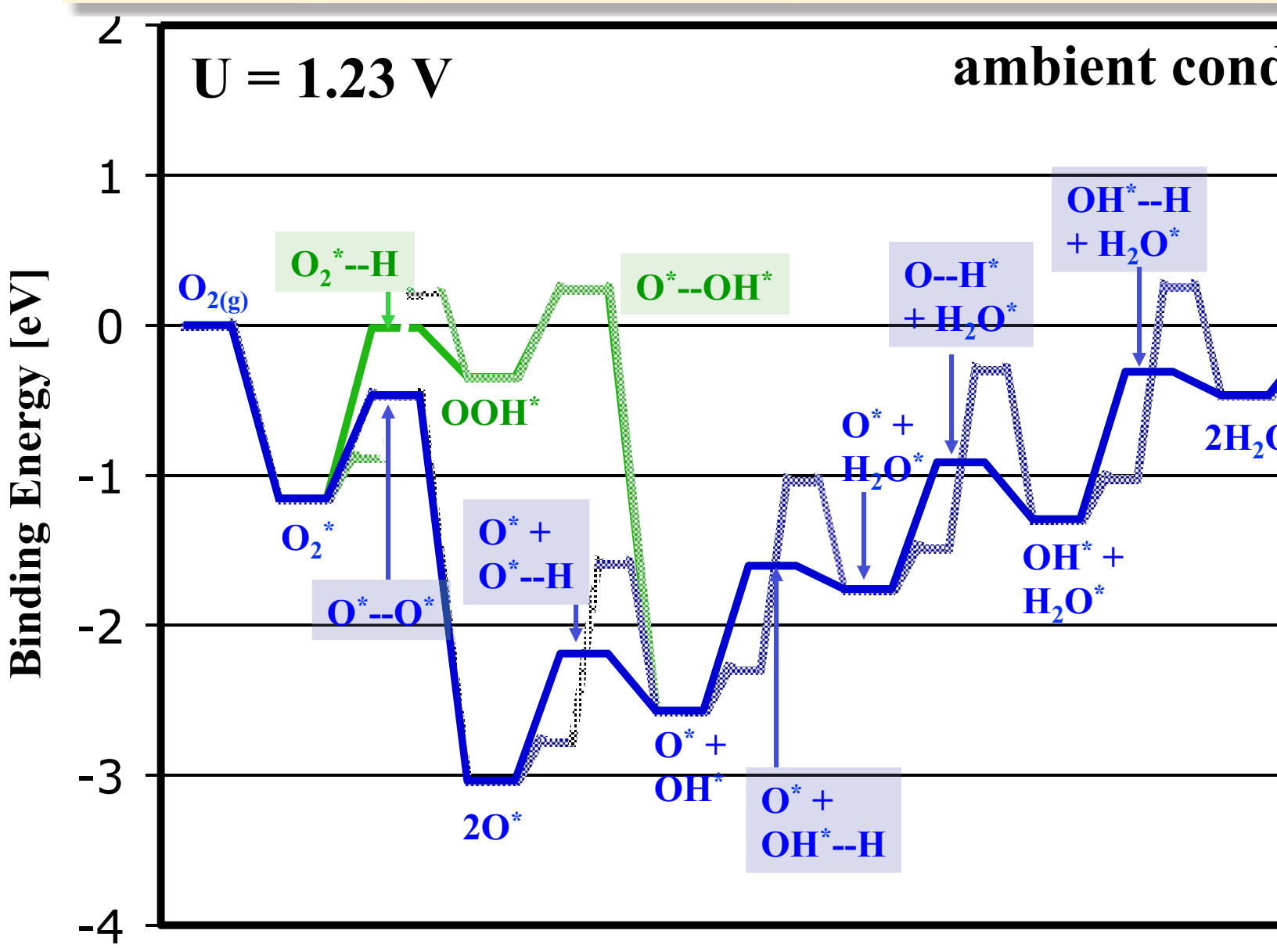

All Mechanisms
(Eley-Rideal + Langmuir-Hinshelwood)

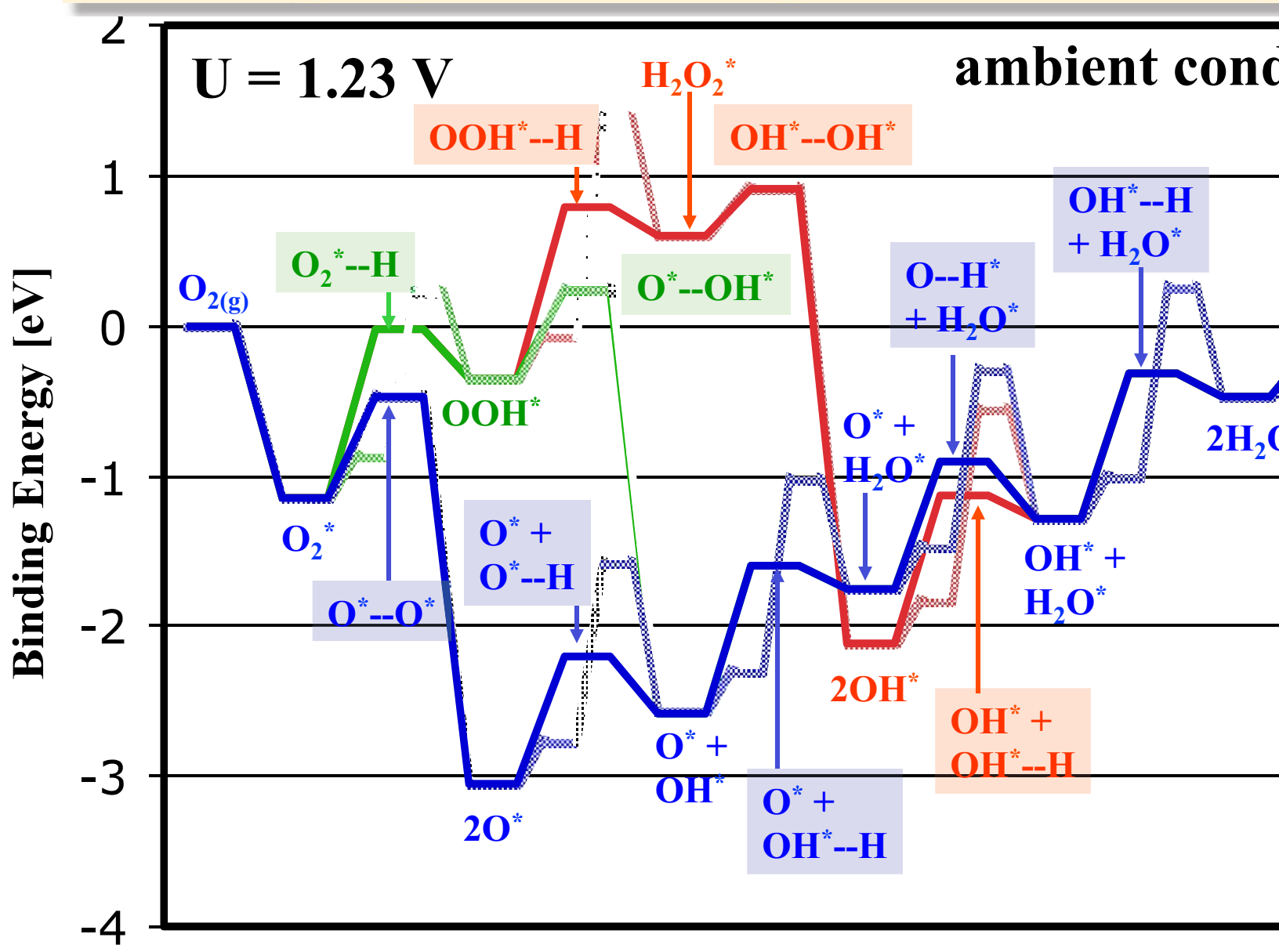

Barriers to form Intermediates

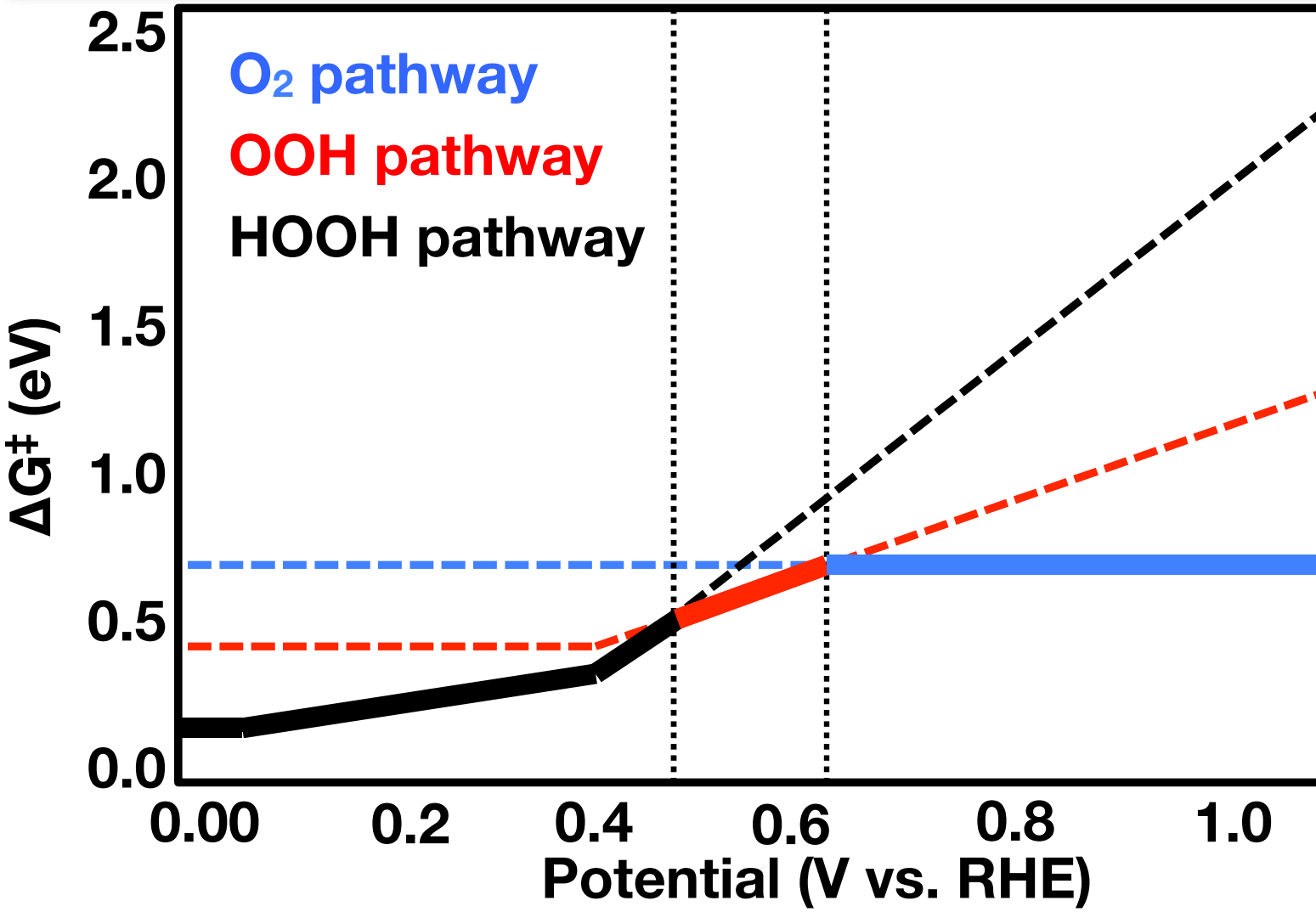

J. A. Keith, G. Jerkiewicz, T. Jacob, *Chem. Phys. Chem.* **11**, 2779 (2010)
J. A. Keith, T. Jacob, *Angew. Chem. Int. Ed.* (hot article), **49**, 9521 (2010)

Differences in barrier (OUT) – barrier (

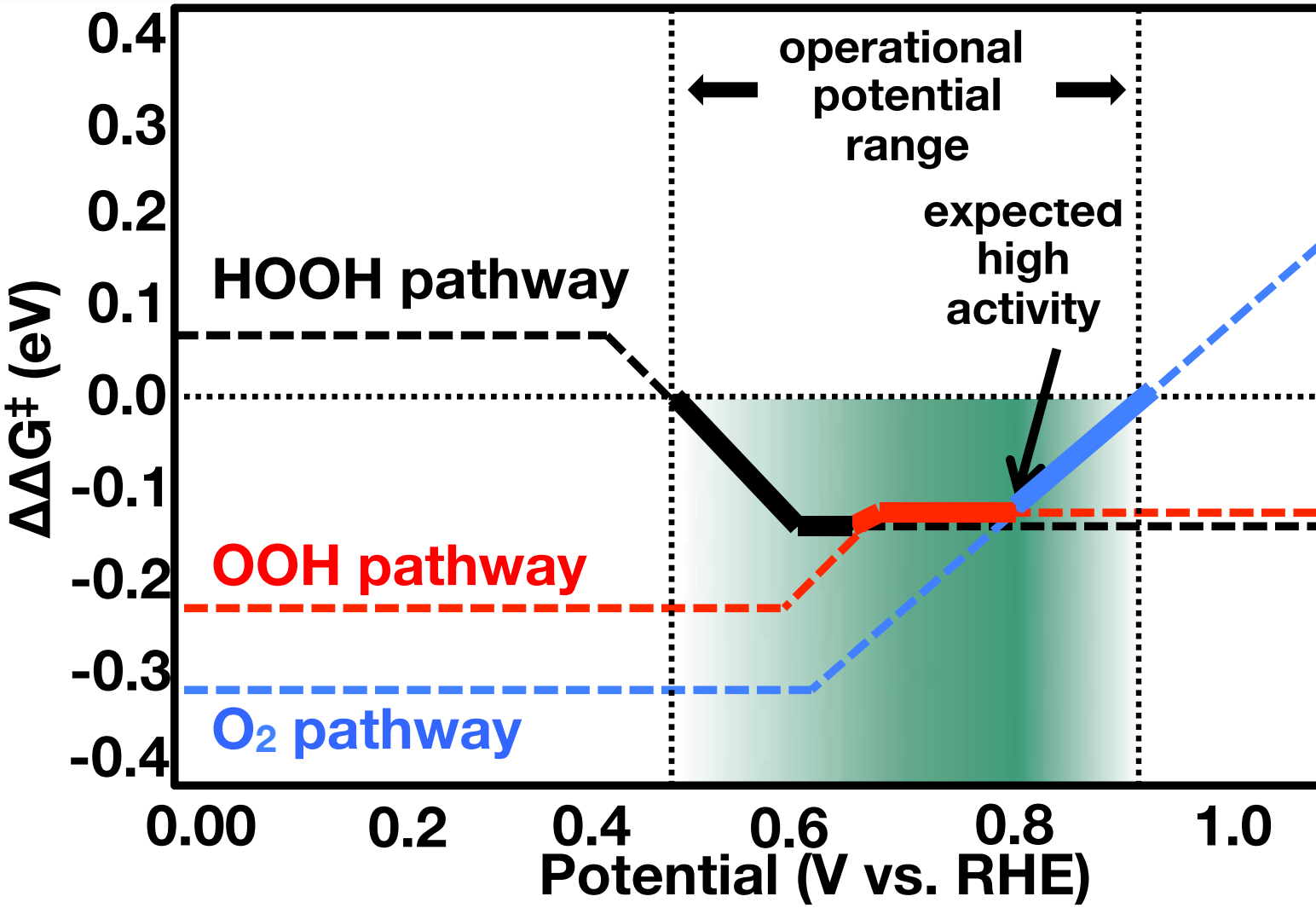

J. A. Keith, G. Jerkiewicz, T. Jacob, *Chem. Phys. Chem.* **11**, 2779 (2010)
J. A. Keith, T. Jacob, *Angew. Chem. Int. Ed.* (hot article), **49**, 9521 (2010)

Differences in barrier (OUT) – barrier (

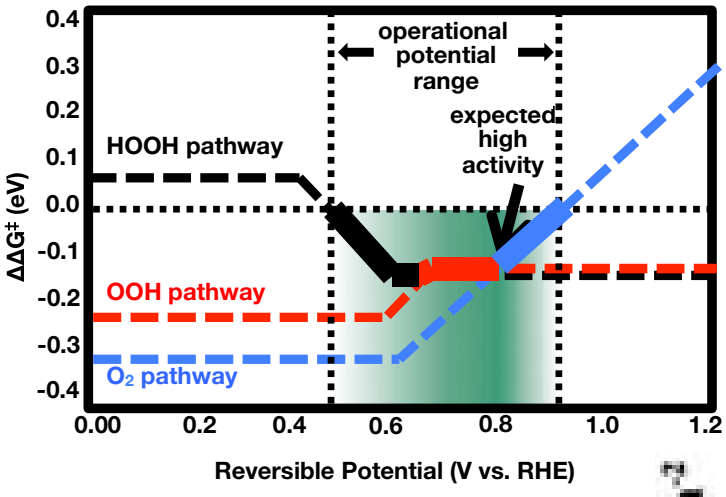

ORR on Pt(111) disk electr

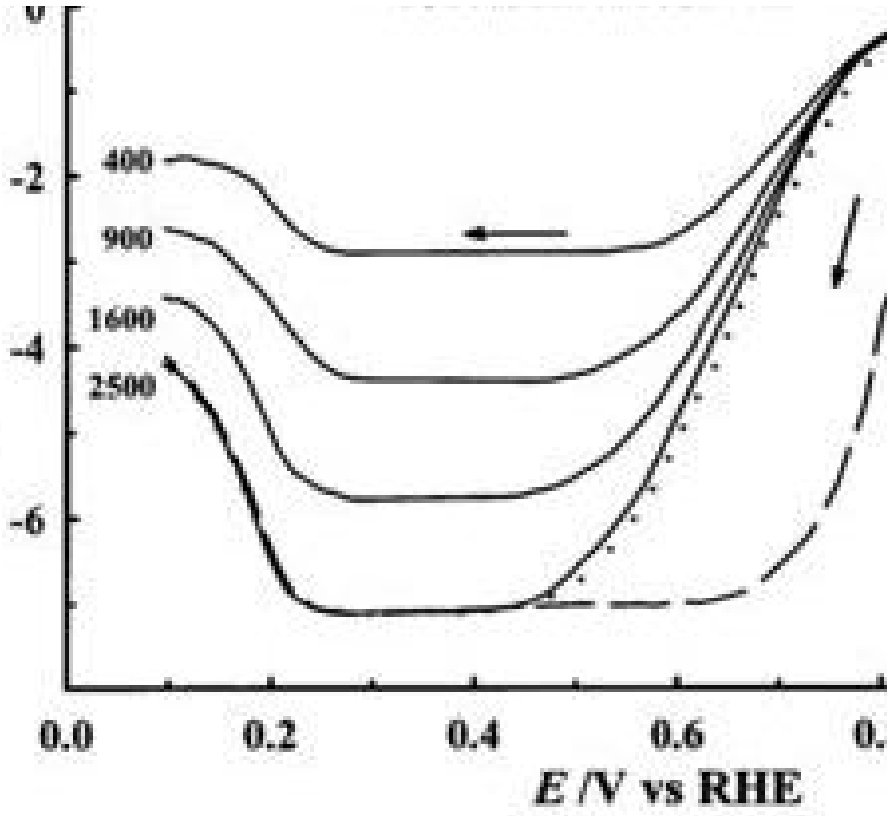

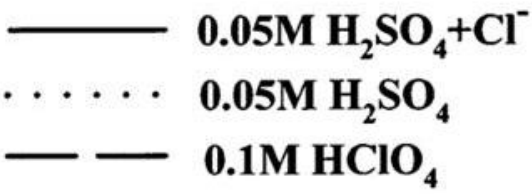

V. Stamenkovic *et al.*, *J. Electroanal. Chem.*, **500**, 44 (2001).

Cathode Reaction with ReaxFF (reactive forcefield)

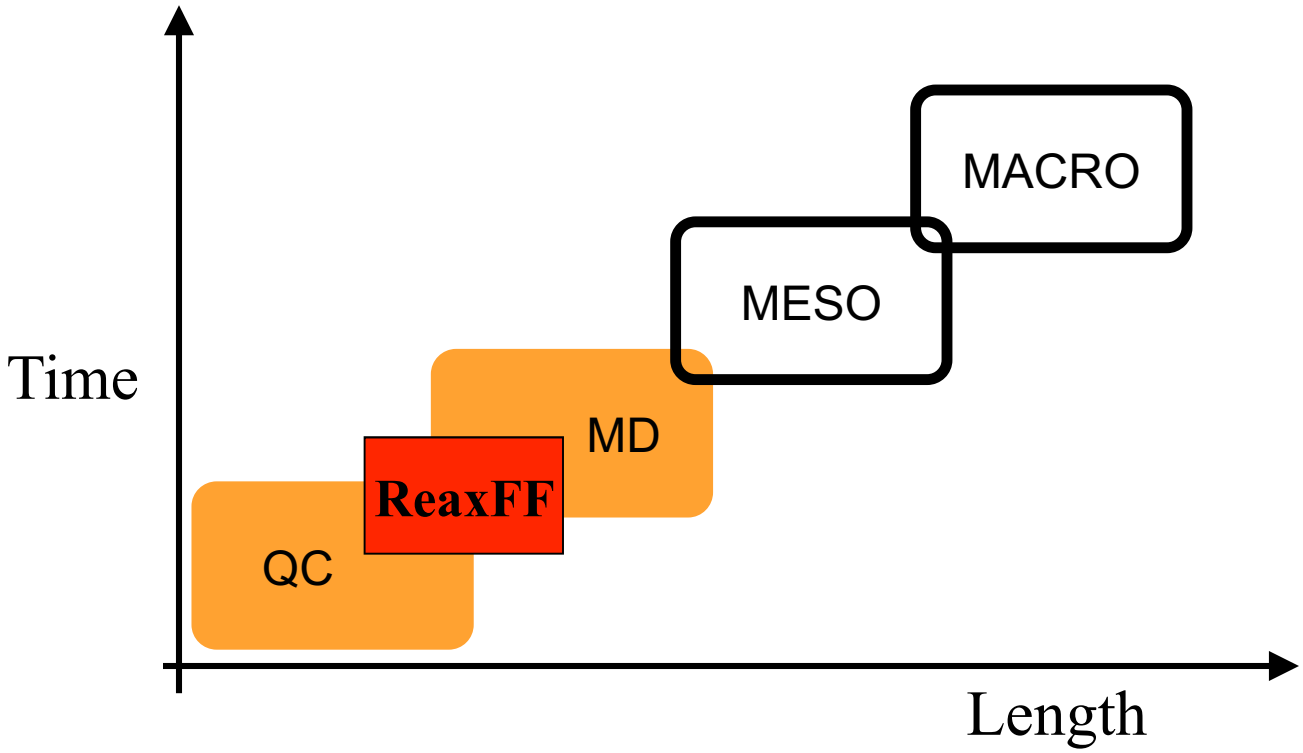

ReaxFF

non-reactive forcefields
(only spheres and springs)

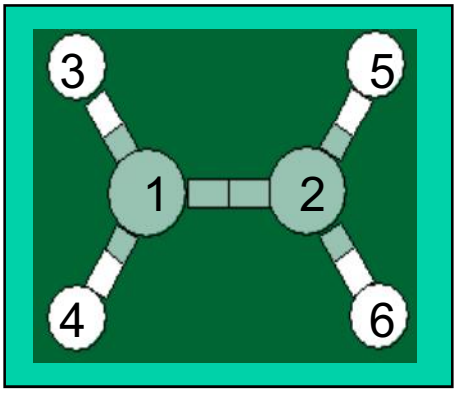

Reactive fo

1: x_1 y_1 z_1
2: x_2 y_2 z_2
3: x_3 y_3 z_3
4: x_4 y_4 z_4
5: x_5 y_5 z_5
6: x_6 y_6 z_6

Atom positions

1: 2 3 4
2: 1 5 6
3: 1
4: 1
5: 2
6: 2

Bonding table

1: x_1 y_1
2: x_2 y_2
3: x_3 y_3
4: x_4 y_4
5: x_5 y_5
6: x_6 y_6

Atom posit

fixed

MD Routine

analyz
bond

MD Rou

System Energy

$$E_{system} = \underbrace{E_{bond} + E_{vdWaals} + E_{Coulomb}}_{\text{2-body}} + \underbrace{E_{val}}_{\text{3-body}} + \underbrace{E_{over} + E_{under}}_{\text{multibody}}$$

Every term depends on bond order (BO_{ij}):

$$BO_{ij} = \exp\left[p_{bo,1}\cdot\left(\frac{r_{ij}}{r_o^{\sigma}}\right)^{p_{bo,2}}\right] + \exp\left[p_{bo,3}\cdot\left(\frac{r_{ij}}{r_o^{\pi}}\right)^{p_{bo,4}}\right] + \exp\left[p$$

Example:

$$E_{tors} = \underbrace{f(BO_a)\cdot f(BO_b)\cdot f(BO_c)}\cdot\left\{\frac{1}{2}V_2\cdot\left(1-\cos 2\omega_{ijkl}\right)\cdot f\left(BO_b^{\pi}\right)+\frac{1}{2}V_3\cdot(1\right.$$

ensures torsion angle energy contribution disappears when bond **a**, **b** or **c** dissociates (similar to valence angle)

H_2 dissociation on Pt(111)

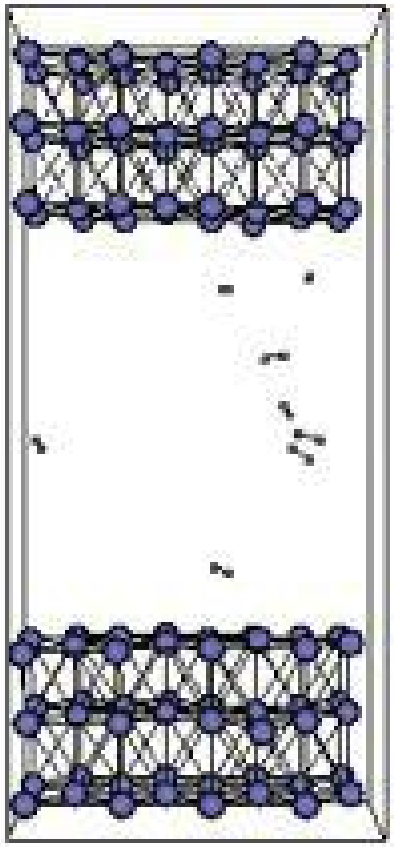

8 H_2-molecules in contact
with a perfect 96-atom (111) Pt-surface.
MD-simulation at 298K

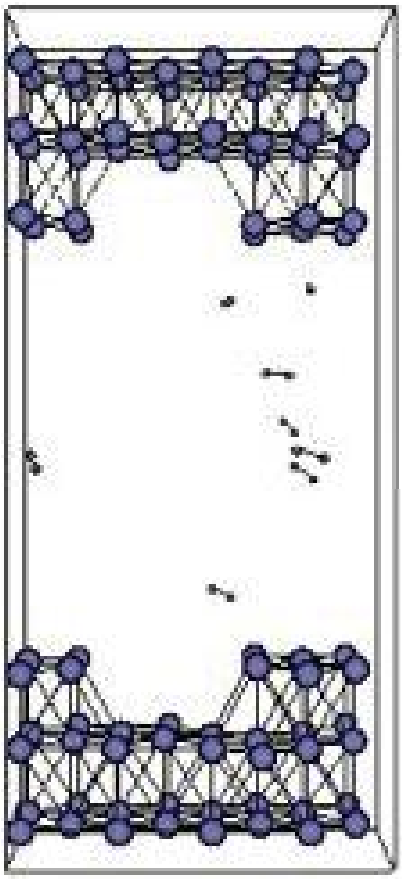

8 H_2-molecules in contact
with a stepped 84-atom (111) Pt-surface.
MD-simulation at 298K

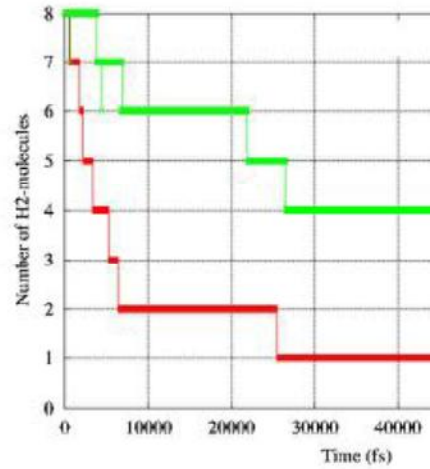

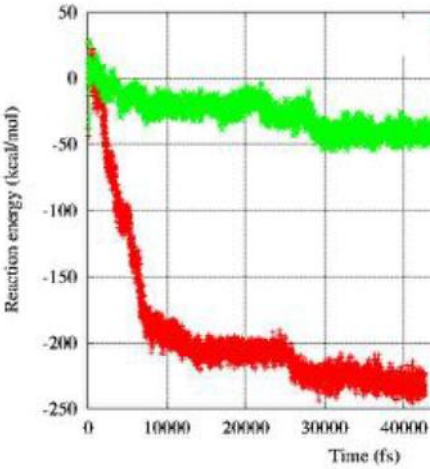

- Surface defec
increase reacti

$H_2 + O_2$ reactions on Pt(111)

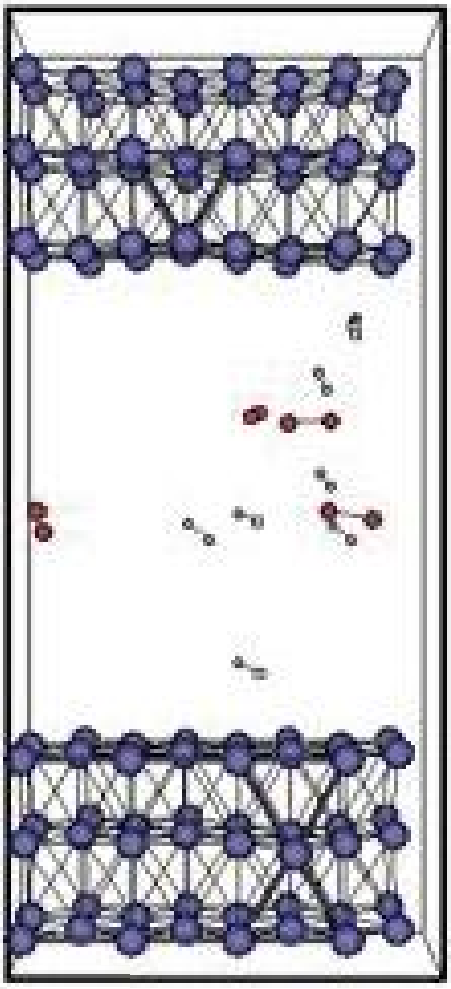

8 H_2+ 4 O_2 in contact with a perfect 96-atom (111) Pt-surface. T=1000K

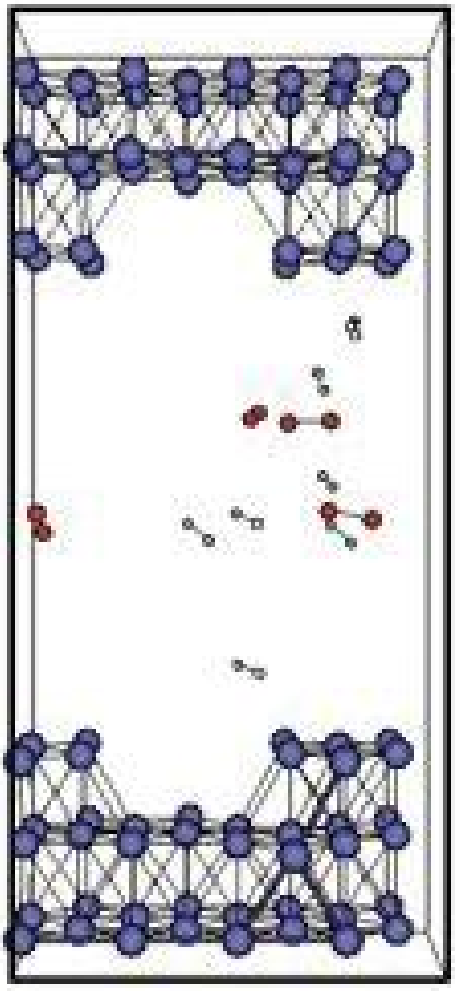

8 H_2 + 4 O_2 in contact with a stepped 84-atom (111) Pt-surface. T=1000K

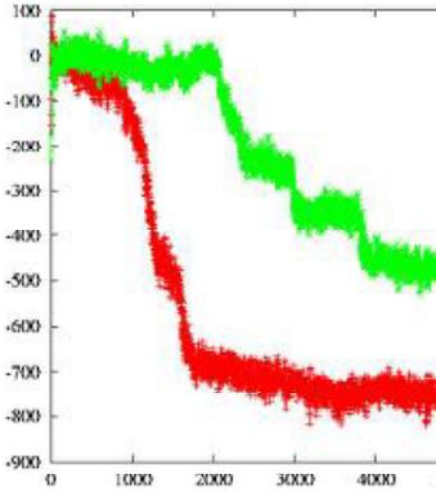

-Perfect surface ge
H_2O, stepped surfa
oxidized

- Need to compare
with QC-data for s
defects

- Energy profile fo
surface clearly sho
generation events

$H_2 + O_2$ reaction on Pt(111)

Restrained MD (

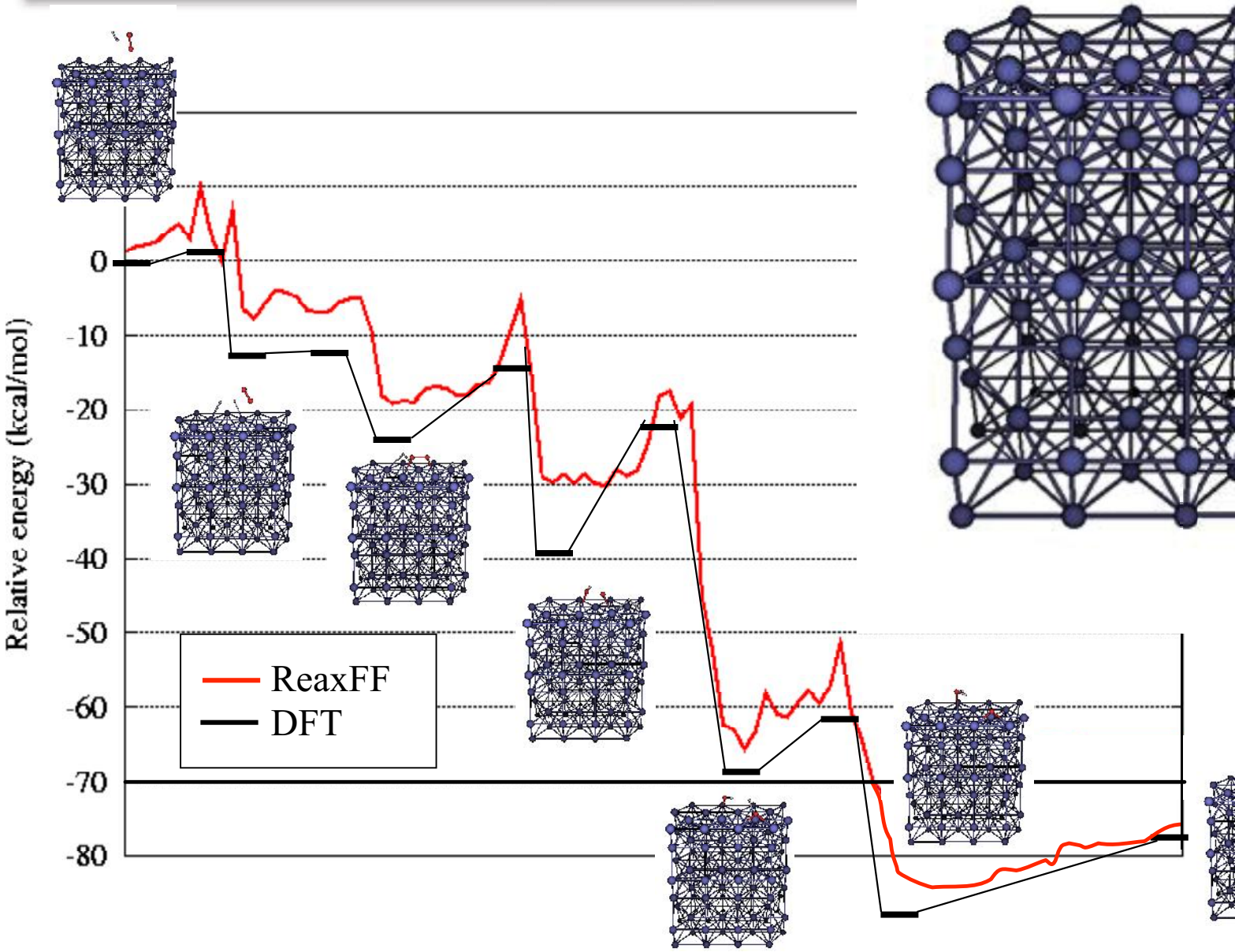

Nanoparticles under Reaction Conditi

Idealized nanoparticles

Idealized particle with low-index faces
(e.g. Wulff-construction)

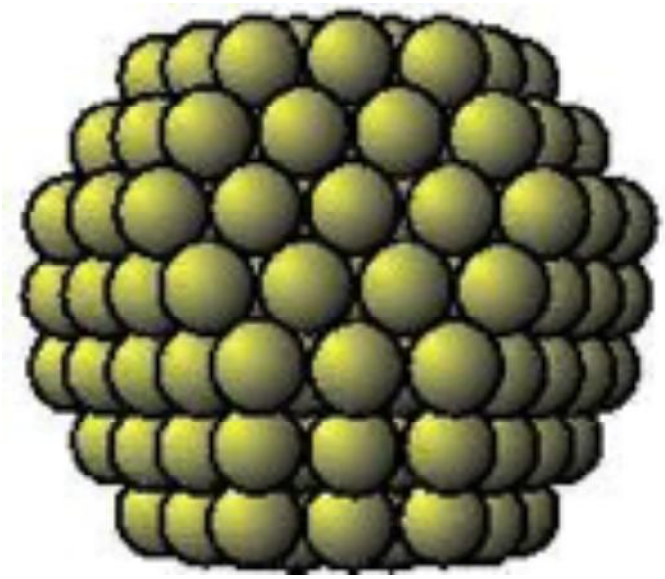

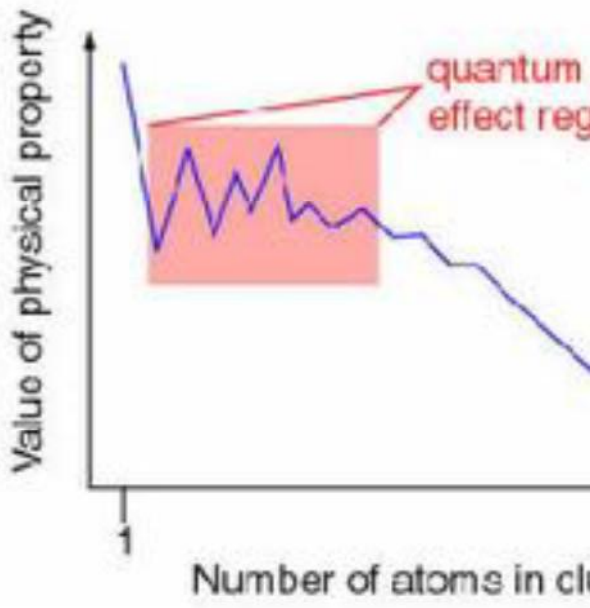

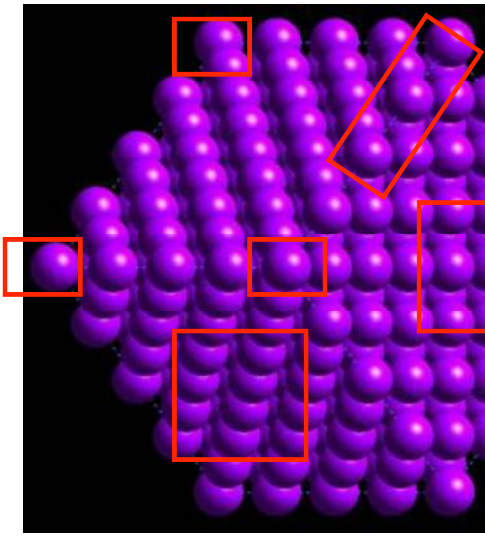

Structure of Pt nanoparticles

Structural distribution depends on preparation metho

Pt_5

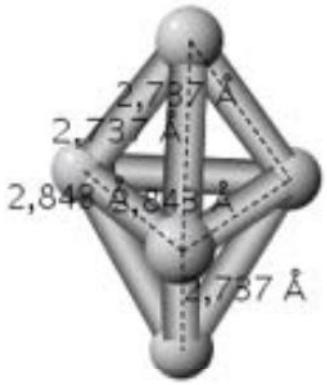

Energy minimization

After annealing proc

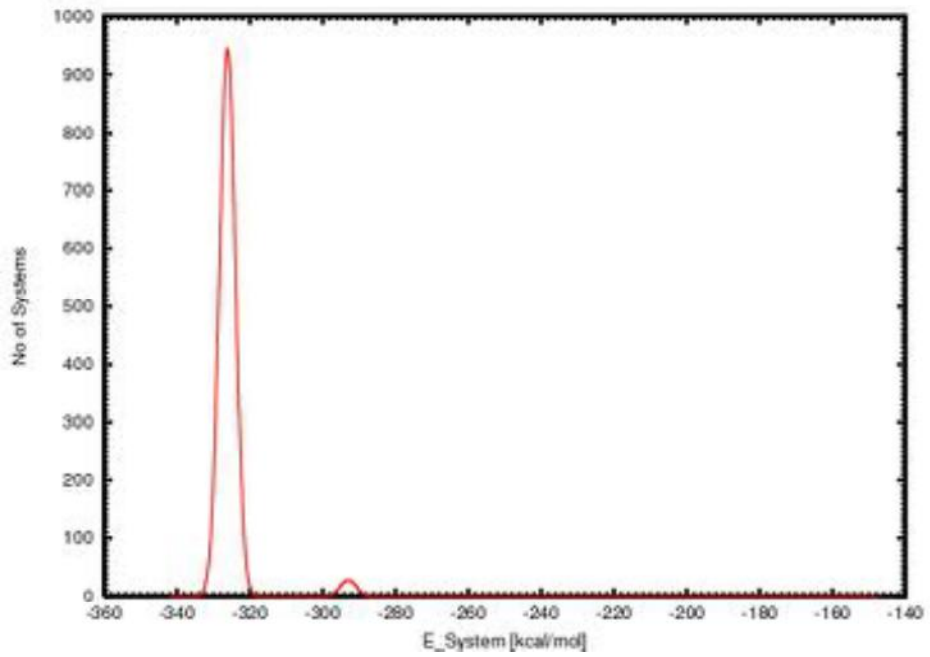

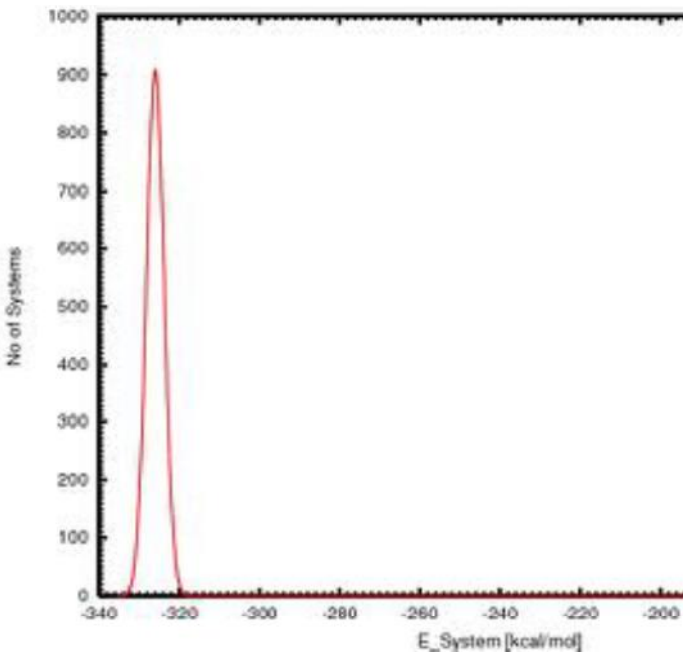

Structure of Pt nanoparticles

Pt_{13}

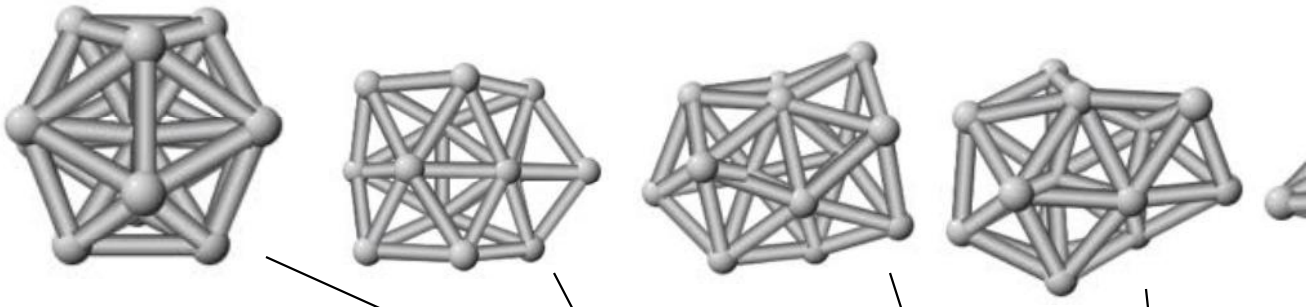

Energy minimization

After annealing proc

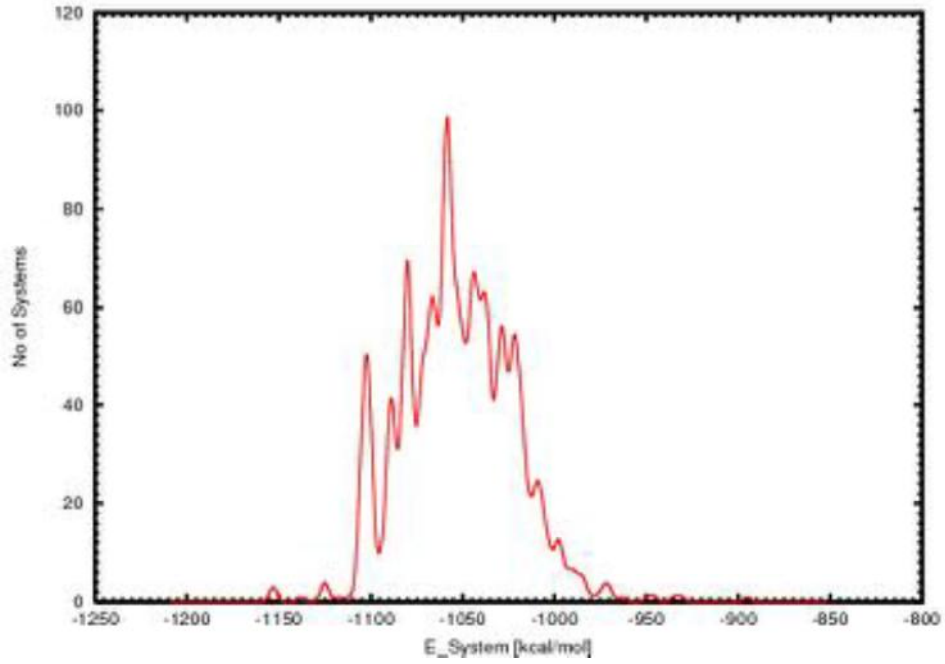

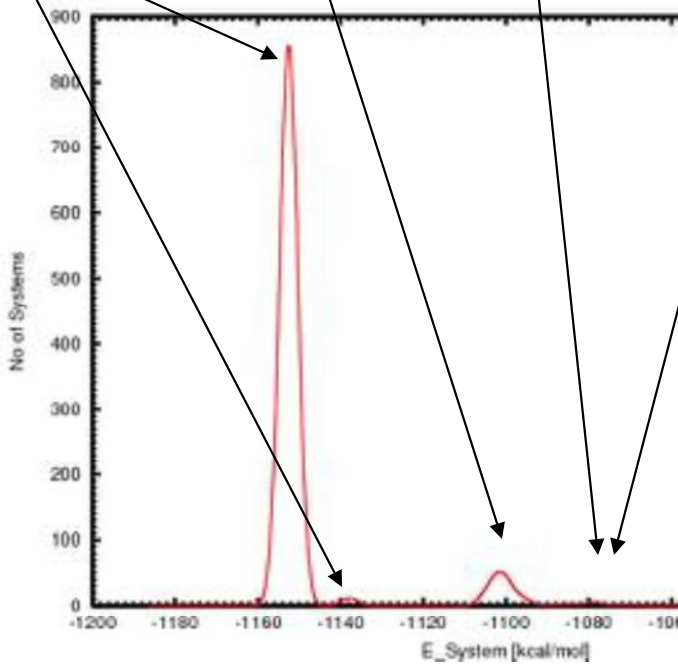

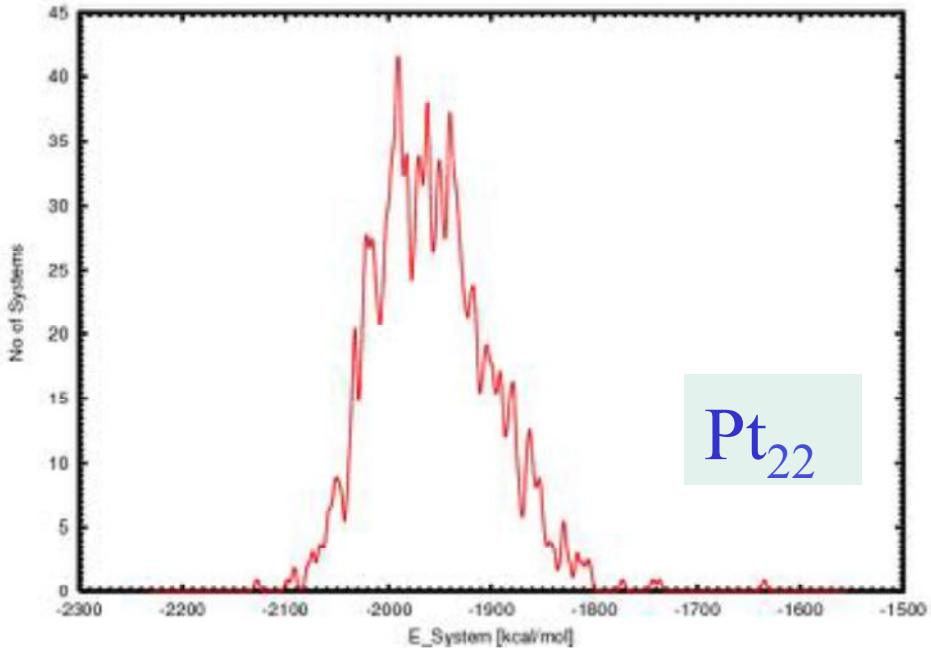

Pt_{22}

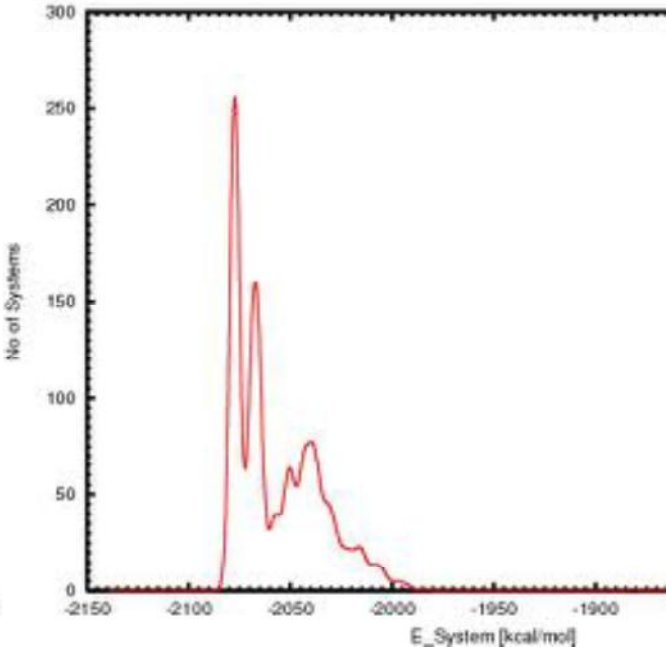

Energy minimization

After annealing proc

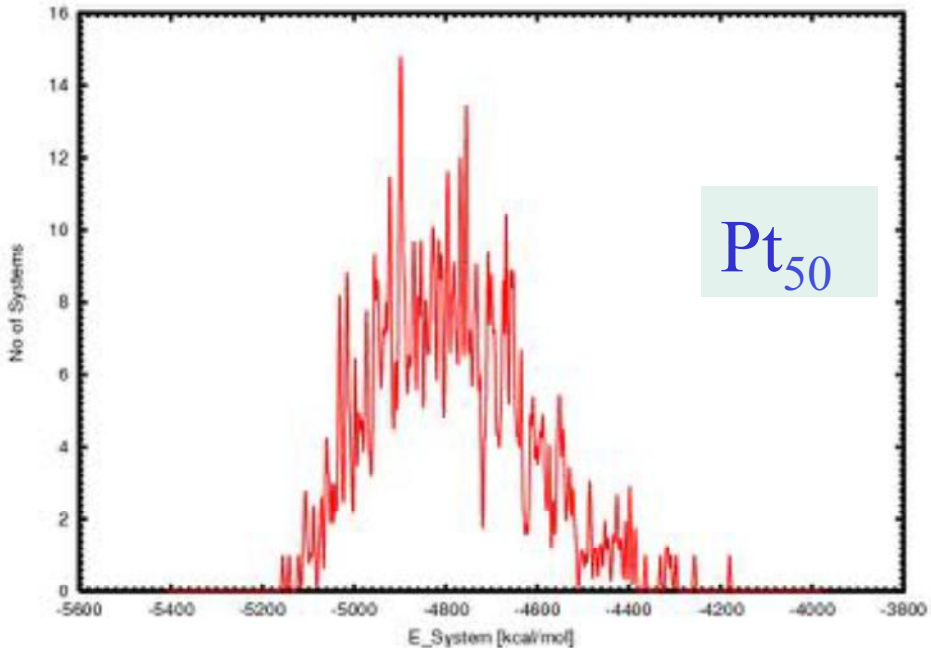

Pt_{50}

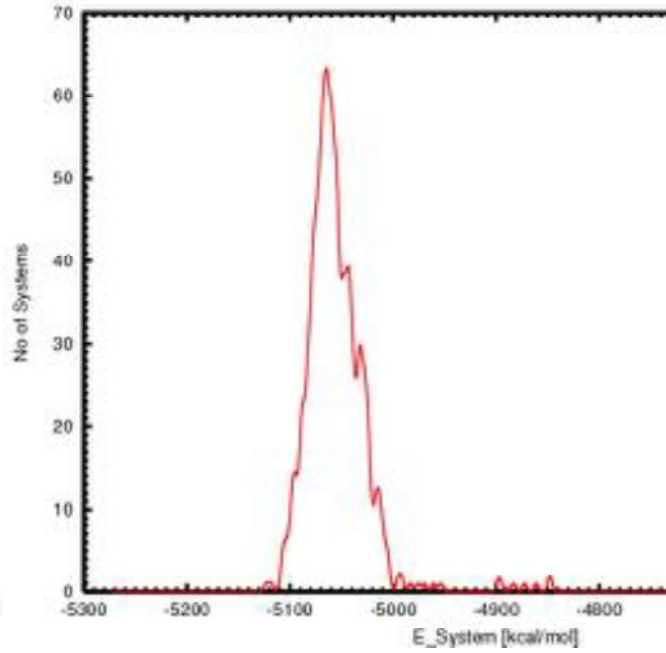

DFT Calculations on Re Surfaces

Re(0001)

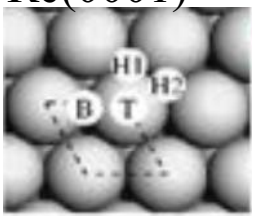

Re(10-10)

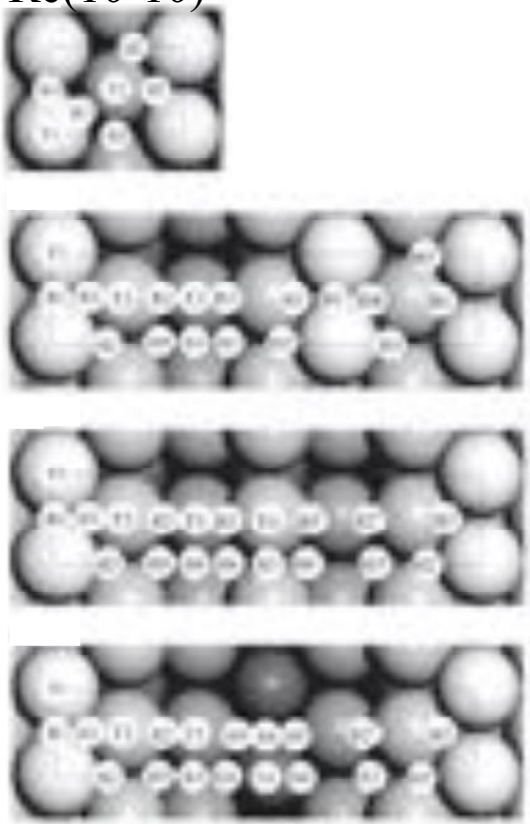

Re(10-11)

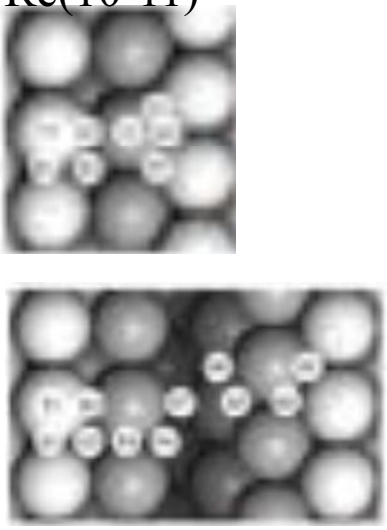

Re(11-2

Re(13-4

• CASTEP-code* • plane wave • GGA-PBE and LDA • ultraso

* M.D. Segall *et. al.*, J. Phys. Condens. Matter. **14**, 2717 (2002).

Equilibrium Shape of Re Particle

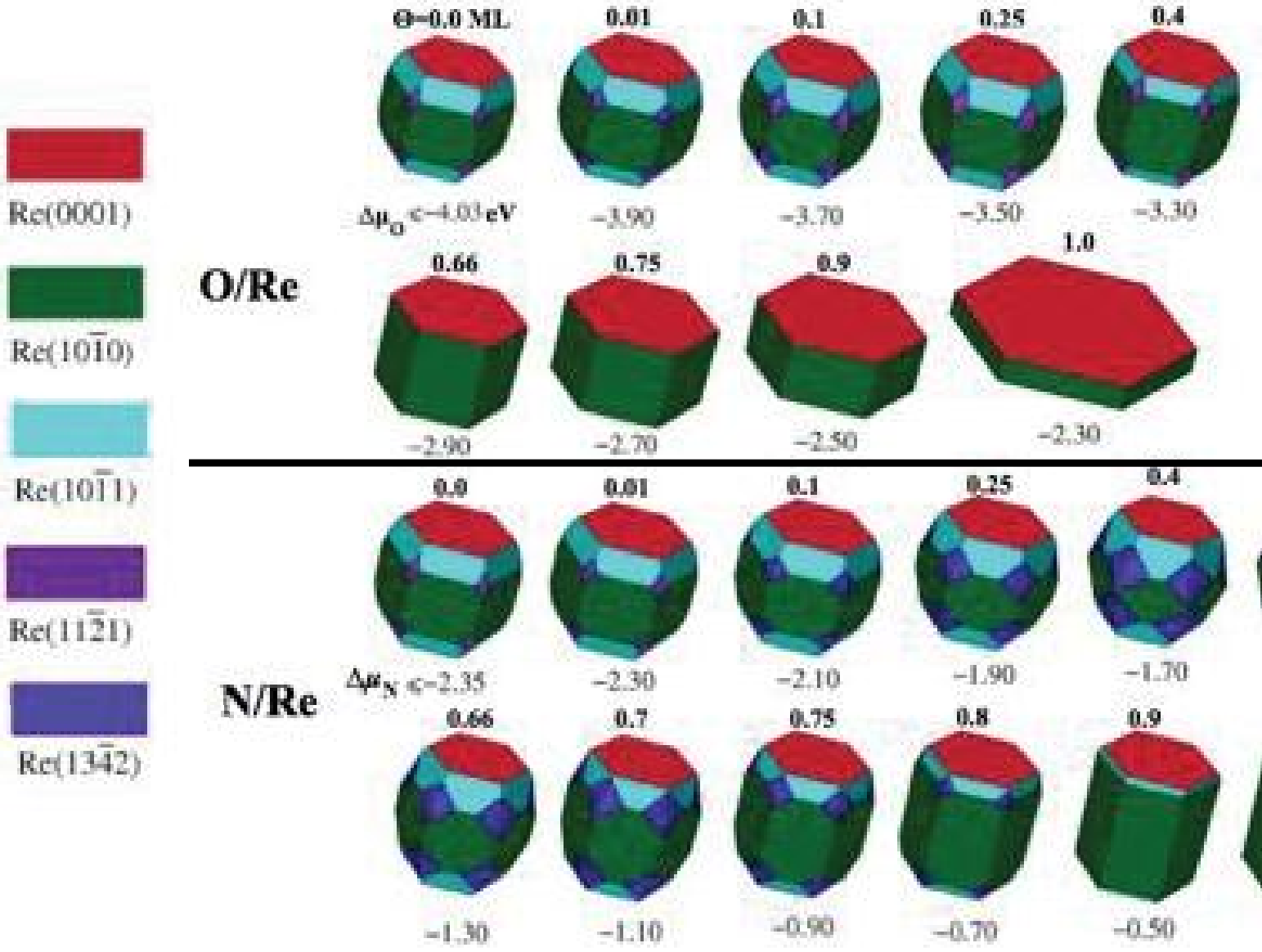

Binding energy vs. particle-shape

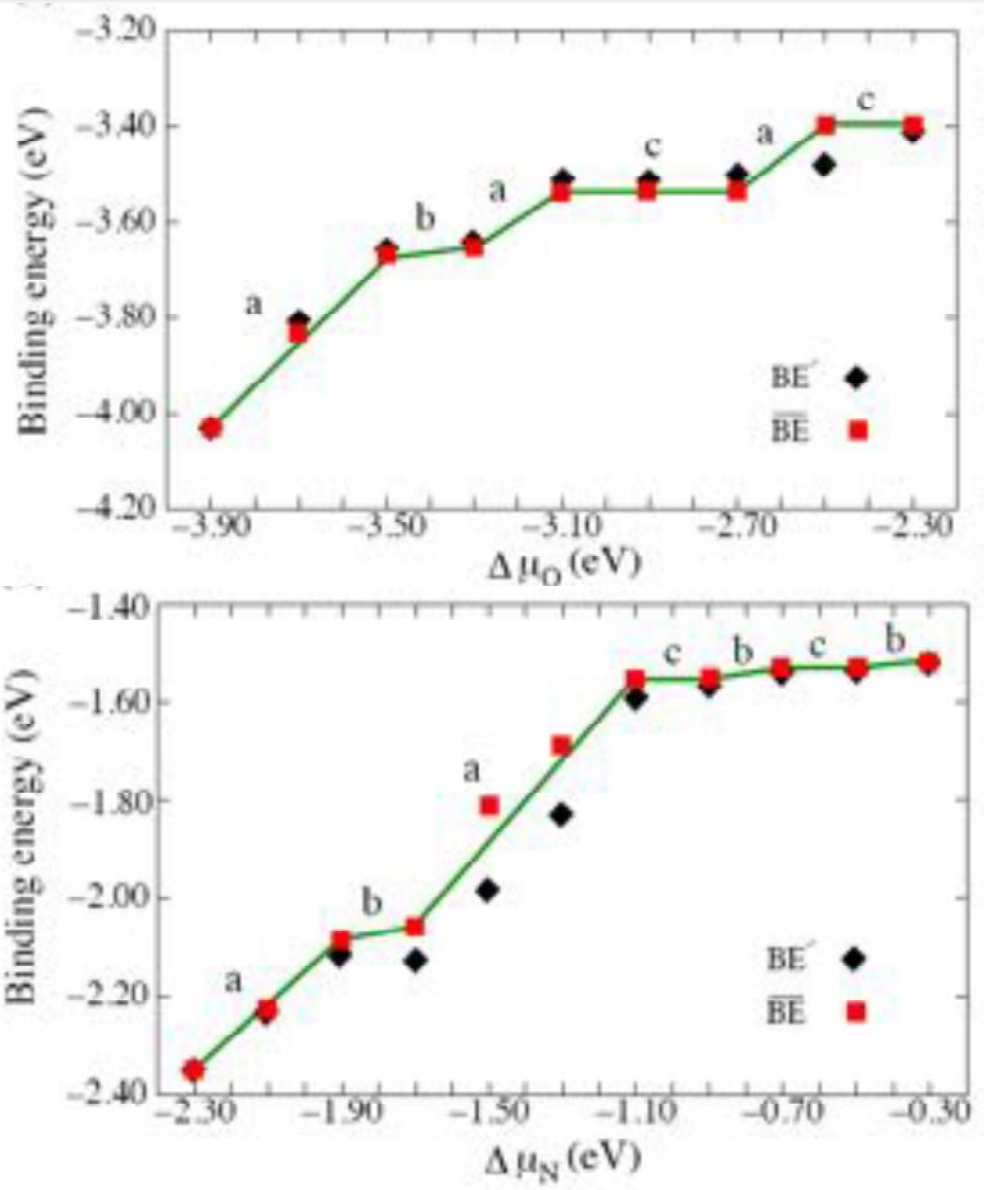

Bimetallic alloys

periodic

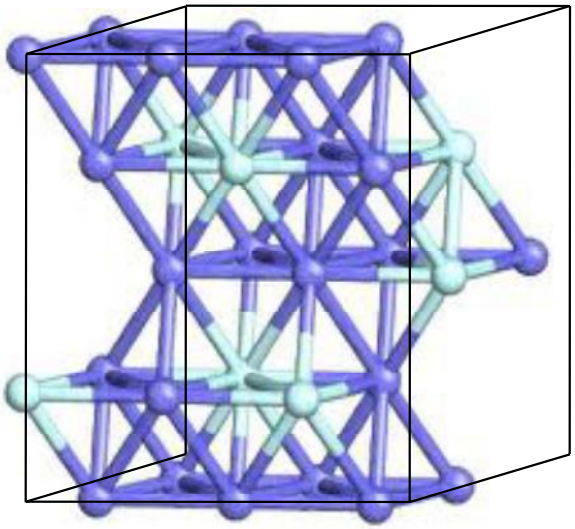

particles

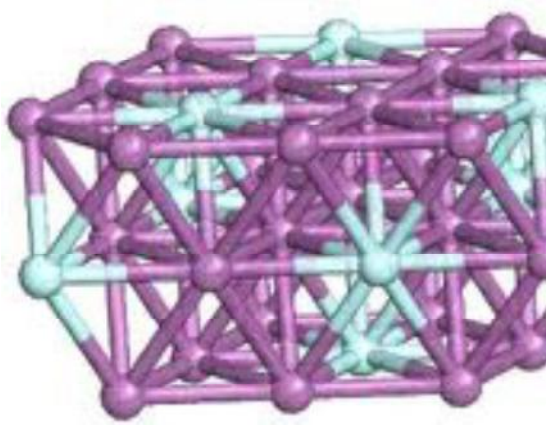

Particle morphologies

analyzed Pt_2Ni_1 nanoparticles

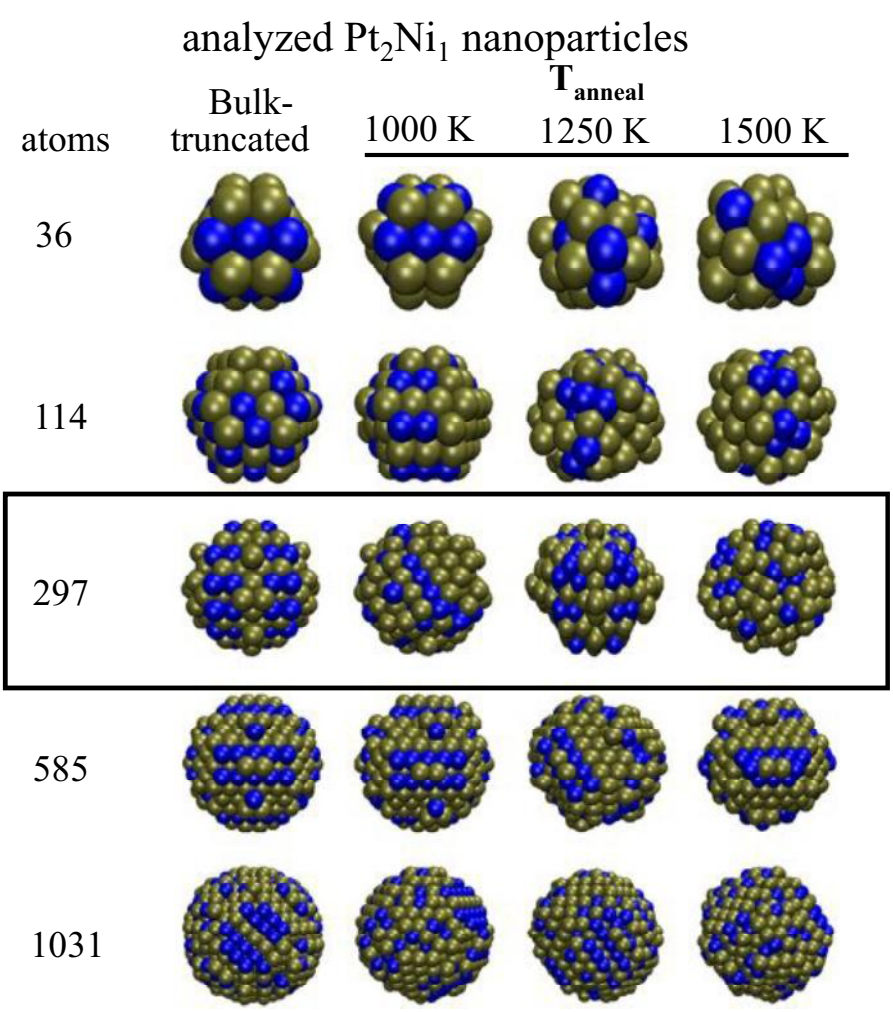

→ broad shape distribution with the maximum not be

Bulk

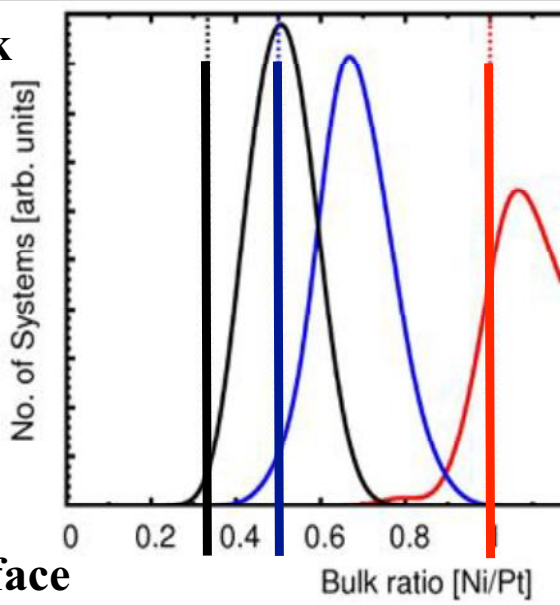

Surface

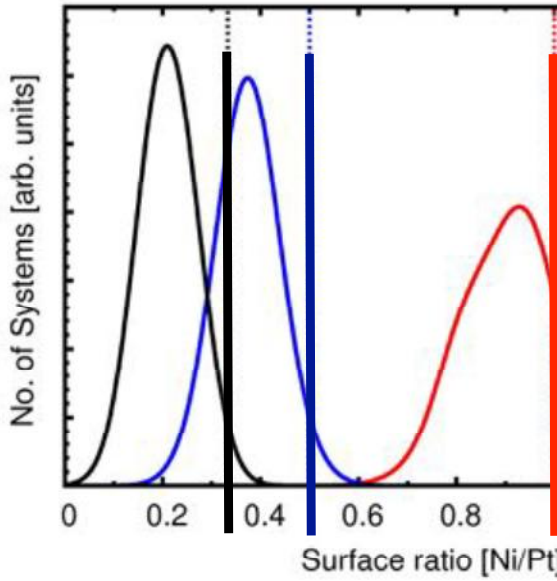

Surface plane composition

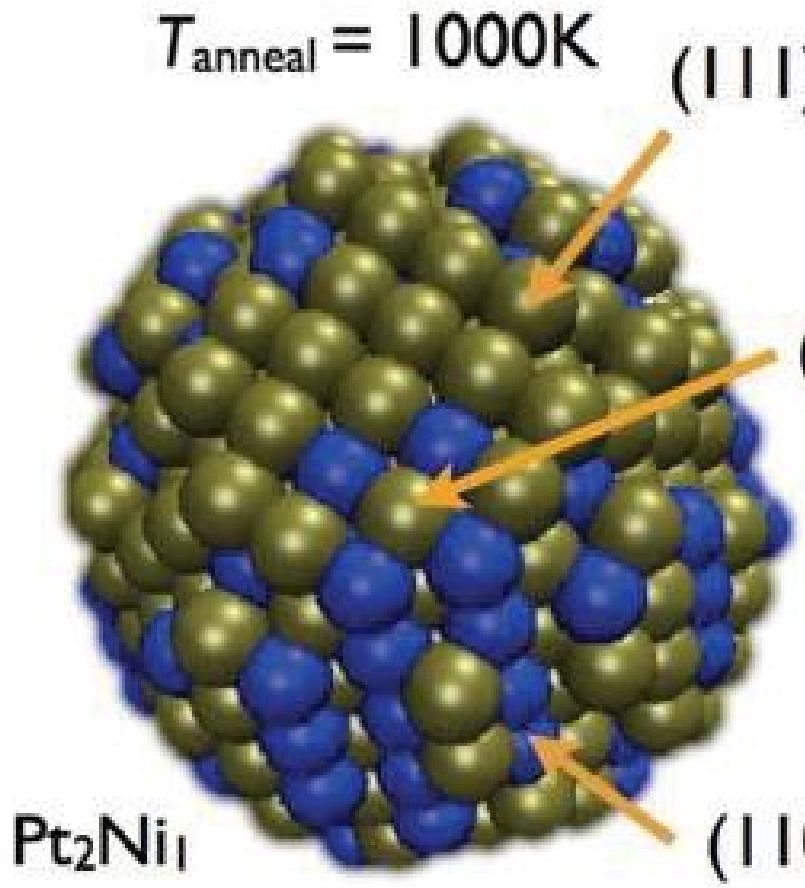

are mostly fully covered with Pt

still contains a certa amount of Ni

seems to be dominated Ni surface segregation

M. A. Vasiliev, J. Phys. Chem. D, 30, 3037 (1997).
Y. Gauthier, Y. Joly, R. Baudoing, L. Rundgren , Phys. Rev. B., 31, 6216 (1985).

→ agrees with experiments for Pt_xNi_1 single crystal surfaces

Dynamic Behavior

Pt_3Ni nanoparticles in 0.05M H_2SO_4, 20mV/s

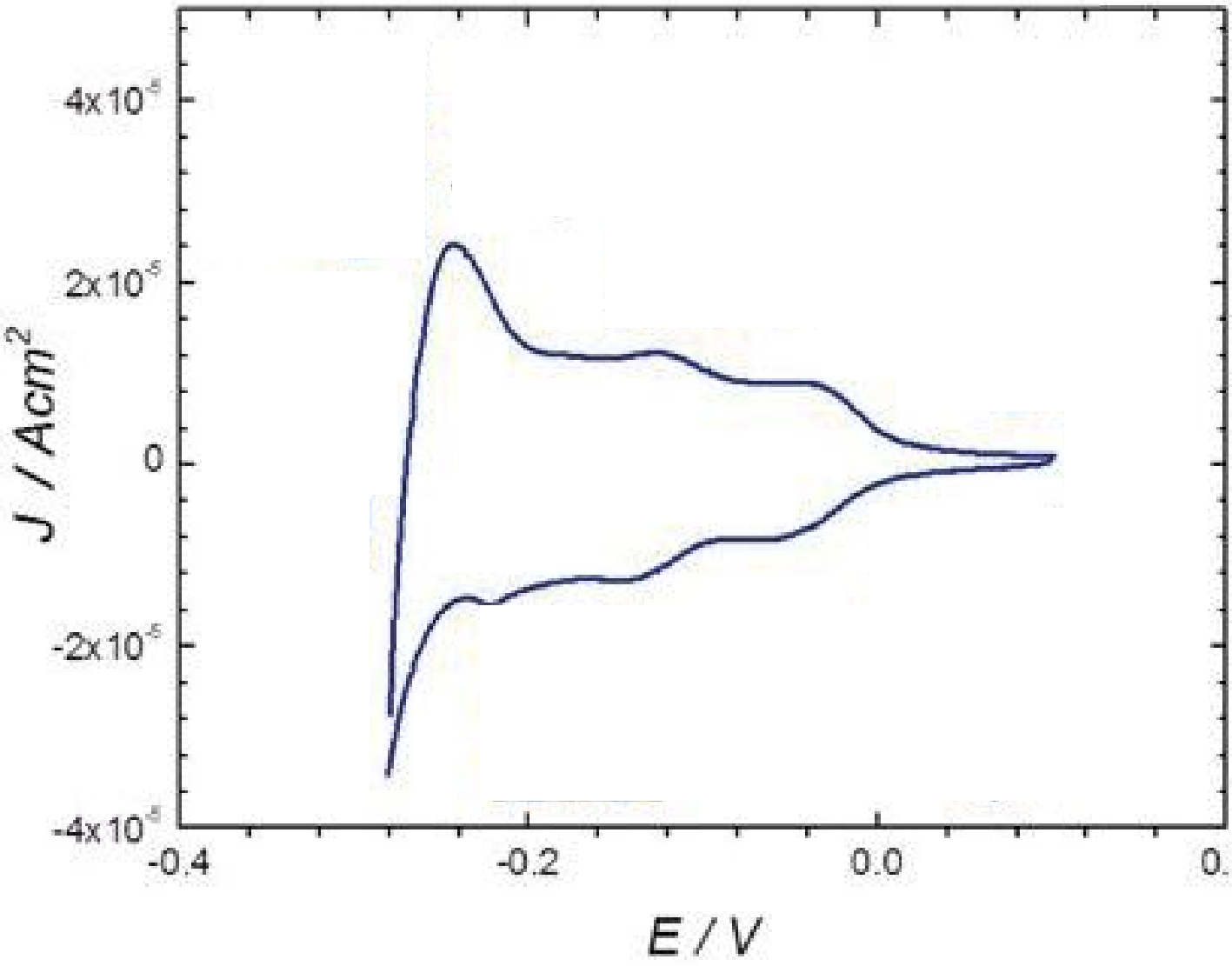

Breathing Catalyst

EXAFS-measurements

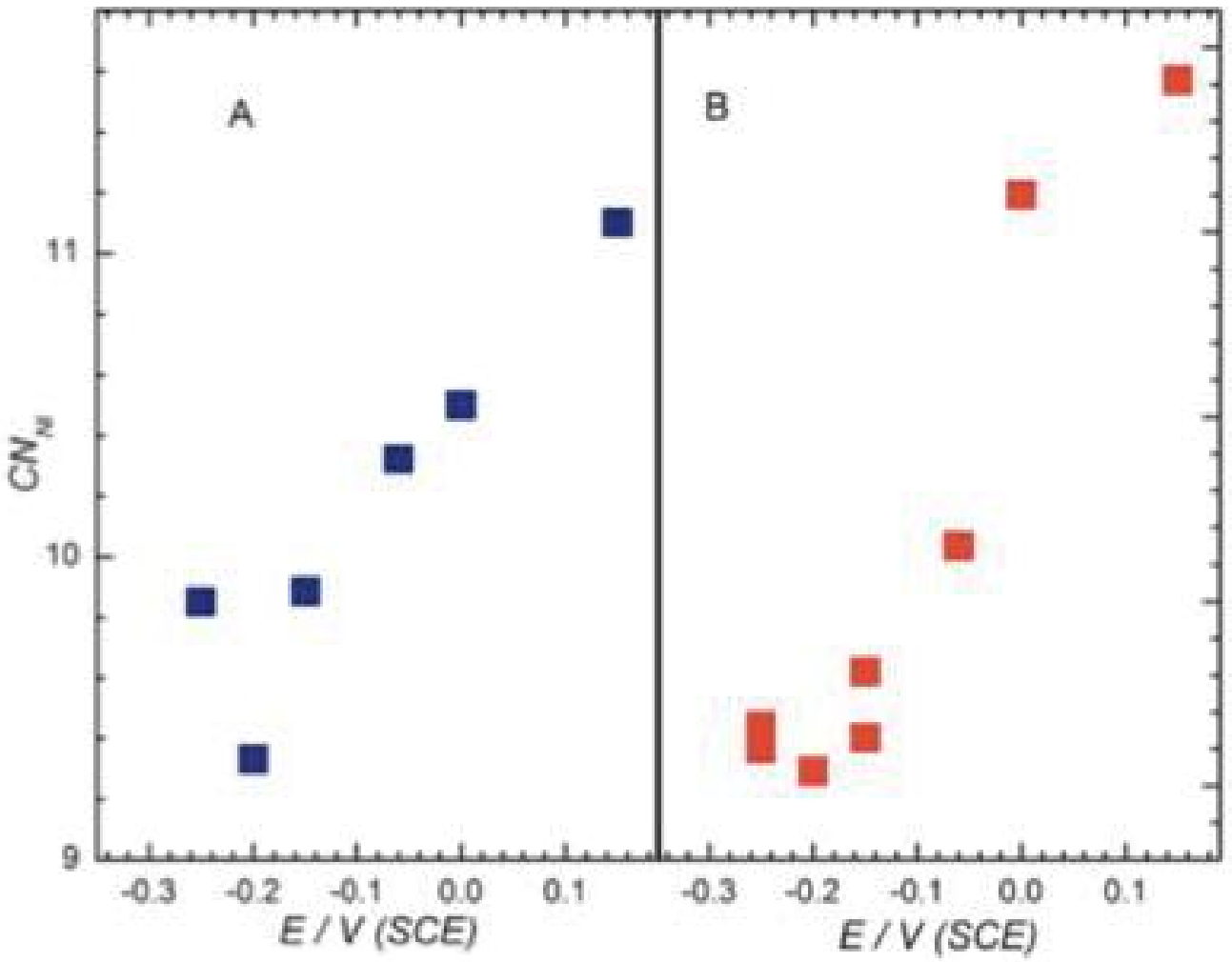

H. Hoffmanova et al., Langmuir, 29, 9046 (2013).

Breathing Catalyst

Pt_3Ni nanoparticles in 0.05M H_2SO_4, 20mV/s

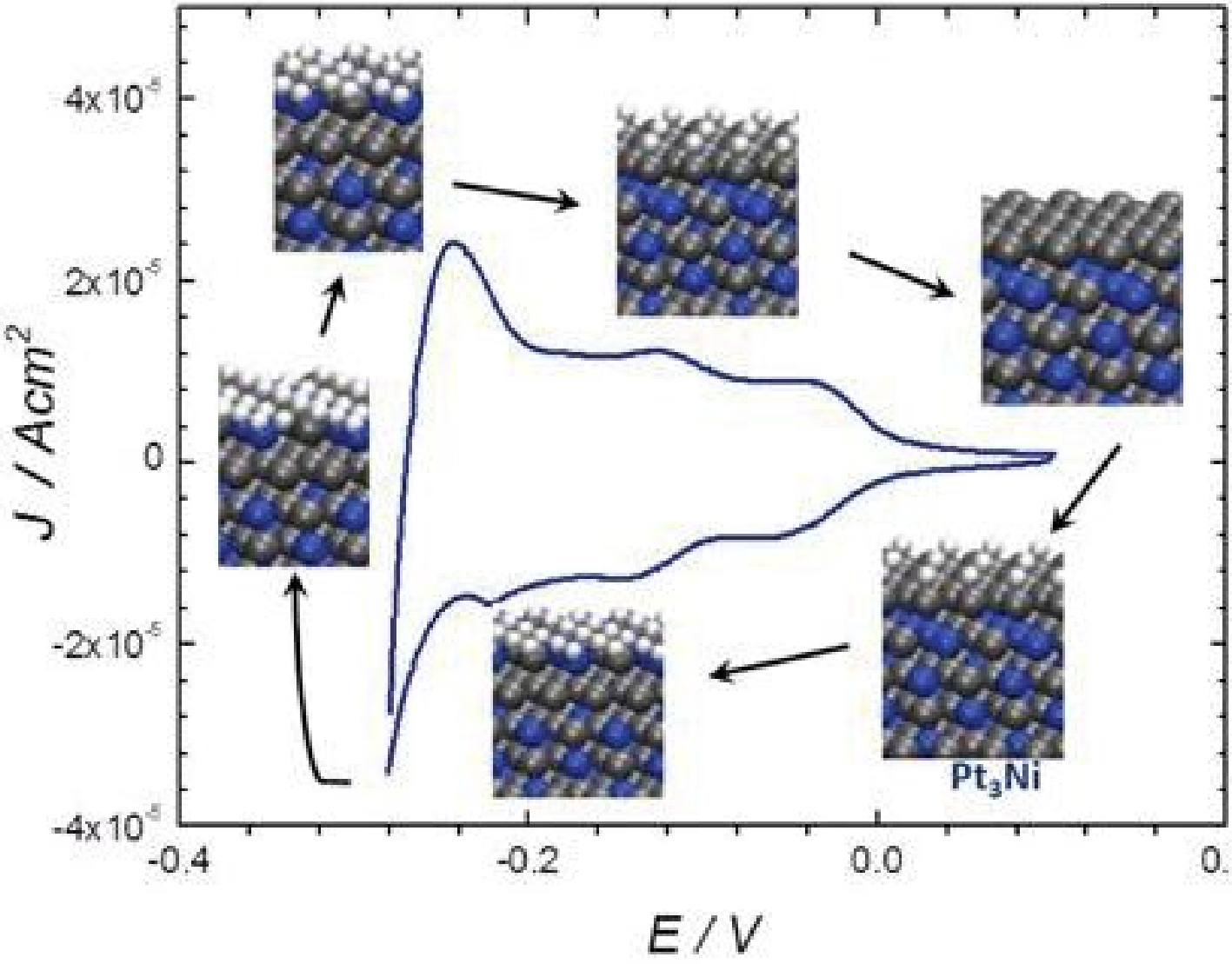

AuPd: A breathing catalyst

High H-concentration
(H:Pd ratio)

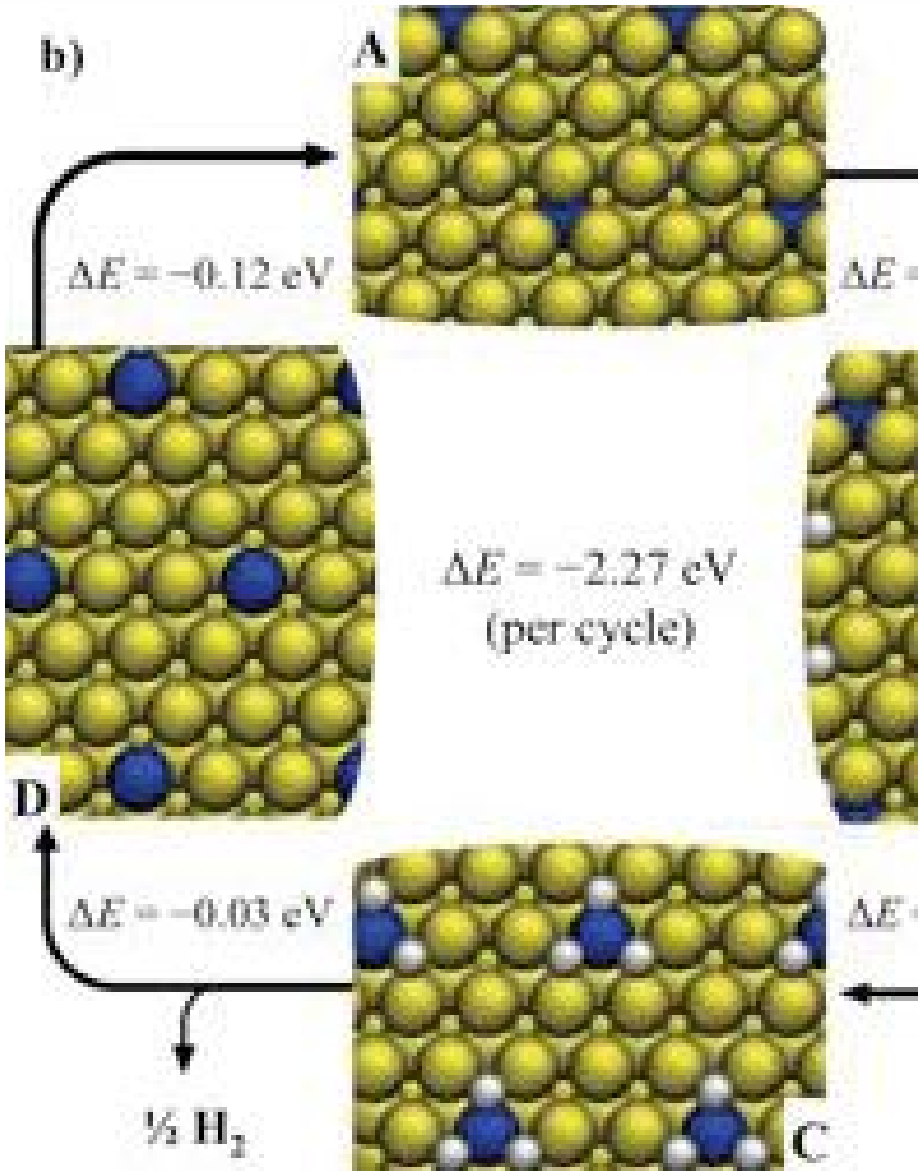

H_2 Evolution on Au-Pd alloys

Cyclic voltammogram of nanoparticulate Au_4Pd alloy catalyst (5 nm part
0.05 M H_2SO_4 (polarization rate of 10 mV/s).

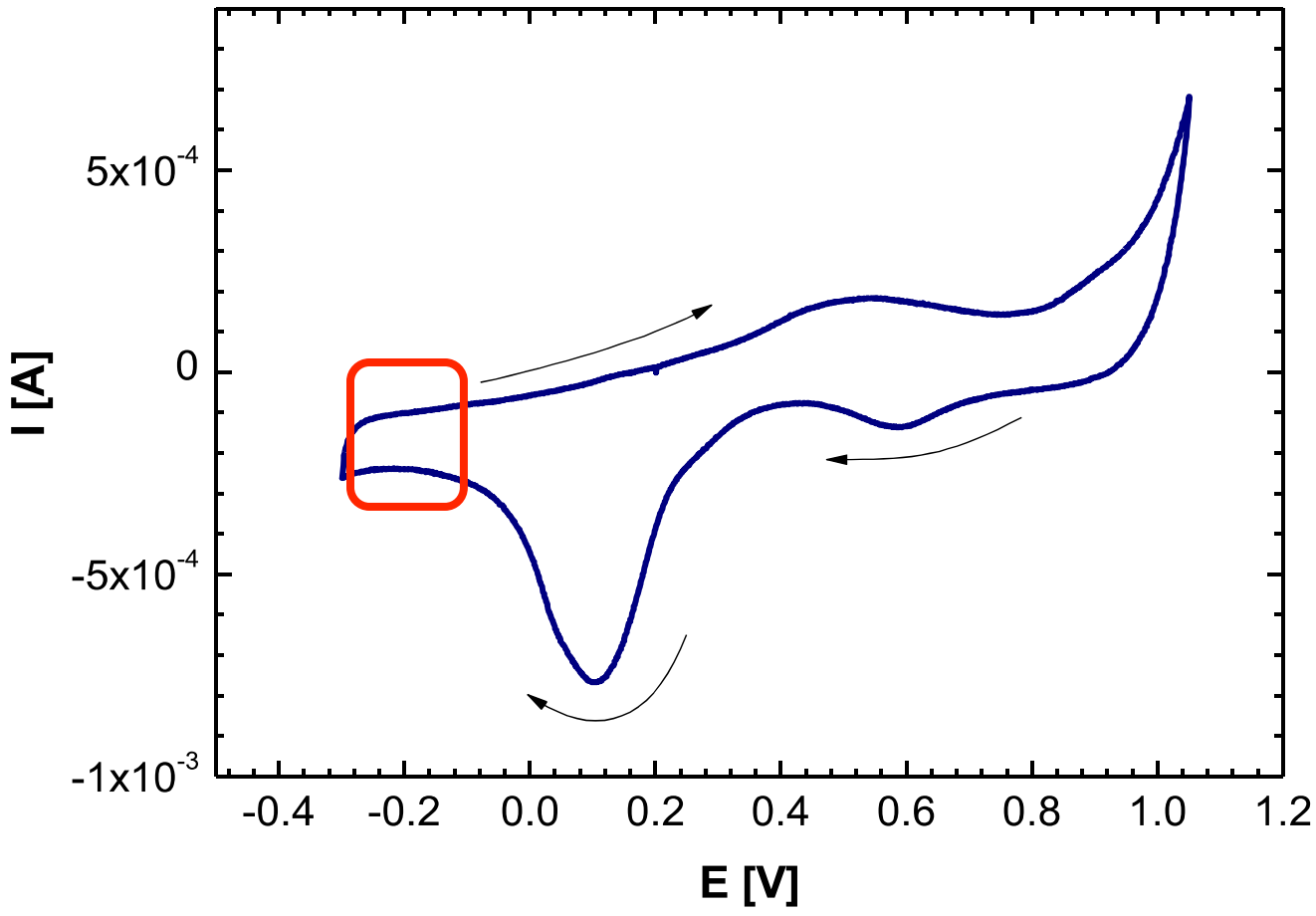

H adsorption and H_2 Evolution on Au-Pd allo

k^3-normalized EXAFS functions extracted from X-ray absorption spe

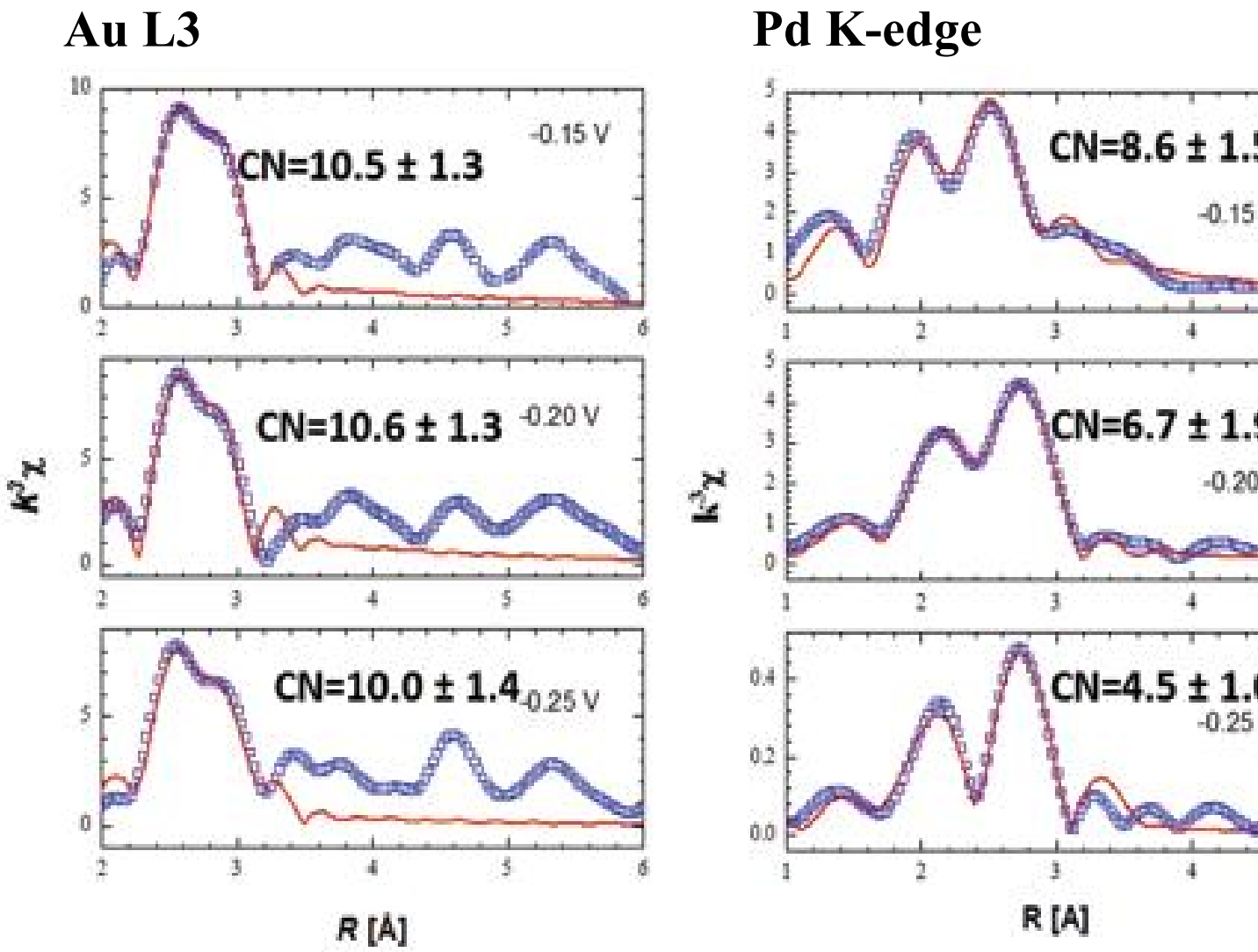

Examples of Diffusion Processes Involving Vaca in 3x3, 6 Layer Au(111) Slab

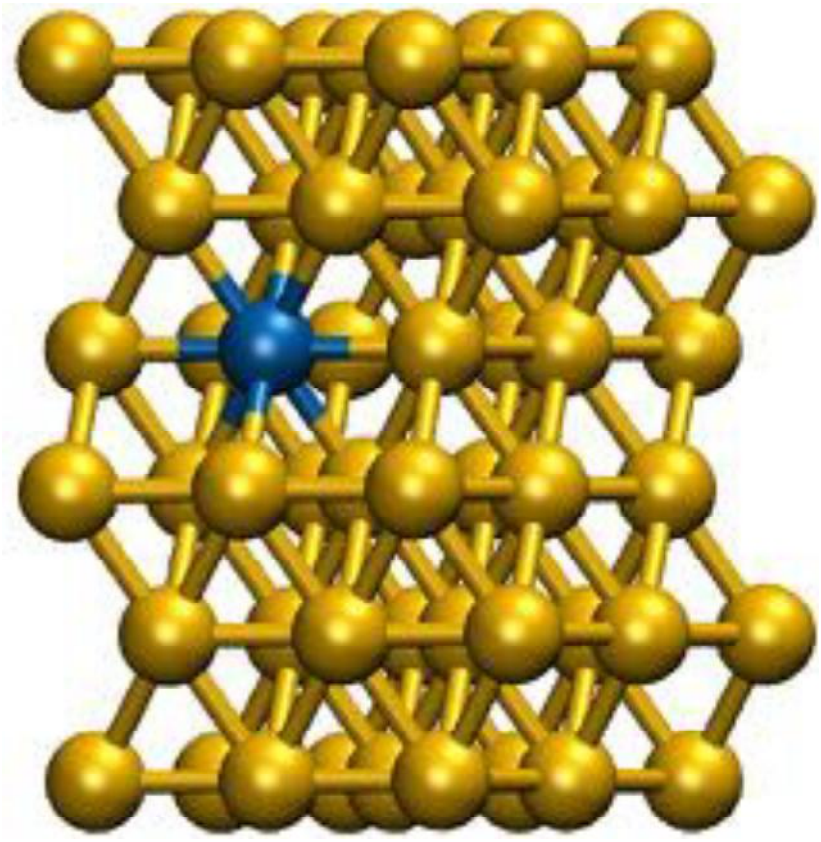

3rd layer to 3rd layer diffusion

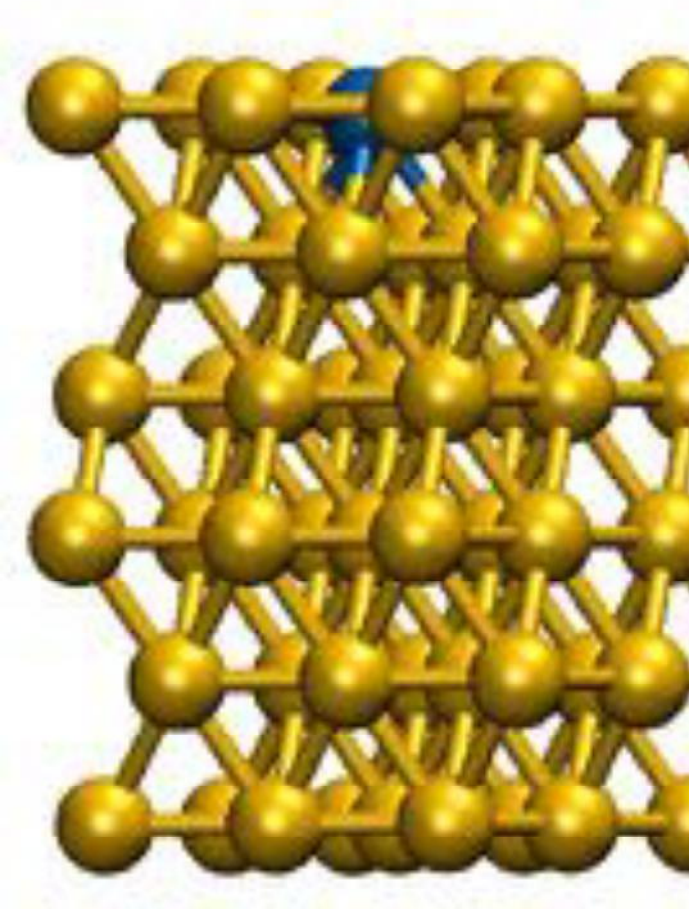

Ad atom to 1st layer diffusion

Examples of Surface Migration Processes on 3x3, 6 Layer Au(111) Slab

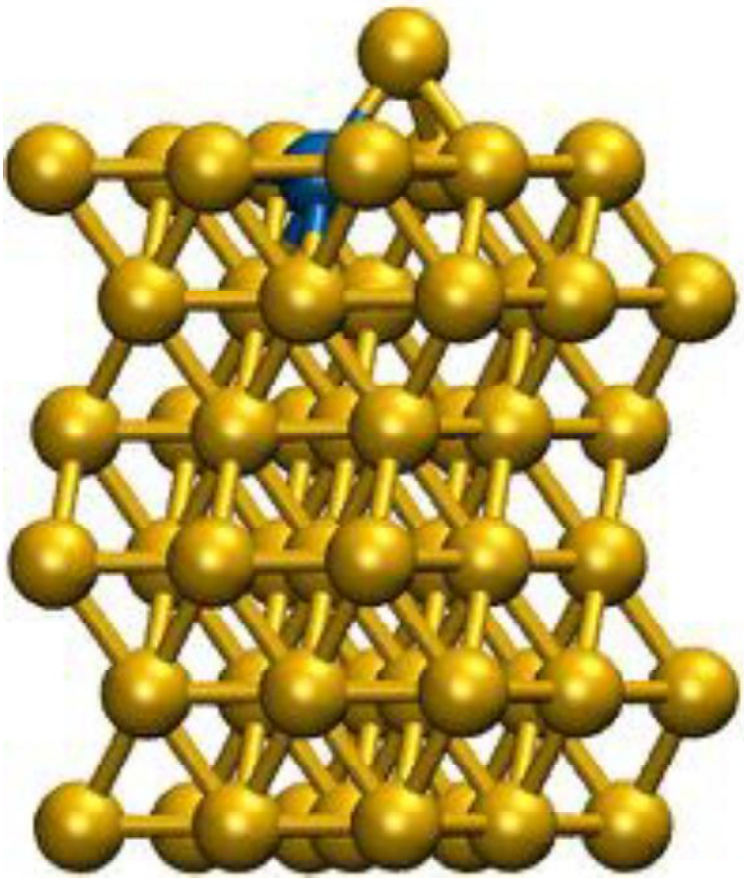

1st barrier in surface-bulk exchange

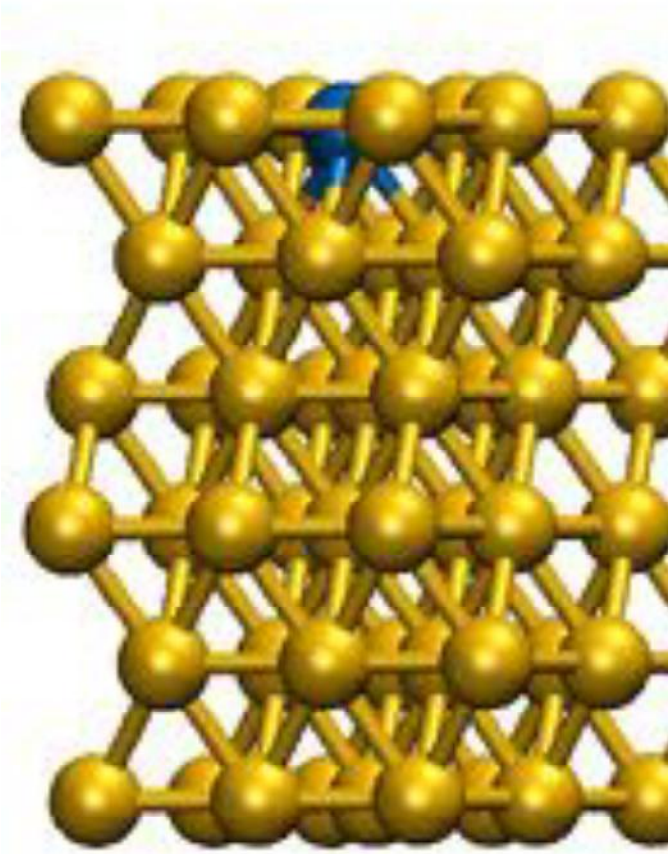

2nd barrier in surface-bulk exchang

Pd substitution near (111) step on Au(

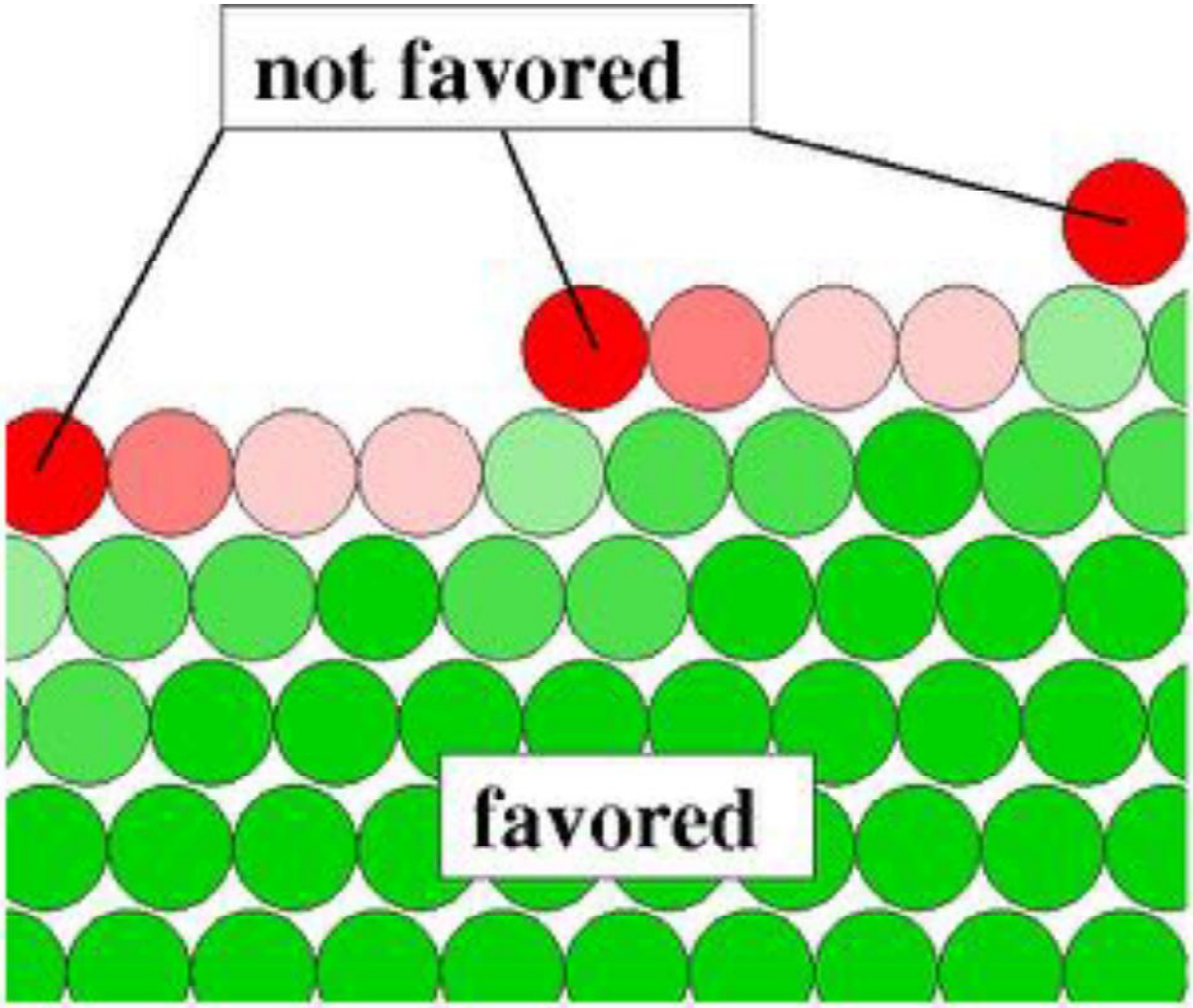

Clean surfaces

pure Au

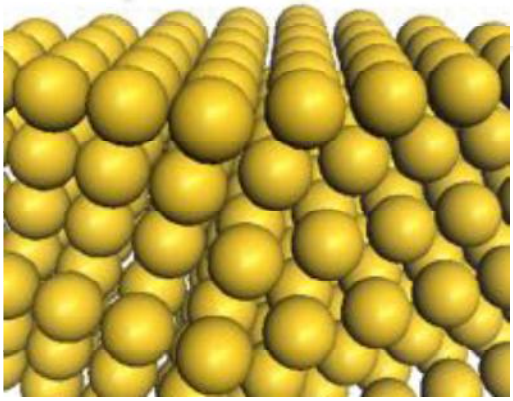

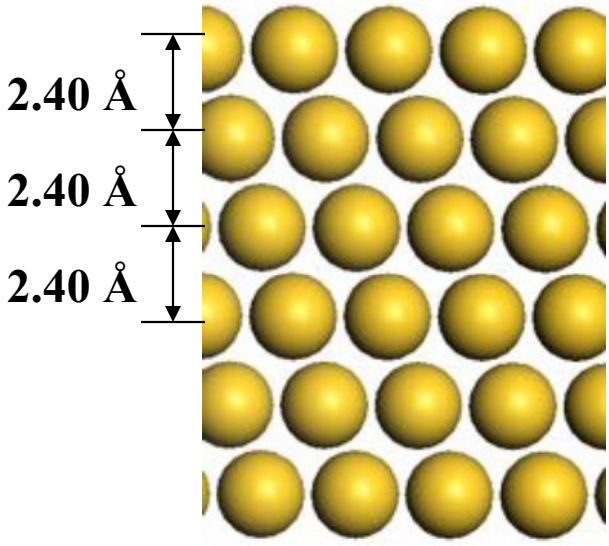

$AuCu_{surf}$

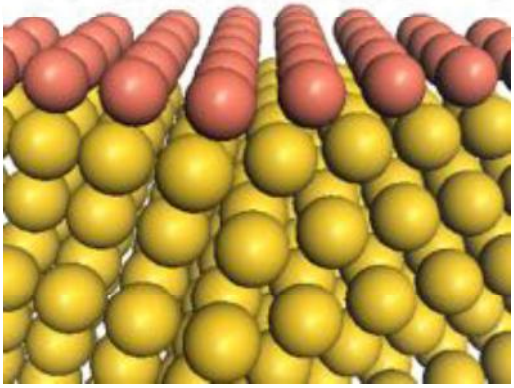

$\Delta E = 0.0$ eV

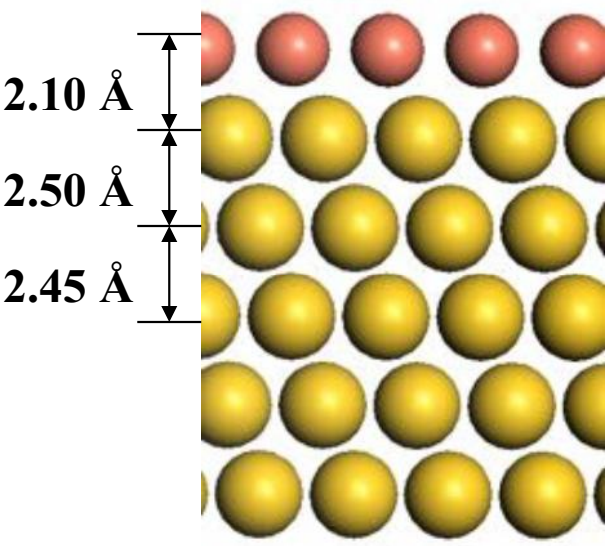

Au

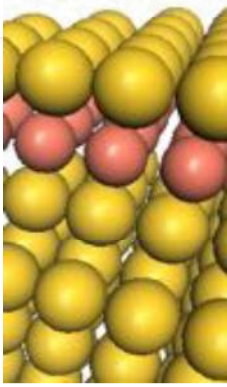

$\Delta E =$

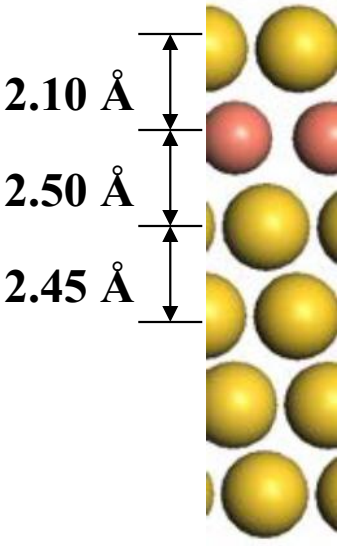

Oxygen-covered surfaces

pure Au

$AuCu_{surf}$

Au

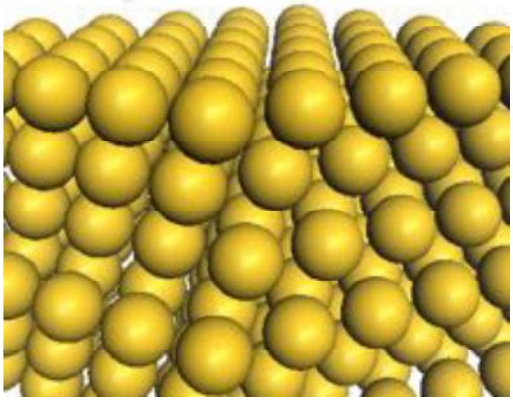

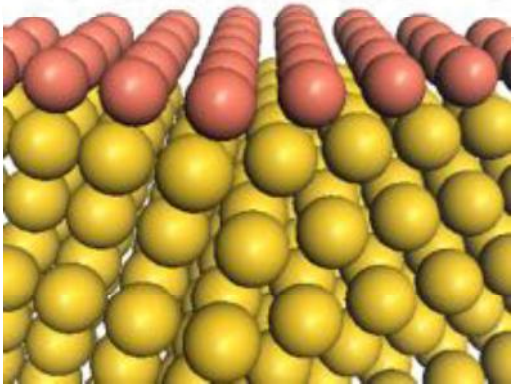

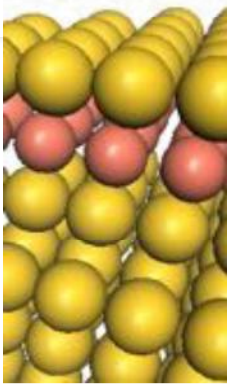

$\Delta E = 0.0$ eV

$\Delta E =$

1.41 Å
2.36 Å
2.43 Å

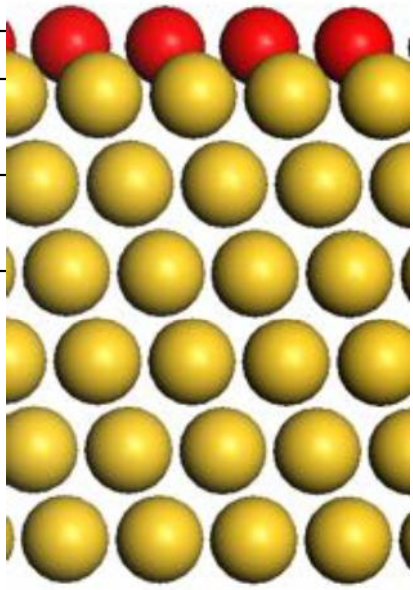

0.74 Å
2.23 Å
2.55 Å

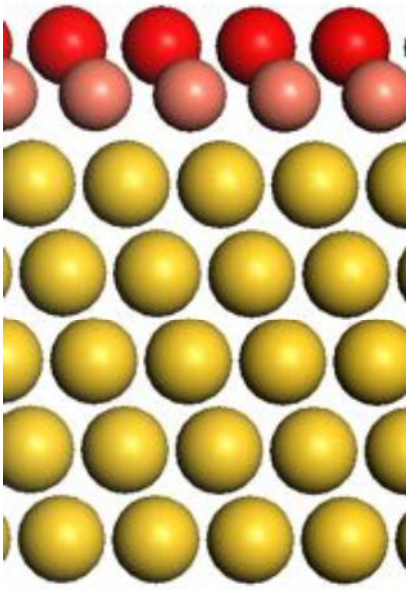

1.37 Å
1.94 Å
2.28 Å

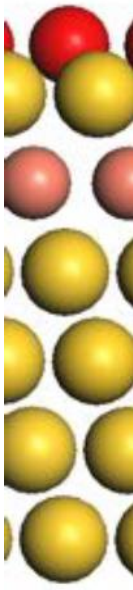

Core-Shell Particles

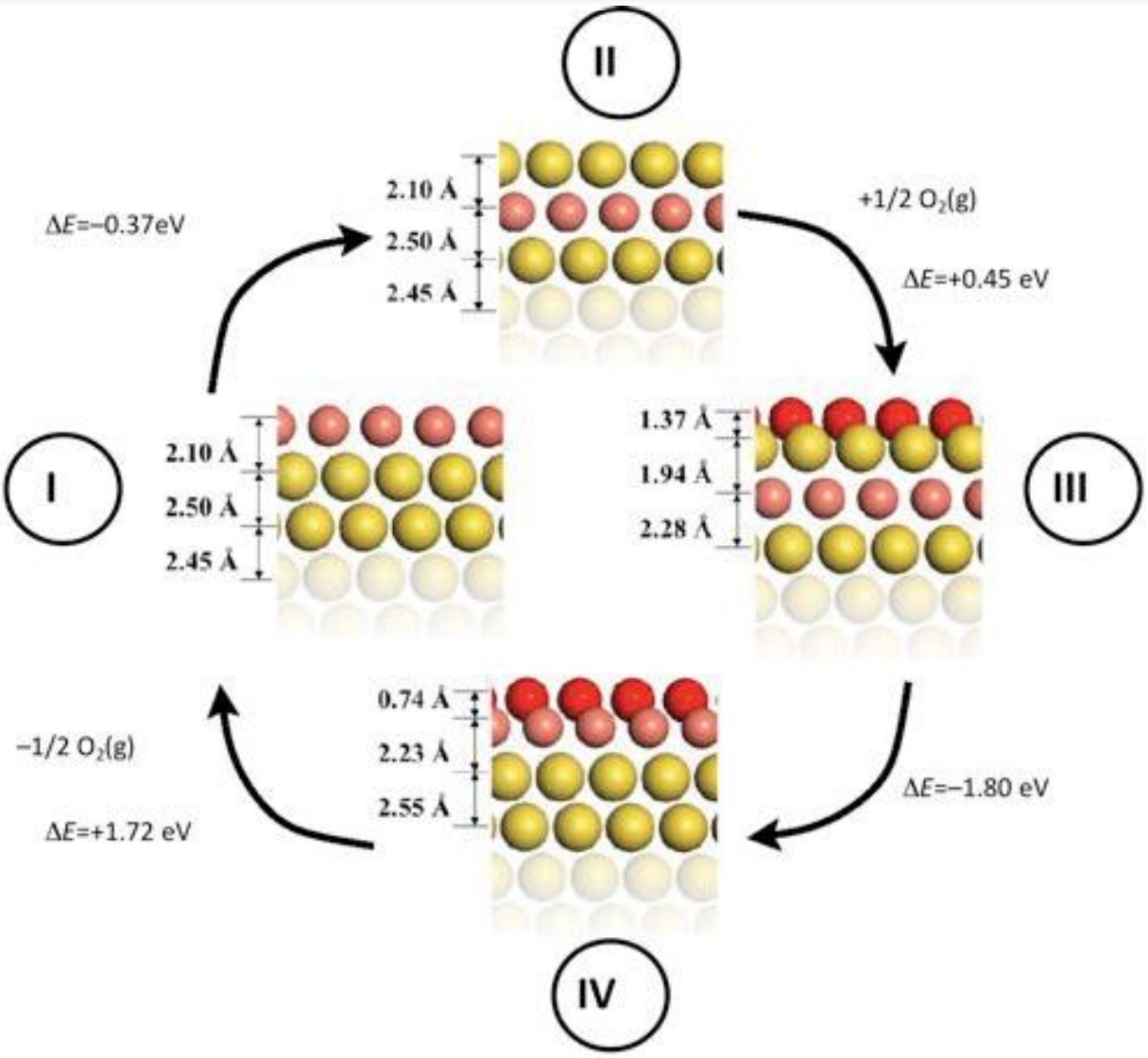

Ref.: E. Völker *et al. Phys. Chem. Chem. Phys.*, **14**, 7448 (2012).

Surface Structuring – Bridging between single crystals and nanoparticles

Facet-Formation

planar Ir(210)

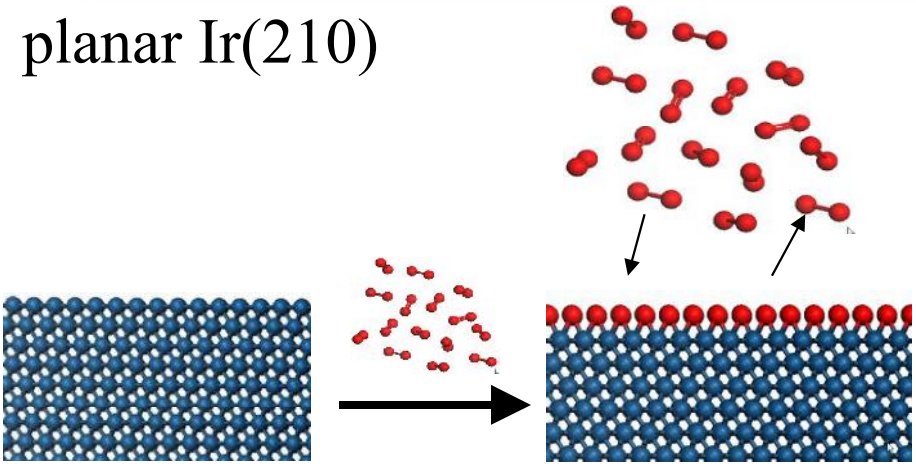

$p_{O_2}=5\times10^{-8}$ Torr,

$T_a \geq 600$K

T=300K

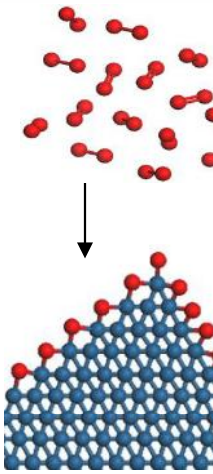

cleanliness → AES, TPD
structure → LEED, STM

faceted Ir(210)

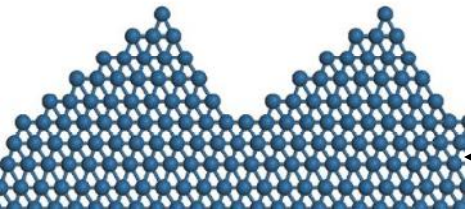

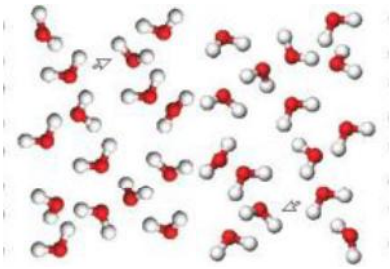

$p_{H_2}=5\times10^{-9}$ Torr
$T = 400$K

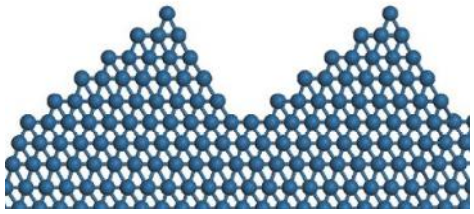

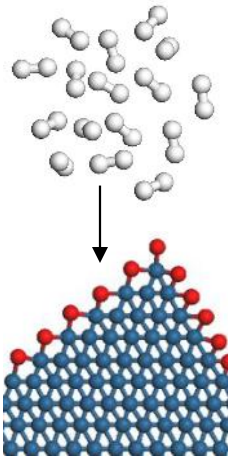

Structure of the nanoscale pyramids

LEED-Experiments:

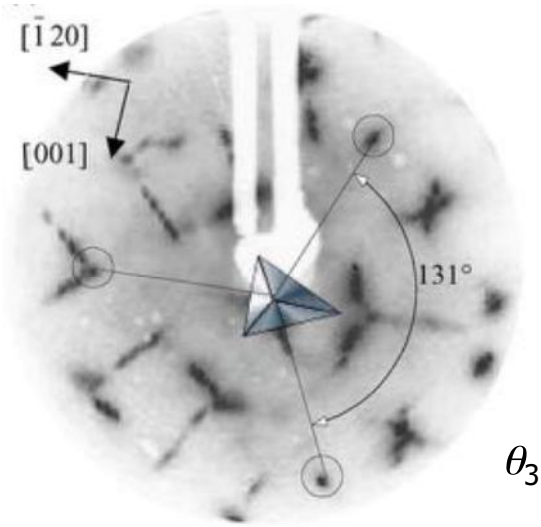

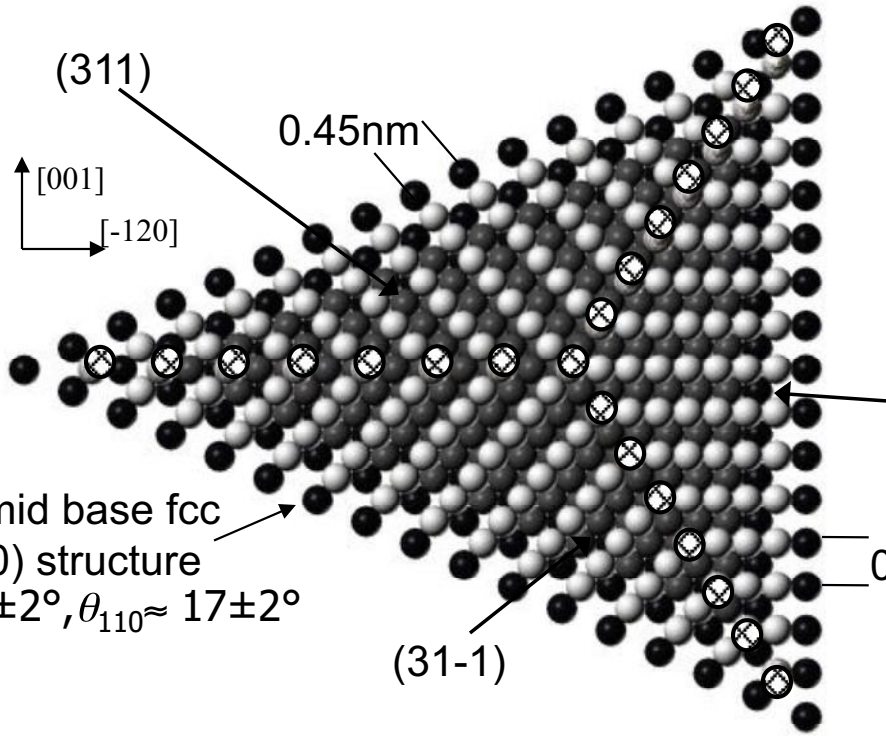

Stability Condition:

$$S_1/\cos\theta_{311}\cdot\gamma_{311}(T,p_O)+S_2/\cos\theta_{110}\cdot\gamma_{110}(T,p_O)<\gamma_{210}(T,p_O)$$

(S_i: normalized coefficients for the partial contribution to the faceted surface [S_1=0.
θ_i: facet tilt angles [geometrical considerations: θ_{311}≈19.29°,θ_{110}≈18.44°])

(p,T)-surface phase diagram

a planar Ir(210)

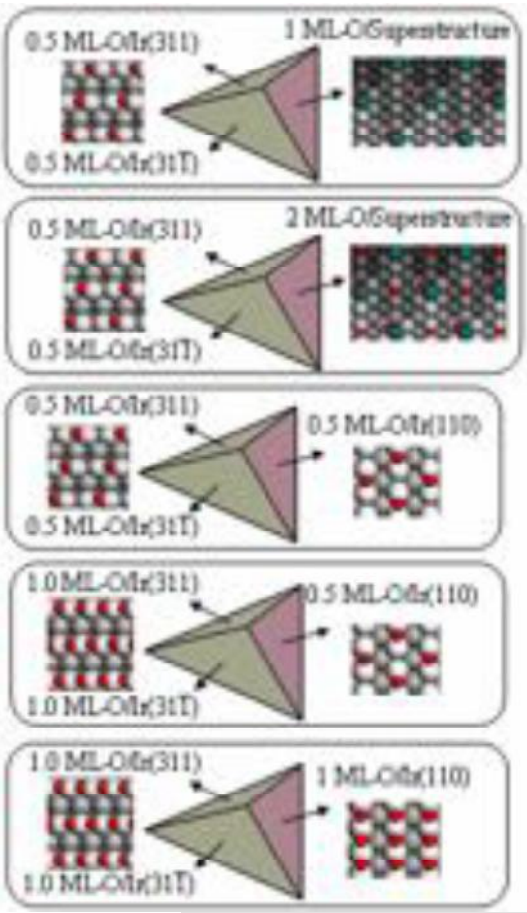

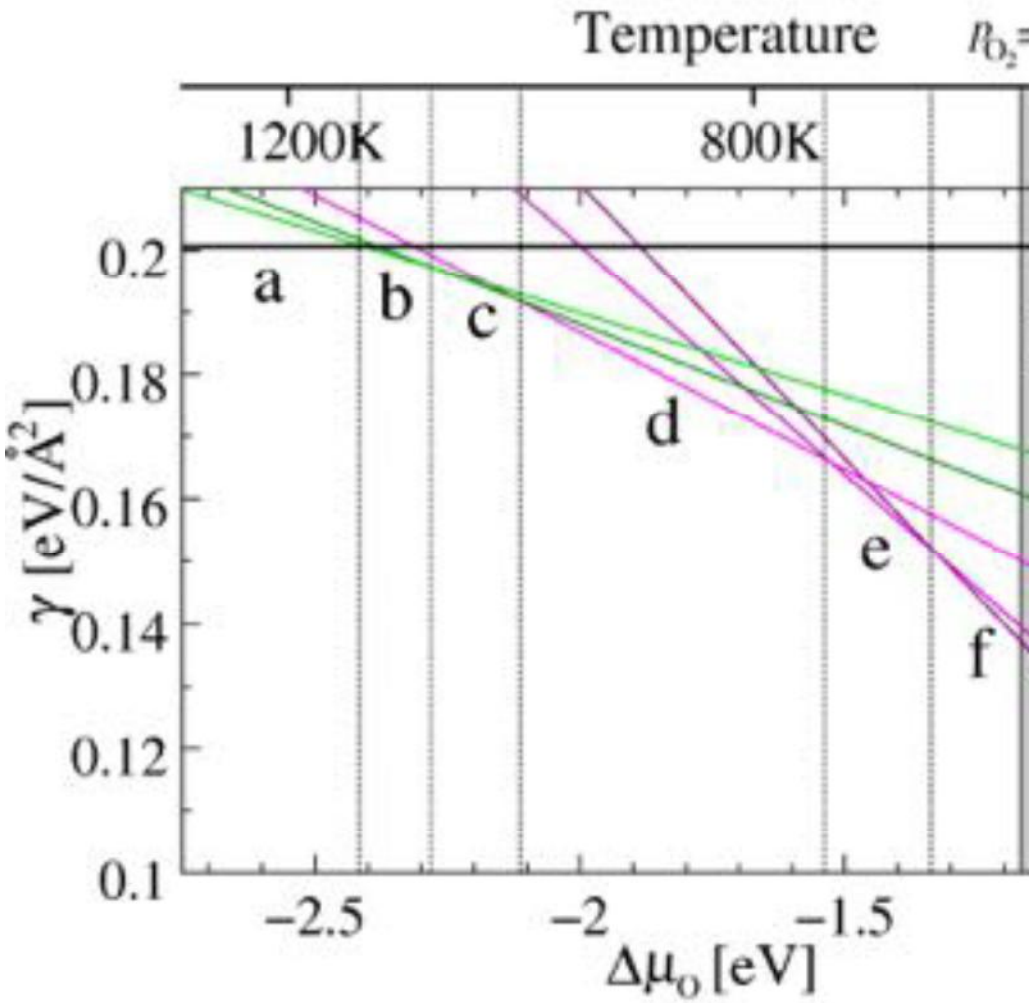

P. Kaghazchi, W. Chen, H. Wang, I. Ermanoski, T. E. Madey, TJ, *ACS Nano*,

Ir/O $(a, T, \Delta\phi_e)$ — Phase Diagr

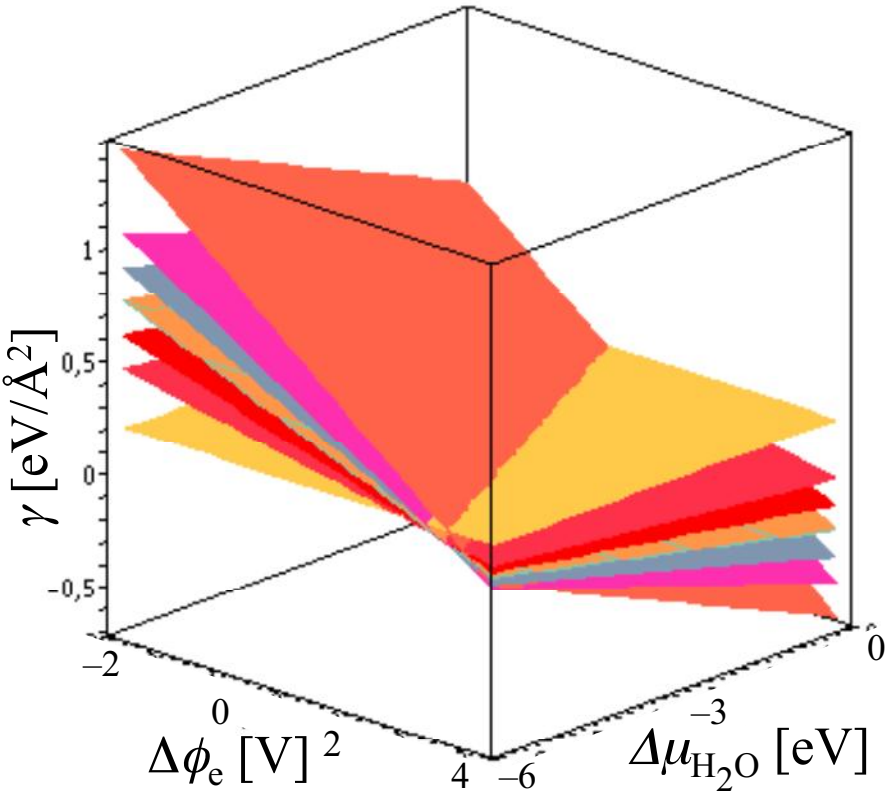

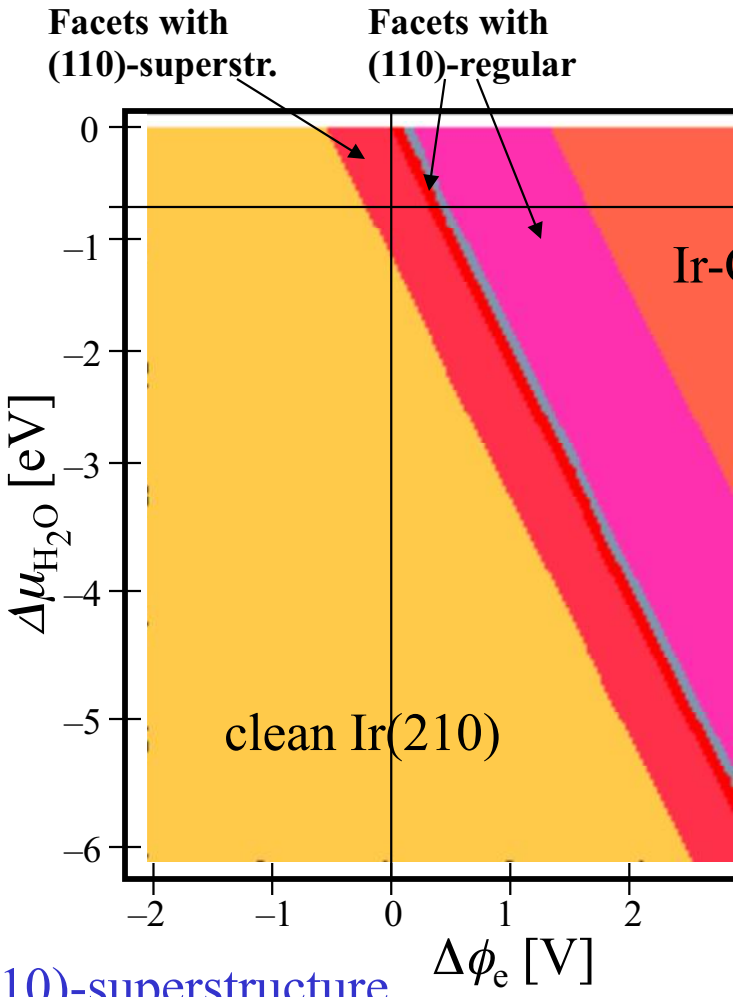

- $\Delta\phi_e \leq -0.3$V: clean Ir(210)
- $-0.3\text{V} < \Delta\phi_e \leq 0.9$V: Facets with Ir(110)-superstructure
- $\Delta\phi_e < 0.95$V: Facets with Ir(110)-regular

P. Kaghazchi, K. A. Soliman, F. C. Simeone, L. A. Kibler, TJ, *Faraday Diss.*, **140**, 69 (2008)

Experimental: Surface Preparati

Annealing in the absence of oxygen by inductive heating

inert (Ar,N_2) or reducing (H_2,C

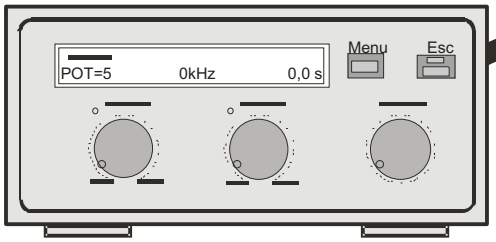

Himmelwerk HU 2000

Faceted Ir(210) in 0.1M H_2SO_4

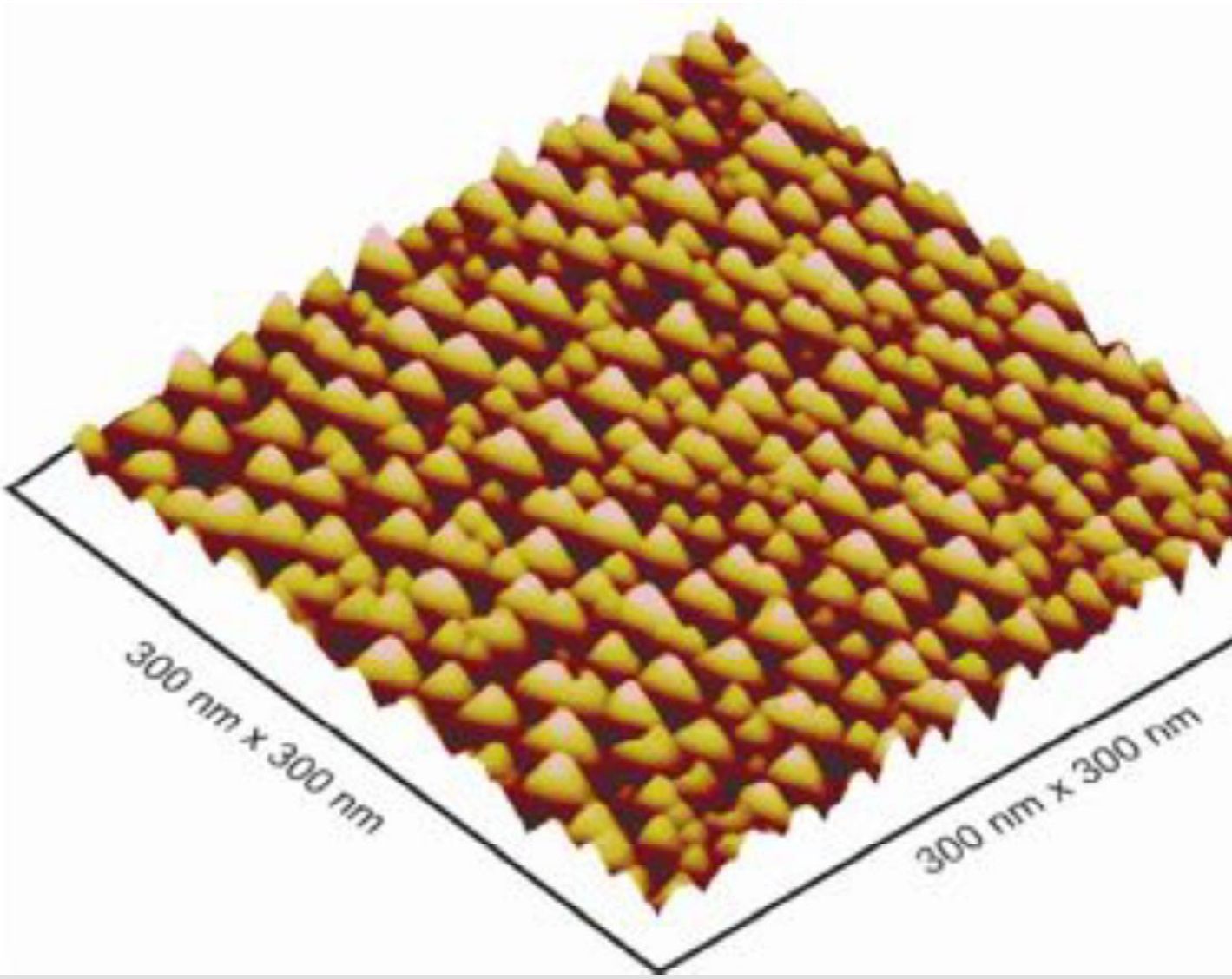

P. Kaghazchi, K. A. Soliman, F. C. Simeone, L. A. Kibler, TJ, *Faraday Diss.*, **140**, 69 (2008)

Characterization by *in-situ* STM

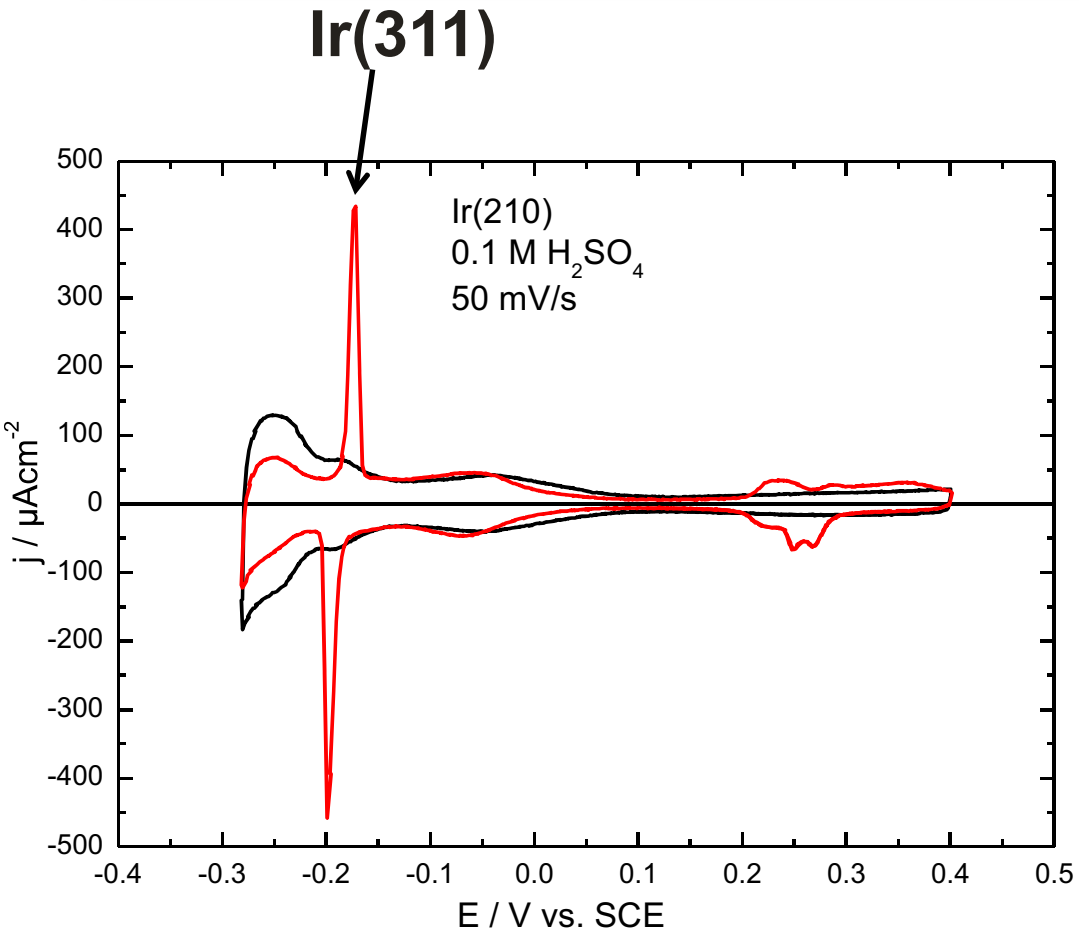

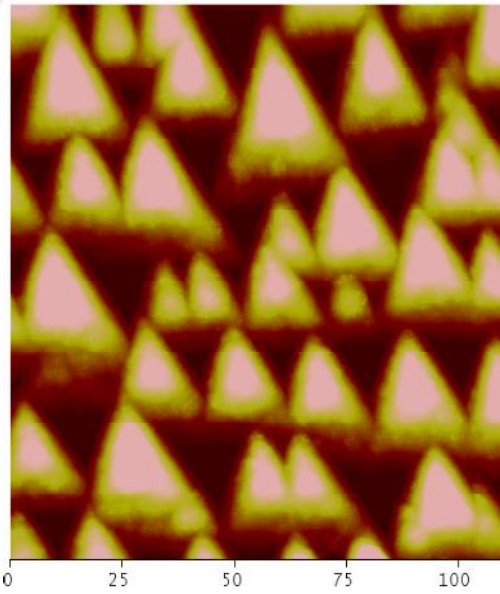

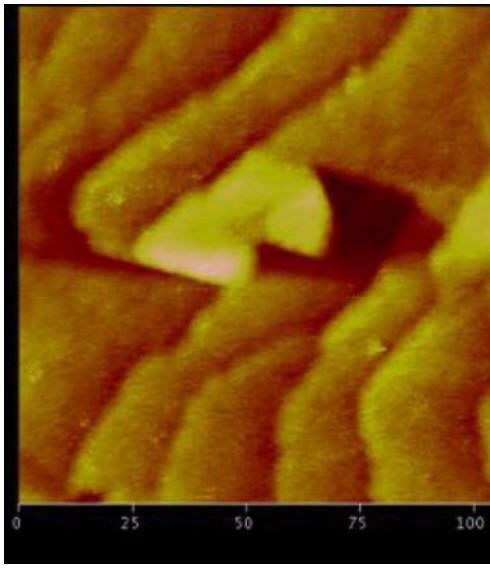

Structure Stability in $HClO_4$

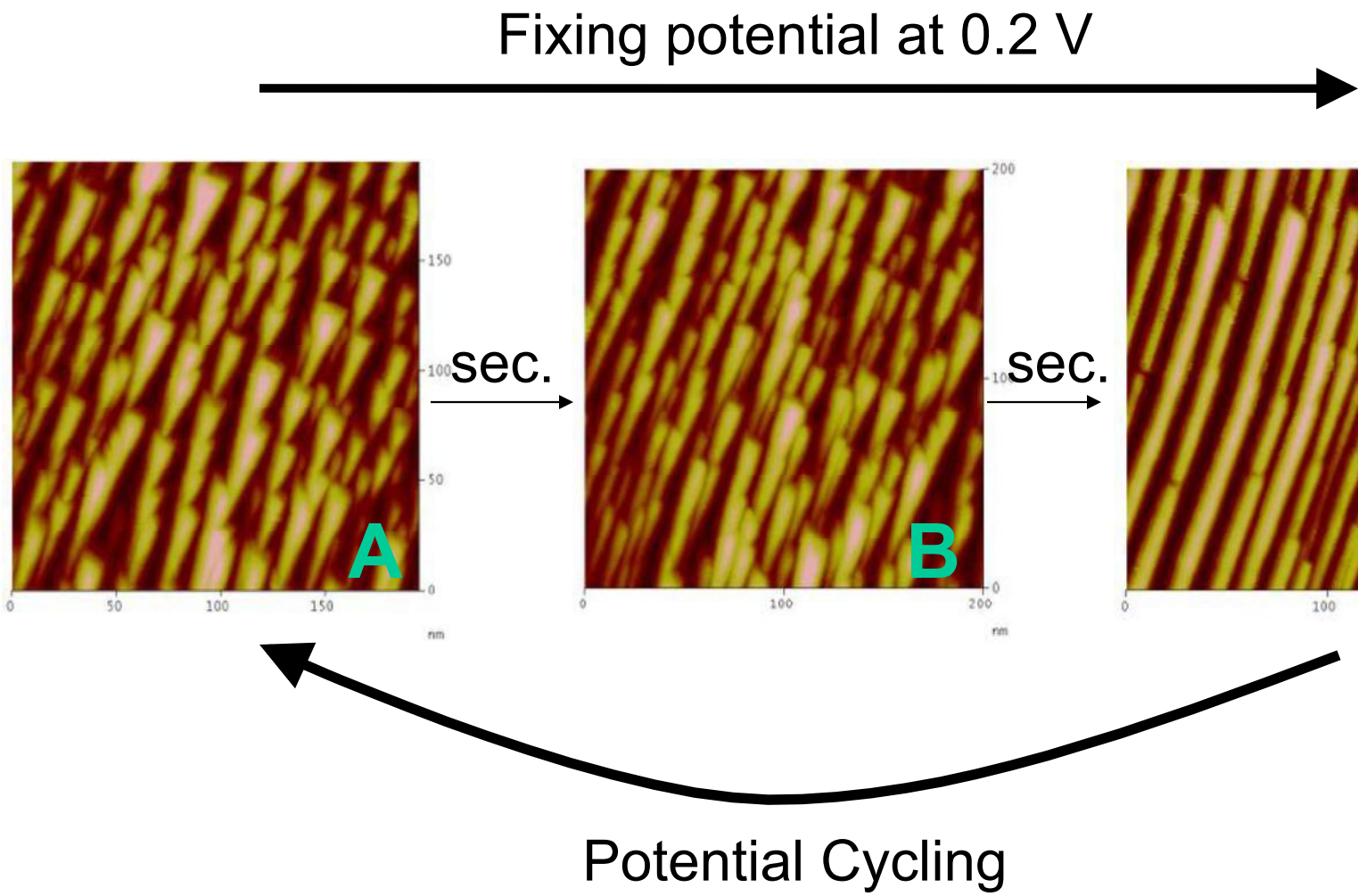

CO oxidation (UHV)

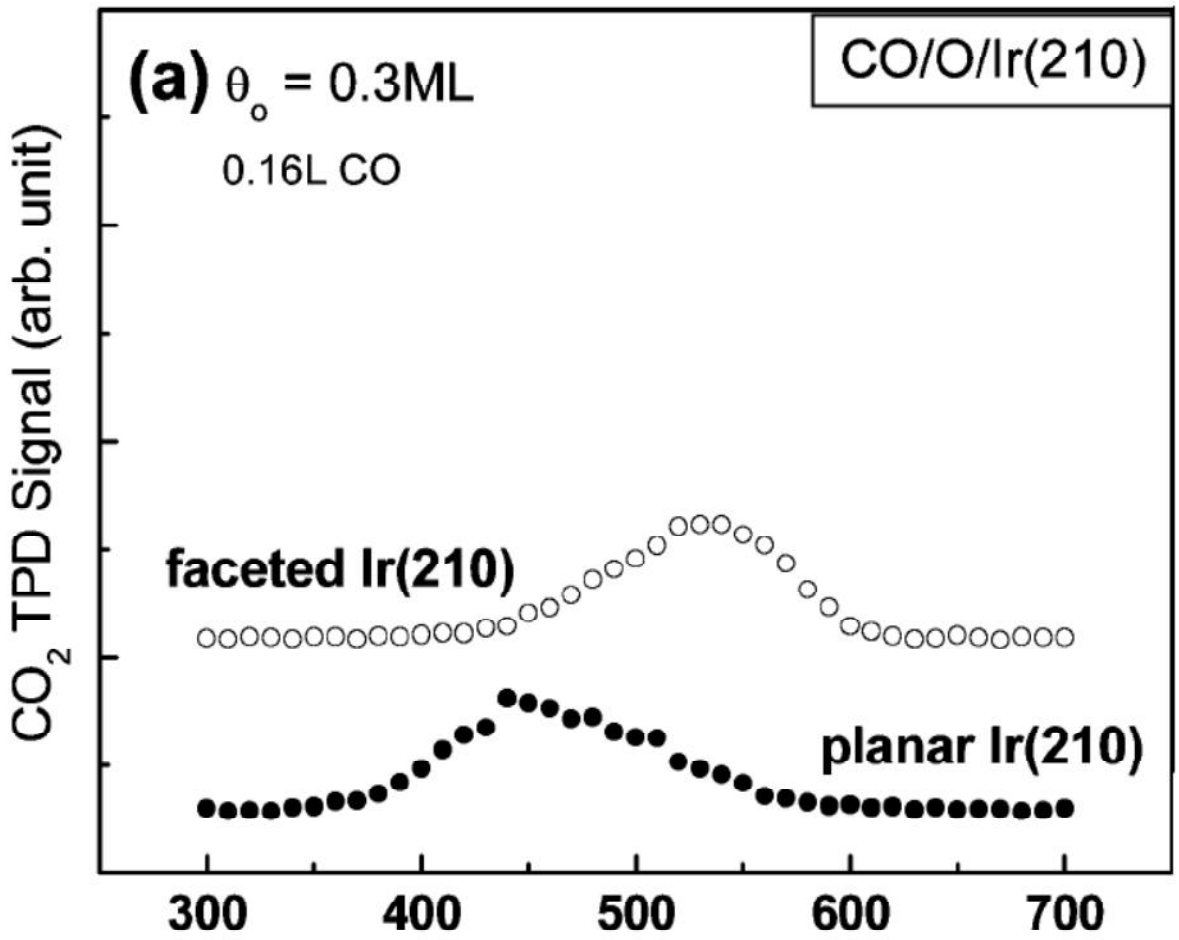

Ten

W. Chen, I. Ermanoski, T. E. Madey, TJ, *Langmuir*, **22**, 3166 (2006).

CO adlayer oxidation (electrochemica

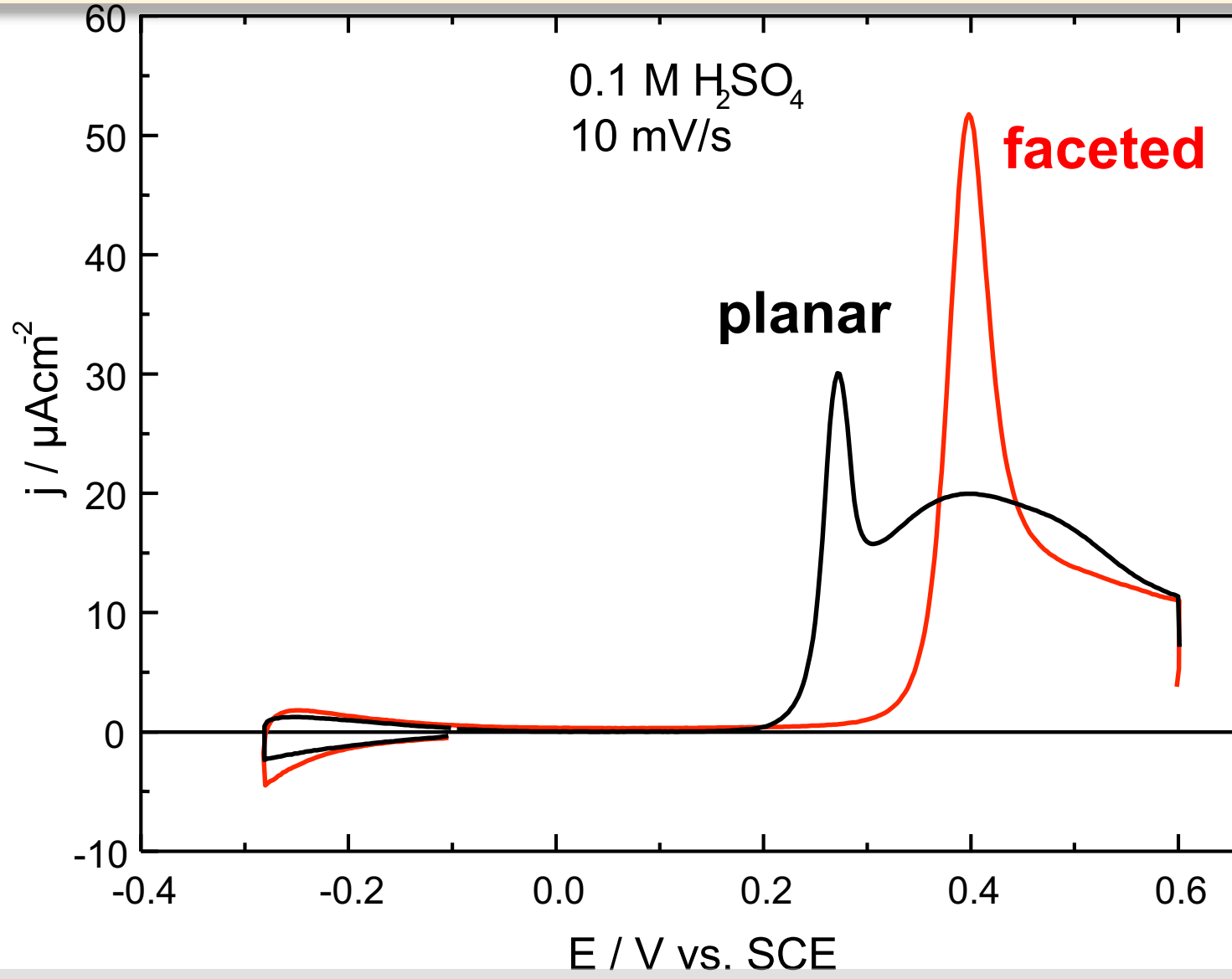

P. Kaghazchi, K. A. Soliman, F. C. Simeone, L. A. Kibler, TJ, *Faraday Diss.*, **140**, 69 (2008)

NO decomposition (UHV) **2NO → N_2 +**

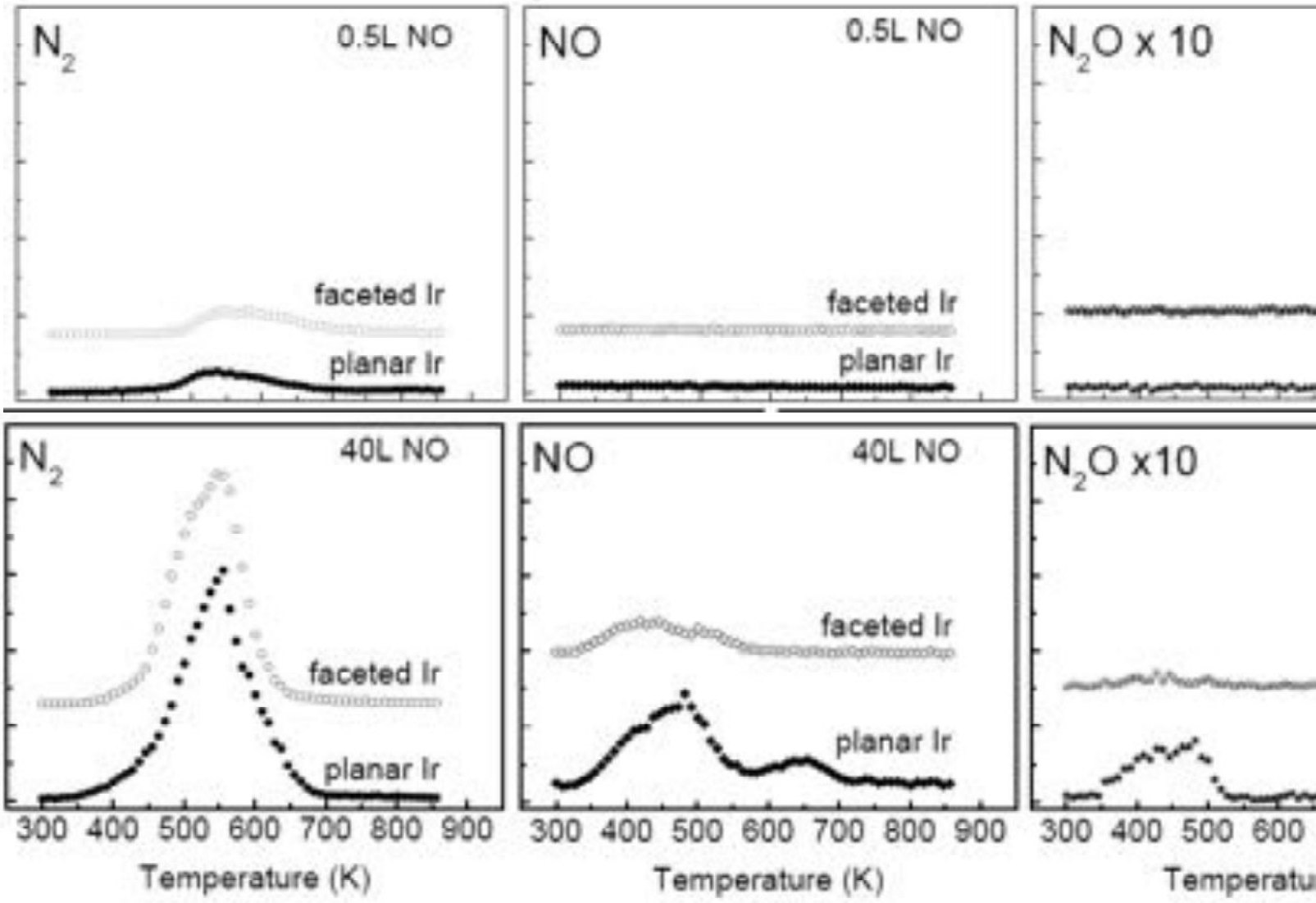

W. Chen, T. E. Madey, A. L. Stottlemyer, J. G. Chen, P. Kaghazchi, TJ, JPC-C, 112,

Re(11-21)-faceting

O-induced

x-slope STM image, 1000Å×1000Å

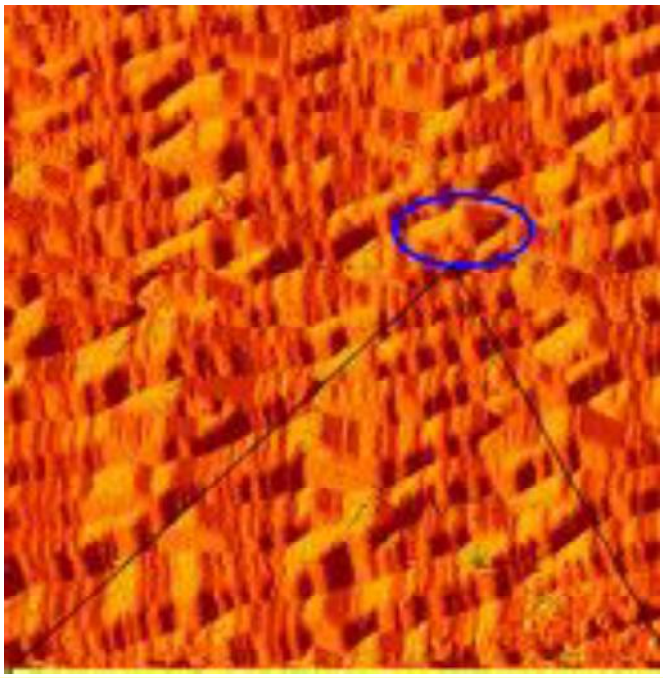

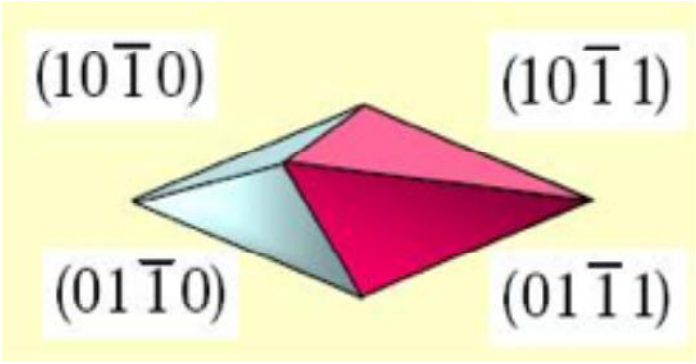

N-induced

STM image, 1000Å×

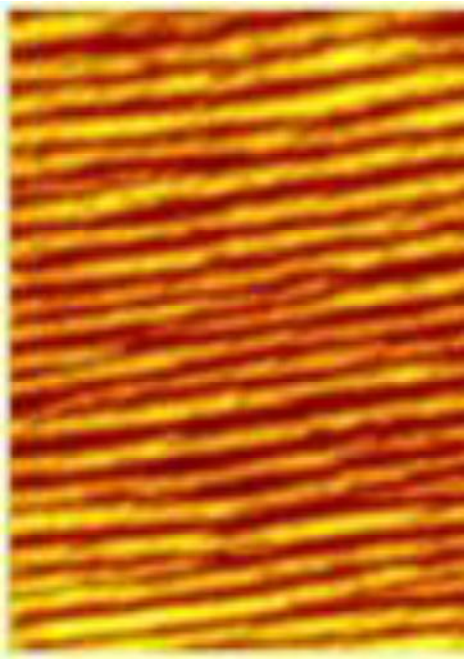

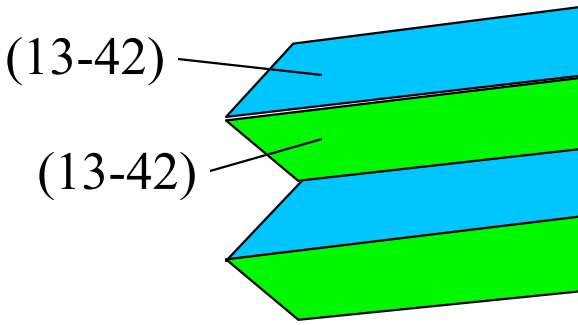

Ir-nanoparticles

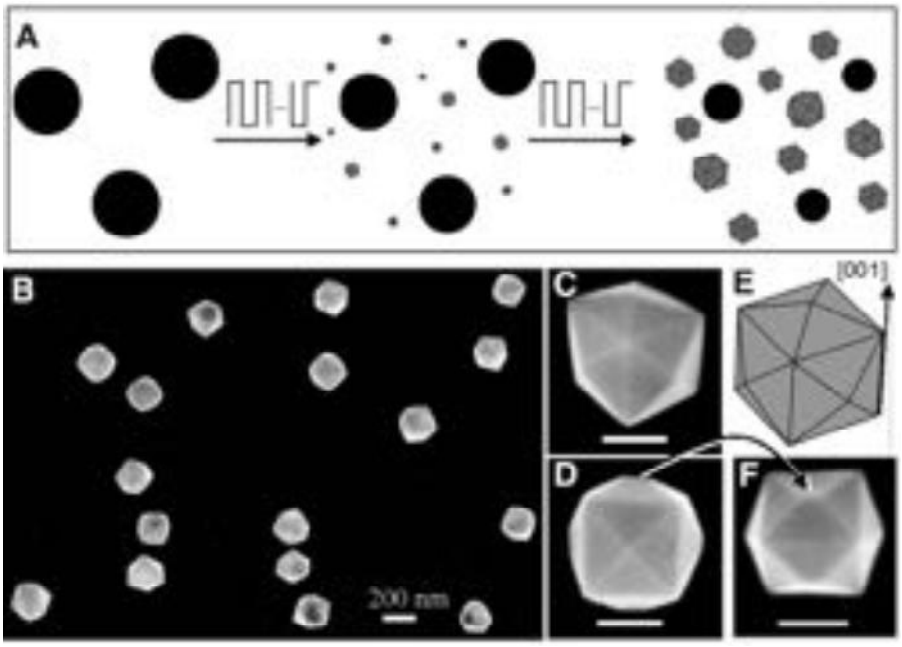

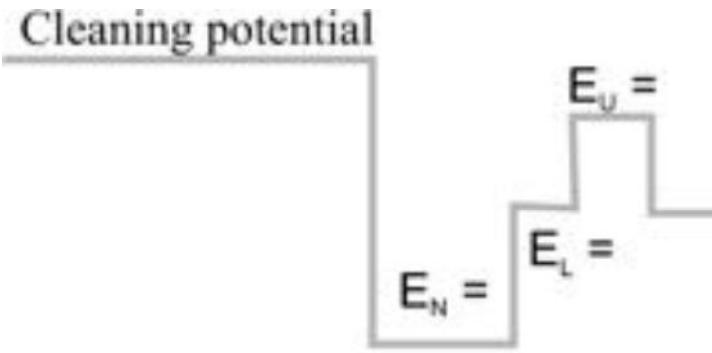

Synthesis of tetra-hexahedral platinum nanocrystals with high-index facets

Tian et al., Science, 316

Ir-nanoparticles: Synthesis by potential cyc

SEM characterization

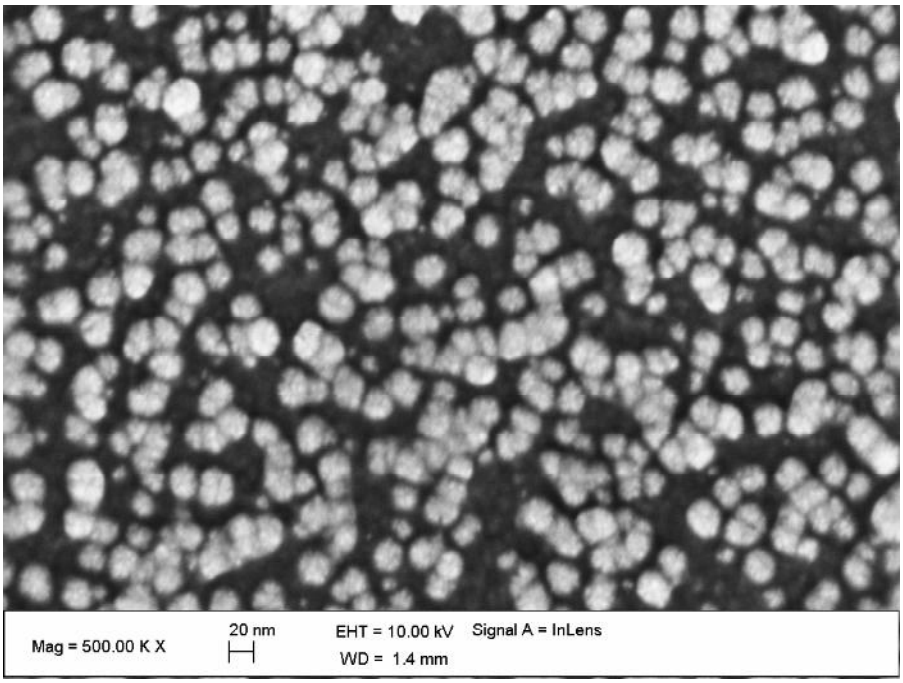

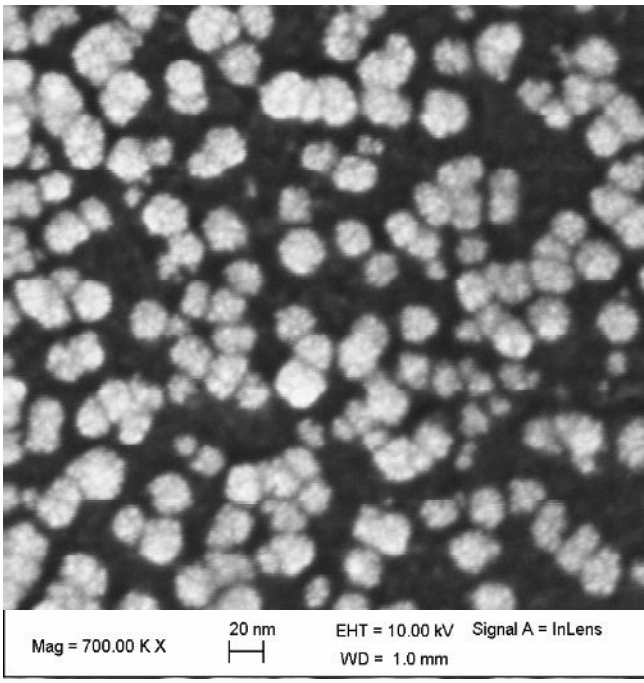

after Ir deposition from 1mM $IrCl_4$ + 0.5 H_2SO_4 between 0.1 V and -0.9 V at 10 mV s^{-1}

Ir-nanoparticles: Synthesis by square-wave

SEM characterization

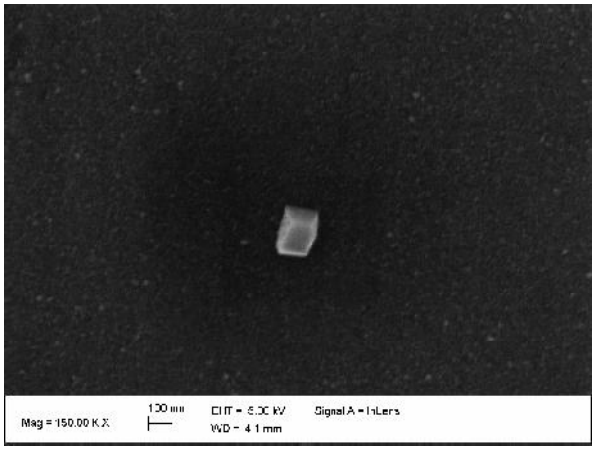

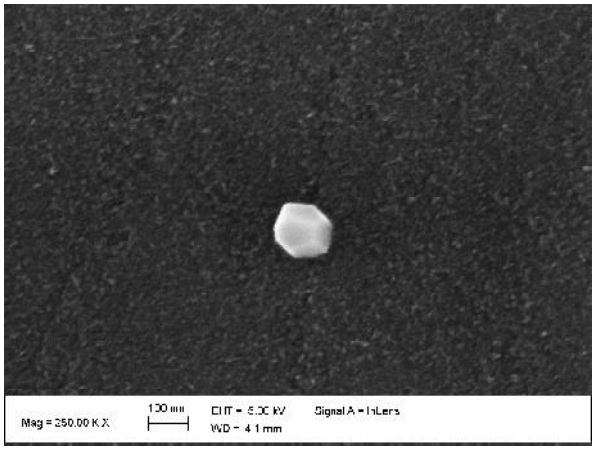

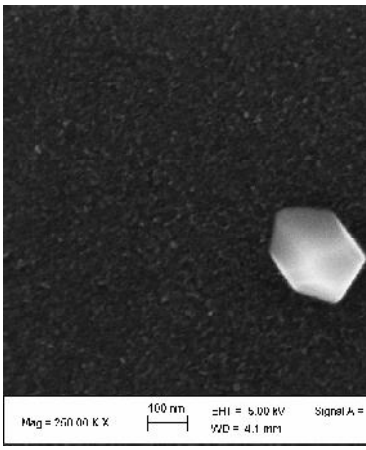

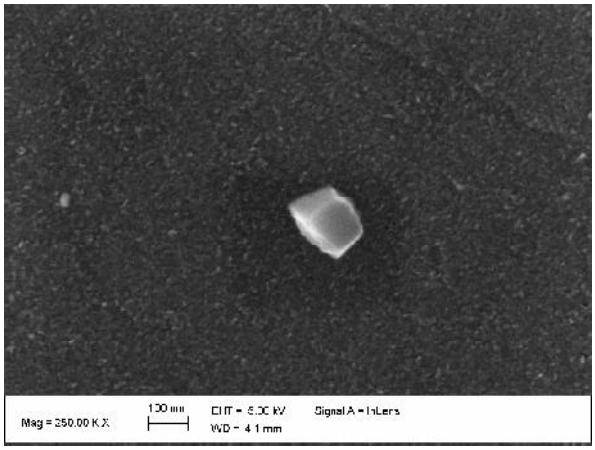

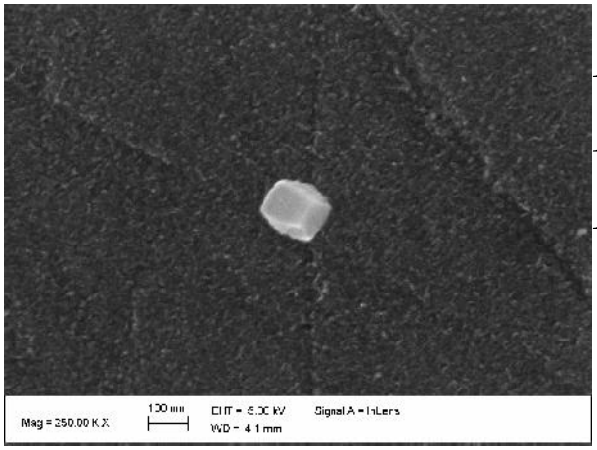

$E_N = -0.90$ V

$E_L = -0.40$ V

$E_U = 0.61$ V

Summary

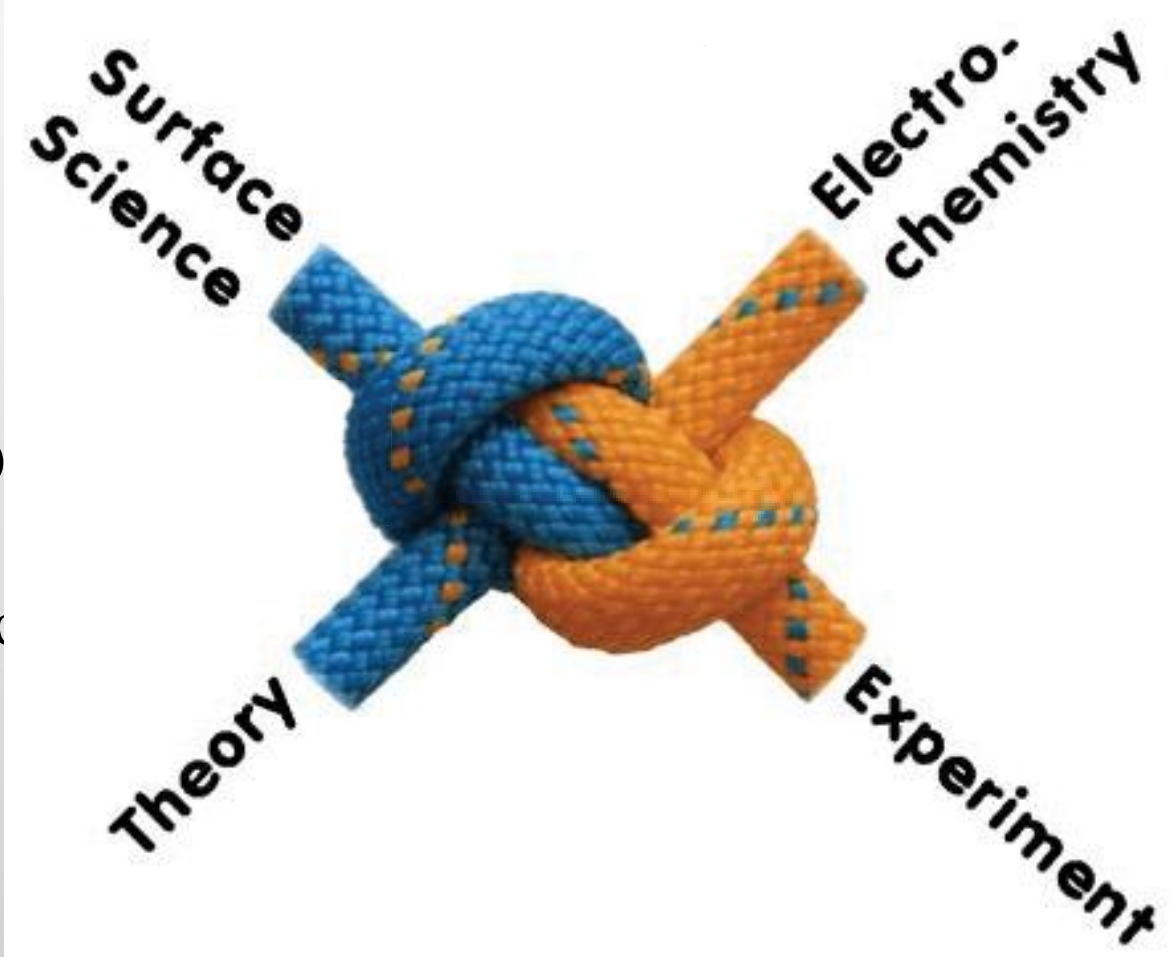

Mo **eti**

rgie

co **acti**

(reactive)
environment

The Gang

Acknowledgements

Funding

- Deutscher Akademischer Austauschdienst (DAAD)
- Alexander von Humboldt Stiftung (AvH)
- Fonds der chemischen Industrie (VCI)
- BMBF
- Europäische Union (ELCAT-Network), European Research Council (ERC)
- Deutsche Forschungsgemeinschaft (DFG)
- Studienstiftung des dt. Volkes
- Robert Bosch GmbH, Daimler